NASA Contractor Report 165742

HELICOPTER ROTOR LOADS USING A MATCHED ASYMPTOTIC EXPANSION TECHNIQUE

G. Alvin Pierce and
Anand R. Vaidyanathan

Georgia Institute of Technology
A Unit of the University System of Georgia
School of Aerospace Engineering
Atlanta, GA 30332

NASA
National Aeronautics and
Space Administration

Langley Research Center
Hampton, Virginia 23665
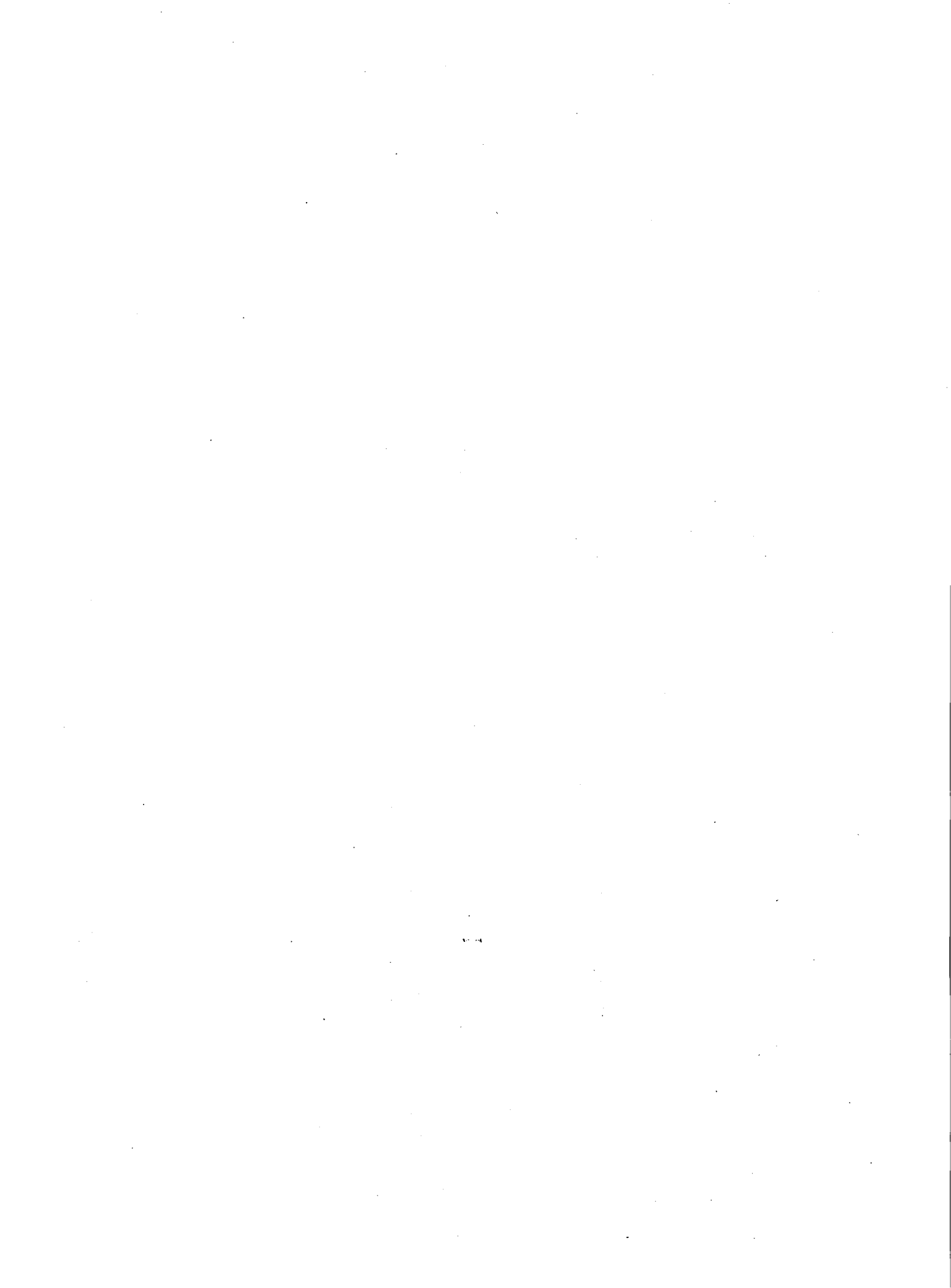
N82- 21156

N82- 21156 #

HELICOPTER ROTOR LOADS USING A MATCHED ASYMPTOTIC EXPANSION TECHNIQUE

By

G. Alvin Pierce

and

Anand R. Vaidyanathan

Prepared by

GEORGIA INSTITUTE OF TECHNOLOGY
SCHOOL OF AEROSPACE ENGINEERING
Atlanta, Georgia 30332

CONTENTS

HELICOPTER ROTOR LOADS USING A MATCHED ASYMPTOTIC EXPANSION TECHNIQUE

G. Alvin Pierce and Anand R. Vaidyanathan
Georgia Institute of Technology

SUMMARY

A variety of approximate methods are available for the estimation of airloads on helicopter rotor blades. These methods vary widely in their degree of approximation, accuracy and detail of prediction. One such method has been suggested by Van Holten which uses an acceleration potential description of the flow field and a matched asymptotic expansion technique to calculate unsteady, three-dimensional airloads on a rotor blade in forward flight.

The study presented here was undertaken to examine the theoretical basis and computational feasibility of the Van Holten method, and to evaluate its performance and range of validity by comparison with experiment and other approximate methods. It is found that, within the restrictions of incompressible, potential flow and the assumption of small disturbances, the method does lead to a valid description of the flow. However, due to the nature of the basic assumptions, the method begins to break down under conditions favoring non-linear effects such as wake distortion and blade/rotor interaction

INTRODUCTION

This study is concerned with the calculation of three-dimensional, unsteady airloads on a helicopter rotor blade in forward flight. A detailed knowledge of these airloads is of importance in problems of noise and vibration reduction and in dynamic and aeroelastic analyses of the rotor blade. Due to the complexity of the flow field a completely general solution to the problem has not been obtained. There are a large number of aerodynamic analyses available in which the actual flow field is simplified considerably to make the problem solution feasible. Most of these methods are described in reference 1 and, with particular reference to the vortex representation in reference 2. The methods range in complexity from simple blade element representations to lifting surface models with freely distorted vortex wakes with associated ranges in computational expense, accuracy and detail of solution.

A commonly used method is based on a combination of simple momentum theory and blade element description, in which a momentum balance is made at each blade section in order to determine an effective incidence, from which force and moment coefficients are determined. Induced velocity over the disk is usually assumed constant, equal to the value obtained from simple momentum theory. Sometimes linear variations of induced velocity across the disk are also assumed. The method does not incorporate three-dimensional and wake effects on the airloads other than by the use of empirical factors. The blade element description is often quasi-steady. Unsteady aerodynamics can be included by using Theodorsen's results (ref. 3) or, with the effect of forward speed variation, Greenberg's results (ref. 4). Real fluid effects are accounted for using wind tunnel test results appropriate to the Mach number and Reynolds number of the blade section. In spite of these shortcomings, this model is perhaps the most widely used in practice, for its main advantages are twofold.

(1)   The blade element representation leaves the model open for incorporation of empirical factors associated with various effects such as reversed flow, dynamic stall, compressibility, etc. (usually determined from two-dimensional wind tunnel tests).

(2)   The relative simplicity of the model makes it ideal for inclusion in a more extensive helicopter analysis. An example of such a model is that of Gormont (ref. 5).

In order to account for the rotor wake, many methods model the blade by a simple lifting line of bound circulation and then calculate the non-uniform induced velocity field generated by the wake of the lifting line, to various degrees of approximation. Finite-chord effects are then represented by a blade element model. In the method due to Willmer (ref. 6), the wake immediately behind the blade is replaced by a plane, semi-infinite wake similar to that of a fixed wing. The remainder of the wake is represented by a series of plane, infinite layers underneath the blade. For simplicity, quasi-steady assumptions are made so that the wake consists only of trailing vorticity. The wake can also be represented by a rigid, helical surface of shed and trailed vorticity from the rotating lifting line. Calculation of the velocity induced by such a wake at a point on the lifting line involves numerical integration with a singularity in the integral, which makes it necessary to extract the finite part of the integral by some means. This difficulty arises because replacing the blade by a lifting line is not a physically acceptable assumption in the vicinity of the blade itself. One way of overcoming this difficulty is to calculate the induced velocity along the three quarter-chord line. The only justification for this procedure is the observation from steady, two-dimensional flow that, with the distributed vorticity lumped into a bound vortex at the quarter-chord point, the boundary condition is satisfied exactly only at the three quarter-chord point. Another method of overcoming the singularity is to take the time (azimuth) average of the effect of the instantaneous wake configuration (ref. 2). This leads to a simplier model which could also have been arrived at by replacing the finite-bladed rotor with an actuator disk. This model consists of an infinite number of blades each carrying an infinitesimal load, so that the wake of a finite number of helical sheets is replaced by a skewed, semi-infinite cylinder filled with vorticity. Another method consists of considering the continuous distribution of vorticity in the helical wake to be lumped into elements of finite circulation at convenient radial and azimuthal intervals (ref. 7).   If the bound circulation on the blade is approximated by a stepped distribution and if the blade is moved impulsively from one azimuth station to the next, then the resulting wake is just a network of straight-line segments, a discretized version of the continuous wake. The contribution of each segment is known directly as a function of its position; hence the wake integration becomes greatly simplified, since it consists only of a finite summation.   The model can be improved to better account for unsteady aerodynamic effects by retaining a continuous sheet for the "near" shed wake (ref. 8).

Under conditions of low inflow through the rotor and low forward speed, the concept of a rigid wake, (i.e., one in which all elements of the wake are convected downward at a constant speed to give the wake a rigid helical shape, is not an acceptable one. Interaction between the blade and the wake, self-induced distortions in the wake and other nonlinear effects become significant. In addition, there is always the process of rapid roll-up of the vortex sheet near the blade tip and the consequent effect of a strong tip vortex on the same blade and the following one. Miller (ref. 9) introduces the concept of a "semi-rigid" wake, in which the downward velocity with which the wake elements are shed varies with azimuth but not with radial position. He divides the wake into a near wake, for which the blade has a surface representation, and a far wake, for which the blade is a lifting line. The bound circulation distribution is also simplified to a constant so that the trailing vorticity consists only of a root and tip vortex. It is also possible to carry out a distorted wake

analysis by starting either with a rigid wake or some given initial wake configuration, using the non-uniform induced velocity field to define a distorted wake for the next iteration and repeating the process until convergence is achieved. An example of such a "free" wake analysis is that of reference 10. For such an iterative process, the computation time and expense for a single wake calculation must be small and the segmented wake model is best suited to this need.

Another approximate method is the "local momentum" approach of reference 11. The blade is treated as a series of elliptical wings, each of which contributes an induced velocity that is constant along its span. This is combined with a momentum balance at each blade element and an "attenuation coefficient" to account for the timewise change of induced velocity at a point after blade passage through it.

In addition to the vortex methods, there are also techniques based on the use of an acceleration potential. Dat (ref. 12) models the blade by a lifting line of acceleration potential doublets along the quarter-chord line of the blade and satisfies the normal velocity boundary condition along the three quarter-chord line. The details of the computational procedure are presented by Costes (ref. 13). Although the acceleration potential formulation leads to potential discontinuities being confined to the blade surface, the computational expense involved is no less than in the vortex (velocity potential) formulation. This approach does have the merit that it can be rigorously extended to compressible flow; however, computations (ref. 13) seem to show that results for compressible flow are well approximated by scaling incompressible flow results.

In considering the full range of available methods, it is seen that even the distorted wake representations are not acceptable under all circumstances. It is possible to account for wake distortion and have good correlation with experiment by making use of experimental information to define a "prescribed", distorted wake. However, to precisely define the prescribed wake for various flight conditions requires an extensive data base of experimental results. This has been achieved so far only for the case of hovering flight (ref. 14). To extend the data base to forward flight would require entensive experiments to cover possible variations of flight conditions. It has been shown (ref. 15) that the use of a prescribed wake does produce acceptable results but the results are highly sensitive to the prescribed wake geometry.

The use of potential vortex filaments to model the rotor wake sometimes leads to excessive, unrealistic wake effects in the computation, which can be avoided only by accounting for factors such as a finite core radius for the actual vortex tube. In view of the number of factors that cannot be rigorously accounted for in a rotor aerodynamic representation, most methods in practice rely on empirical input in one form or another (ref. 16). Any new method proposed for calculating the airloads on a rotor blade in forward flight must therefore have its performance assessed against this background.

A method has been proposed by Van Holten (ref. 17) for calculating the unsteady, three-dimensional airloads on a helicopter rotor blade in forward flight. The method uses the acceleration potential formulation, together with a matched asymptotic expansion technique, to generate a solution accurate to $O(A^{-2})$, where A is the aspect ratio of the blade. This method has not been studied in sufficient detail to determine its value relative to other available techniques. This program has therefore been undertaken to carry out the following with respect to the asymptotic method.

(1) To study the theoretical basis and limits of validity
(2) To verify the expressions derived for computation
(3) To write a computer program for the computational scheme which calculates the pressure distribution on a rotor blade in forward flight

(4) To apply the program to calculate results for some cases for which experimental results are available for comparison

(5) To calculate results for the same cases using other approximate methods so that results may be compared relative to computational expense

(6) To consider the possibility of using measured section properties

(7) To study the efficiency of the computational scheme

SYMBOLS

A	aspect ratio
A_{nk}, B_{nk}	coefficients in collocation form (eq. (9))
a_n, b_n	coefficients of regular solution
a_o, a_1, b_1	blade flapping coefficients
B	number of blades
b	semi-chord
C	Theodorsen function
C_T	thrust coefficient, thrust$/\pi R_1^2 \rho (\Omega R_1)^2$
D_n	derivative expressions (Appendix C)
F_n	functions in pressure gradient condition (eq. (2))
g, h	coefficients of singular solution
I_n	modified Bessel function of first kind
J_n	Bessel function of first kind
K_n	modified Bessel function of second kind
K	number of azimuthwise harmonics
k	reduced frequency, $b\omega/U$
L	total lift on blade
ℓ	sectional lift
M	moment of blade lift about hub
m	sectional pitching moment
N	number of spanwise collocation modes
N_I	number of integration points
P_n^m	associated Legendre function of first kind
p	pressure
Q_n^m	associated Legendre function of second kind
R_o	blade root radius
R_1	blade tip radius

r	cylindrical coordinate
r_b	spanwise coordinate along blade with hub as origin
s	semi-span of rotor or fixed wing
t	time
U	freestream velocity
u, v, w	flow velocity components
V	flow velocity
x, y, z	flow-axes coordinates (fig. 1)
x_a, y_a, z_a	fixed-wing coordinates (figs. 2, 3 and 4)
x_b, y_b, z_b	blade-axes coordinates (figs. 1 and 2)
x_r, y_r, z_r	rotor-axes coordinates (fig. 1)
α_r	tip path plane incidence, forward tilt positive
β	blade flapping angle
γ	blade inertia coefficient (Lock number)
ϵ	linear twist, root pitch angle - tip pitch angle
η	elliptic coordinate
θ	prolate spheroidal coordinate
θ_o	blade root pitch angle
λ, τ	variables of integral (eq. (G7))
μ	advance ratio, $U/\Omega R_1$
ρ	air density
ϕ	elliptic coordinate
χ	cylindrical coordinate
Ψ	prolate spheroidal coordinate
Ψ_b	azimuth angle
Ω	rotor angular velocity
ω	oscillation frequency

Notations:

$(\ )'$	perturbation quantity
$(\overline{\ \ })$	complex amplitude
$(\ )^*$	non-dimensional

THE ASYMPTOTIC METHOD

Analytical Description

The asymptotic method as proposed by Van Holten (ref. 17) for the determination of unsteady, three-dimensional airloads on a helicopter rotor blade is based on the following assumptions:

(a)   Incompressible, potential flow
(b)   Disturbances induced by the rotor are small compared to the forward speed

Each blade of the rotor is presumed to be rigid and rectangular in planform. Coordinate systems which are used to describe the rotor configuration are illustrated in figure 1. The "rotor-axes" coordinates, x_r, y_r, z_r, are oriented such that the x_r-y_r plane is the tip-path plane and the freestream direction is parallel to the x_r-z_r plane. The "flow-axes", x, y, z, are inclined to the rotor-axes by the angle α_r, which is a rotation about y_r, such that the freestream velocity is in the negative x direction. A third system which is fixed to the blade has its origin at the quarter-chord of the mid-span. These "blade-axes", x_b, y_b, z_b, are inclined to the tip-path plane by the coning angle such that z_b coincides with the quarter-chord line.

The momentum equation can be written as

$$\frac{D\vec{V}}{Dt} = \text{grad}\,(-p/\rho)$$

Introducting perturbation quantities $\vec{V}'$ and p' so that $\vec{V} = \vec{U} + \vec{V}'$ and $p = p_\infty + p'$ and using the assumption of small perturbations, it can be shown that the perturbation pressure satisfies the Laplace equation.

$$\nabla^2 p' = 0$$

The complete linearized boundary value problem for the pressure field around the rotor can now be stated:

$$\frac{\partial^2 p'}{\partial x^2} + \frac{\partial^2 p'}{\partial y^2} + \frac{\partial^2 p'}{\partial z^2} = 0 \tag{1}$$

On the blade surface, the pressure gradient in the z direction must attain the value (Appendix A)

$$-\frac{1}{\rho\Omega^2 R_1}\frac{\partial p'}{\partial z} = \frac{x_b}{R_1} F_1\left(\Psi_b, \frac{r_b}{R_1}\right) + F_2(\Psi_b) + \frac{r_b}{R_1} F_3(\Psi_b) \tag{2}$$

such that

$$p' \to 0 \text{ as } (x^2 + y^2 + z^2) \to \infty$$

and

$p' \to -\infty$ along the leading edge such that the velocity component in the z direction along the quarter-chord line is

$$\frac{w}{\Omega R_1} = \left(\frac{w_b}{\Omega R_1}\right)_{x_b = 0} \tag{3}$$

6

The solution to this problem will be divided into a singular part which satisfies $\frac{\partial p'}{\partial z} = 0$ (singular at the leading edge) and a regular part which is non-singular and satisfies the given pressure gradient condition of equation (2).

Singular solution. - In the near field (vicinity of the blade) it is assumed that spanwise variations are characterized by a length of the order of the span while the characteristic length for variations in the other two directions is of the order of the chord. The governing equation for the near field can be written in terms of the nondimensional coordinates

$$x_b^* = x_b/b, \quad y_b^* = y_b/b, \quad z_b^* = z_b/s$$

as

$$\frac{\partial^2 p'}{\partial x_b^{*2}} + \frac{\partial^2 p'}{\partial y_b^{*2}} + \frac{1}{A^2} \frac{\partial^2 p'}{\partial z_b^{*2}} = 0$$

Assuming the near field solution to be described by an asymptotic expansion in inverse powers of the aspect ratio as

$$p'_{near} = p_0 + \frac{1}{A} p_1 + \cdots$$

the lowest order term is found to be a solution of the two-dimensional Laplace equation and can be shown to be

$$p'_{near} = - g(z_b^*, \Psi_b) \frac{\sin \phi}{\cosh \eta + \cos \phi}$$

where (η, ϕ) are elliptic coordinates centered about mid-chord (see fig. 2). The near field solution to $O(A^{-2})$ satisfies the equation

$$\frac{\partial^2 p'_{near}}{\partial \eta^2} + \frac{\partial^2 p'_{near}}{\partial \phi^2} = \frac{1}{A^2} g''(z_b^*, \Psi_b)(\cosh \eta \, \sin \phi - \frac{1}{2} \sin 2\phi)$$

the general solution of this equation is of the form

$$p'_{near}(\eta, \phi, z_b^*, \Psi_b) = - h(z_b^*, \Psi_b) \frac{\sin \phi}{\cosh \eta + \cos \phi} + \sum_{n=1}^{\infty} a_n(z_b^*, \Psi_b) \cosh n\eta \, \sin n\phi$$

$$+ \frac{1}{A^2} g''(z_b^*, \Psi_b)(\frac{1}{2}\eta \, \sinh \eta \, \sin \phi + \frac{1}{8} \sin 2\phi) \qquad (4)$$

In the far field region, the characteristic length may be taken to be of the order of the span in all directions. It is shown in reference 17 that, to $O(A^{-2})$, the far field solution may be represented by a line of dipoles located along the quarter-chord line of the blade.

$$p'_{far} = p_{dip}(r, \chi, z_b, \Psi_b)$$

It is shown in Appendix B that the field of a line of dipoles can be conveniently expressed in terms of prolate spheroidal coordinates (see fig. 3) as

$$P_{dip}(\Psi,\theta,\chi,\Psi_b) = \frac{\sin\chi}{2\pi} \sum_{n=1}^{\infty} A_n(\Psi_b)\, P_n^1(\cos\theta)\, Q_n^1(\cosh\Psi) \tag{5}$$

The near and far field solutions are then matched by requiring that

$$\lim_{\frac{r}{b}\to\infty} P'_{near} = \lim_{\frac{r}{s}\to 0} P'_{far}$$

which ensures that the behavior of the near field solution at distances of the order of the span is like that of the far field solution at distances of the order of the chord. Such a matching is achieved by choosing

$$h(z_b^*,\Psi_b) = g(z_b^*,\Psi_b)$$

$$a_1(z_b^*,\Psi_b) = 2\left[P_{dip}(\Psi',\theta',\chi',\Psi_b) + 2g(z_b^*,\Psi_b) \right]$$

where Ψ', θ', χ' correspond to $r = \frac{b}{2}$, $\chi = \frac{\pi}{2}$, $z_b = z_b$.

$$a_n(z_b^*,\Psi_b) = 0, \quad n \geq 2$$

$$g(z_b^*,\Psi_b) = \frac{A}{2\pi}\sqrt{1 - z_b^{*2}} \sum_{n=1}^{\infty} A_n(\Psi_b)\, P_n^1(z_b^*) \quad .$$

The composite solution for the singular part is obtained as

$$P'_{sing} = (P'_{near})_{sing} + (P'_{far})_{sing} - (P'_{common})_{sing}$$

where

$$P'_{common} = \lim_{\frac{r}{b}\to\infty} P'_{near} = \lim_{\frac{r}{s}\to 0} P'_{far}$$

The complete singular part is then

$$P'_{sing} = P_{dip}(\Psi,\theta,\chi,\Psi_b) + g(z_b^*,\Psi_b)\frac{1}{2A}\frac{\sin\chi}{r/(R_1 - R_0)} - g(z_b^*,\Psi_b)\frac{\sin\phi}{\cosh\eta + \cos\phi}$$

$$+ 2(\cosh\eta\,\sin\phi - \frac{r}{b}\sin\chi)\left[P_{dip}(\Psi',\theta',\chi',\Psi_b) + 2g(z_b^*,\Psi_b) \right]$$

$$+ \frac{d^2 g}{dz_b^{*2}}\frac{1}{2A^2}\left[\eta\,\sinh\eta\,\sin\phi + \frac{1}{4}\sin 2\phi - \frac{r}{b}\sin\chi\,\ln(\frac{2r}{b}) \right] \tag{6}$$

8

<u>Regular solution.</u> -- The regular part of the pressure field must satisfy the following pressure gradient condition.

$$
-\frac{1}{\rho\Omega^2 R_1^2}\left(\frac{\partial p'_{reg}}{\partial\eta}\right)_{\eta=0} = \frac{1}{8A^2}\left(1-\frac{R_0}{R_1}\right)^2 (\sin\phi + \sin 2\phi)\, F_1\left(\Psi_b, \frac{r_b}{R_1}\right)
$$

$$
+ \left(1-\frac{R_0}{R_1}\right)\frac{\sin\phi}{2A}\left[F_2(\Psi_b) + \frac{r_b}{R_1}F_3(\Psi_b)\right]
$$

As observed in the previous section, the near field solution to lowest order is a solution of the two-dimensional Laplace equation which is $O(A^{-1})$. Consideration of the equation for the next higher order only adds terms of $O(A^{-3})$ and can therefore be neglected. It is shown (ref. 17) that the near field regular solution is

$$
\frac{1}{\rho\Omega^2 R_1^2}(p'_{near})_{reg} = \left[F_2(\Psi_b) + \frac{r_b}{R_1}F_3(\Psi_b)\right]\frac{1}{2A}\left(1-\frac{R_0}{R_1}\right)e^{-\eta}\sin\phi
$$

$$
+ F_1\left(\Psi_b, \frac{r_b}{R_1}\right)\frac{1}{8A^2}\left(1-\frac{R_0}{R_1}\right)^2\left[e^{-\eta}\sin\phi + \frac{1}{2}e^{-2\eta}\sin 2\phi\right]
$$

The first term, of $O(A^{-1})$, can be shown to have a far field expansion of $O(A^{-2})$ and hence the second term, of $O(A^{-2})$ need not be considered for the far field. By matching the near and far field solutions and combining them with a common part, it is shown in reference 17 that the complete regular part of the pressure field is given by

$$
\frac{p'_{reg}}{\rho\Omega^2 R_1^2} = \left[F_2(\Psi_b) + \frac{r_b}{R_1}F_3(\Psi_b)\right]\frac{1}{2A}\left(1-\frac{R_0}{R_1}\right)\left[e^{-\eta}\sin\phi - \frac{\sin\chi}{2r/b}\right]
$$

$$
+ F_1\left(\Psi_b, \frac{r_b}{R_1}\right)\frac{1}{8A^2}\left(1-\frac{R_0}{R_1}\right)^2\left[e^{-\eta}\sin\phi + \frac{1}{2}e^{-2\eta}\sin 2\phi\right]
$$

$$
+ \left[F_2(\Psi_b) + \frac{R_0}{R_1}F_3(\Psi_b)\right]\frac{1}{4A^2}\left(1-\frac{R_0}{R_1}\right)\frac{\sin\chi\cosh\Psi\sin\theta}{(\sinh^2\Psi + \sin^2\theta)\sinh\Psi}
$$

$$
+ F_3(\Psi_b)\frac{1}{8A^2}\left(1-\frac{R_0}{R_1}\right)^2\frac{\sin\chi\sin\theta}{(\cosh\Psi-\cos\theta)\sinh\Psi} \tag{7}
$$

The complete solution for the pressure field can now be written as $p' = p'_{sing} + p'_{reg}$, and is completely known except for the function $g(z_b^*, \Psi_b)$ that occurs in the singular part. To determine this function, the transverse pressure gradient on a fluid particle is integrated along a linearized trajectory from far upstream to a point on the rotor disk.

This yields the transverse velocity induced by the pressure field at that point, which can then be set equal to the known transverse velocity on the blade at the same point. Since the unknown function occurs inside the integral, the normal velocity boundary condition leads to an integral equation of the form (eq. A4)

$$\left.\frac{w_b}{\Omega R_1}(r_{bo}, \Psi_{bo})\right|_{x_b = 0} = -\int_{-\infty}^{\Psi_{bo}} \frac{\partial}{\partial\left(\frac{y_b}{R_1}\right)}\left(\frac{p'}{\rho\Omega^2 R_1^2}\right) d\Psi_b \tag{8}$$

The expression for the known velocity on the blade and the form of the linearized trajectory are presented in Appendix A.

Computational Scheme

The standard method of solving the above integral equation (eq. 8) for the unknown function is to assume a collocation function for g (z_b^*, Ψ_b) with a finite number of unknown coefficients and then satisfy the equation at the same number of collocation points to generate a system of equations for the coefficients. Since the unknown depends on both radius and azimuth, it would have to be represented by a finite sum of products of radial modes and azimuthal harmonics. Van Holten (ref. 17) assumes the following form

$$g^*(z_b^*, \Psi_b) = A(1 + z_b^*)\left[A_{00} + \sum_{k=1}^{K}\left\{A_{0k}\cos k\Psi_b + B_{0k}\sin k\Psi_b\right\}\right]$$

$$+ \frac{A}{2\pi}\sqrt{1 - z_b^{*2}}\sum_{n=1}^{N}P_n^1(z_b^*)\left[A_{n0} + \sum_{k=1}^{K}\left\{A_{nk}\cos k\Psi_b + B_{nk}\sin k\Psi_b\right\}\right] \tag{9}$$

This involves a total of $(N+1)(2K+1)$ unknown coefficients. The radial modes are dictated by the result of matching and the fact that the dipole line field has been expressed in prolate spheroidal coordinates. The field of the dipole line now has the form

$$p_{dip}^*(\Psi, \theta, \chi, \Psi_b) = -\frac{\sin\chi\sin\theta}{\sinh\Psi(\cosh\Psi - \cos\theta)}\left[A_{00} + \sum_{k=1}^{K}\left\{A_{0k}\cos k\Psi_b + B_{0k}\sin k\Psi_b\right\}\right]$$

$$+ \frac{\sin\chi}{2\pi}\sum_{n=1}^{N}P_n^1(\cos\theta)Q_n^1(\cosh\Psi)\left[A_{n0} + \sum_{k=1}^{K}\left\{A_{nk}\cos k\Psi_b + B_{nk}\sin k\Psi_b\right\}\right] \tag{10}$$

The first term of the collocation function has been used to represent the contribution of the regular part of the solution to the far field.

The pressure field of the dipole line given by equation (10) can be substituted into the

10

boundary condition of equation (8). The resulting integral equation is then evaluated at each of the collocation points which are located at r_{br}, Ψ_{bs}. The collocation indicies r and s are respectively associated with the radial modes and azimuthal harmonics. The result is a system of linear simultaneous equations for the unknown coefficients that can be written symbolically in the form.

$$\frac{w_b}{\Omega R_1}(r_{br},\Psi_{bs}) - w_{rs}^* = w_{rs,oo}^* A_{00} + \sum_{k=1}^{K}\left[w_{rs,okc}^* A_{0k} + w_{rs,oks}^* B_{0k}\right]$$

$$+ \sum_{n=1}^{N}\left[w_{rs,no}^* A_{n0} + \sum_{k=1}^{K}\left\{w_{rs,nkc}^* A_{nk} + w_{rs,nks}^* B_{nk}\right\}\right] \qquad (11)$$

Since $1 \le r \le (N+1)$ and $1 \le s \le (2K+1)$, there are $(N+1)(2K+1)$ such equations, representing the boundary condition applied at that many points on the rotor disk, to solve for the same number of coefficients.

Each of the starred quantities represents an azimuthwise integral, from $-\infty$ to Ψ_{bs}, of the function associated with the corresponding A_{ij} or B_{ij}. Since the pressure field also contains terms that are completely specified by the regular part of the solution, the integral contribution of these terms appears as w_{rs}^*. The first term of equation (11) is the specified normal velocity on the blade due to the blade motion. The starred terms may be considered to be influence coefficients since they represent the contributions to the induced velocity of those portions of the pressure field corresponding to a unit value of their associated coefficients.

Mention must be made of the behavior of the integrands in the azimuthwise integrations. The field of the dipole line becomes singular at its origin, namely, the quarter-chord line of the blade. However, this singularity is cancelled out by an equal and opposite one in the common part, leaving only the near field solution in the vicinity of the blade. Further, the near field solution itself has a singularity at the leading edge of the blade, of the thin airfoil type (square root). This singularity is integrable and is evaluated by numerical integration up to a point close to the leading edge and replacing the remainder of the integral with a simplified analytical expression. Complete expressions for the starred integral coefficients are written out in Appendix C, for a single blade. For the case of a multi-bladed rotor, the computation is simply repeated successively for the pressure fields of the other blades by assuming that the pressure field of each blade to be identical in form but shifted appropriately in azimuth dependence relative to the reference blade.

The integrands also require the computation of associated Legendre functions of the first and second kind, $P_n^m(x)$ and $Q_n^m(x)$. Both may be computed by using the recursive relations for solutions of the associated Legendre equations. However, the function of the second kind decreases rapidly with an increase in the argument and, beyond a certain range, use of the recursive relations leads to an unacceptable loss of significant figures. In this range of the argument, the functions are computed using asymptotic expansions. The scheme of computation used for these functions and explicit expressions for some of them are given in Appendix D.

The numerical integration utilizes the Gauss-Chebyshev scheme by dividing the entire

azimuth interval into sub-intervals of size $\Delta \Psi_b$ and applying the rule over each.

$$\int_{\Psi_{b1}}^{\Psi_{b2}} f(\Psi_b) \, d\Psi_b = \frac{\pi}{N_I} \sum_{i=1}^{N_I} a_i \, f(\Psi_{bi})$$

where

$$x_1 = (\Psi_{b1} + \Psi_{b2})/2$$

$$x_2 = (\Psi_{b2} - \Psi_{b1})/2$$

$$\Psi_{bi} = x_1 + x_2 \cos\left[(2i-1)\pi/2N_I\right]$$

$$a_i = \sqrt{(\Psi_{bi} - \Psi_{b1})(\Psi_{b2} - \Psi_{bi})}$$

Although the integration is supposed to begin at an infinite distance upstream, the computations are begun at a position where the fluid particle is about three rotor radii upstream of the collocation point. In accordance with the form chosen for the collocation function, $(N+1)$ points are chosen along the blade span at each of $(2K+1)$ azimuth locations.

The input required for the computation can be classified under the following headings.

(1)   Blade geometry: root radius, aspect ratio, number of blades, linear twist

(2)   Flight condition: forward speed, inclination of tip path plane to flight path

(3) · Blade motion: collective pitch angle at the root, coning angle, cyclic pitch coefficients in the tip path plane (or, equivalently, flapping coefficients in the control plane)

Due to the assumption of linearized potential flow, it may be expected that computed airloads would differ from measured airloads because of differences in the lift curve slope. Neither can the computed loads be expected to satisfy flapping equilibrium about the hinge, as measured loads would. Since the solution features that are of primary interest are the variations (chordwise, spanwise and azimuthwise), the use of specified blade motion parameters (taken from experimental measurements) would only obscure the comparison of predicted variations with measured values. For this reason, it is better to consider the blade motion parameters as unknowns and solve for them using appropriate additional equations. If only first harmonic pitch and flapping are retained, then the additional unknowns are four in number: collective pitch, coning angle and the two first harmonic flapping coefficients. The four extra equations are:

(1)   Average value of total blade lift x number of blades = given rotor thrust

(2) to (4)   Moment equilibrium of a rigid blade about the flapping hinge (constant, first harmonic cosine and sine components). For the flapping hinge on the rotor hub, the constant component is determined by the blade inertia (Lock number), while the first harmonic components are both zero.

This procedure is used in all the computations of this investigation. The final equations are presented in Appendix E. The augmented set of equations, $(N+1)(2K+1) + 4$

in number, are solved simultaneously for the (N+1) (2K+1) unknown coefficients in the pressure solution and the four blade motion parameters. With the pressure solution completely known, auxiliary quantities such as sectional lift, sectional pitching moment, sectional center of pressure, total blade lift, aerodynamic moment about the hub and center of the sectional lift distribution can be readily computed. Expressions for these quantities are also given in Appendix E.

Other Methods Used for Comparison

Wilmer's method. - This method (ref. 6) is an attempt to extend the Prandtl lifting line model to rotary wings. The blade is modeled by a lifting line along the quarter-chord. The azimuthal variation of the bound circulation is assumed to be quasi-steady, so that the wake consists of only trailing vorticity. That part of the wake immediately behind the blade is modeled by a plane, semi-infinite trailing vortex sheet so that the velocity induced by this sheet is obtained from simple lifting line theory for fixed wings. The rest of the helical wake is replaced by a series of infinite, plane vortex sheets under the blade. The induced velocity contribution of each layer is given by a spanwise integral that can be evaluated by either simple numerical integration or the theorem of residues. The distribution of bound circulation can then be determined by a collocation method. The entire computation is simple and fast. The solution may be expected to be bad near the downstream edge of the disk where the wake curvature is large, thus the assumption of plane wakes is not valid.

Actuator disk approach. - This model can be formulated by starting with a lifting line for the blade and rigid helical sheets for the wake. The induced velocity contribution of the wake from a blade at any field point will then be given by an integral, the result of which depends on the coordinates of the field point and the azimuth position of the blade (ref. 2). The simplification consists of averaging this result over the azimuth, which is equivalent to considering the single blade (or finite number of blades) to be spread out over an infinite number of blades, each carrying an infinitesimal load. The discrete helical wake is also averaged, becoming a skewed, semi-infinite cylinder filled with vorticity. Since the wake is a surface of velocity potential discontinuity, a disk section of the wake cylinder is replaced by a disk of flow doublets. The induced velocity contribution of this disk is integrated over the length of the cylinder to obtain the total wake effect. The computational scheme for this model, as described in reference 2, reduces the calculation to a series of simple operations, through the use of special functions and integral representations. The basic assumptions of the actuator disk approach may be expected to be less acceptable at low forward speeds where a discrete, distorted wake representation is necessary.

Segmented vortex wake method. - This approach also starts with a lifting line model for the blade and a wake representation as a helical sheet. The simplification consists of discretizing the continuous variation of flow quantities on the blade and in the wake. The bound circulation distribution on the blade is approximated by a stepped variation which, in turn, leads to a trailing wake made up of a finite number of line vortices each carrying a finite circulation. The continuous rotation of the blade is also discretized into impulsive movement between a finite number of azimuth stations. This leads to a shed wake consisting of a finite number of shed line vortices carrying finite shed circulation. The result is that the continuous wake sheet is replaced by a vortex lattice of straight line segments, streamwise and radial. The induced velocity contribution of each segment is known directly as a function of its position relative to the blade. The total wake effect is then obtained by a finite summation so that the computational scheme is quickly executed.

The disadvantage of such a model, as it stands, is that unsteady effects are not adequately represented without a large number of azimuth steps. On the other hand, the approach has the advantage that wake distortions can be handled readily so that it may be used either for an iterative calculation of a distorted wake or to accommodate a prescribed, distorted wake from experimental observation.

For all the methods considered for comparison, the blade motion parameters are considered unknown and solved for in the same way as in the computational scheme for the asymptotic method.

RESULTS OF THE STUDY

Analytical Study

In the course of developing a solution for the pressure field of a rotor blade in forward flight, Van Holten (ref. 17) considers some simpler flow problems. The first is an application of the acceleration potential for the analysis of steady flow past a two-dimensional thin airfoil for which the classical solution is obtained. Next the acceleration potential formulation, together with the matched asymptotic expansion technique, is applied to the problem of steady flow past a straight, rectangular wing, for which solutions to $O(1/A)$ and $O(1/A^2)$ are obtained. Van Holten shows that the solution to $O(1/A)$ is identical with Prandtl's lifting line solution while the solution to $O(1/A^2)$ is identical with the extended lifting line solution of Weissinger (ref. 18).

In the current study, the acceleration potential method has been applied to the problem of a two-dimensional thin airfoil with oscillatory downwash, as described in Appendix F. Particular solutions were obtained for two cases: an airfoil in harmonic pitching and heaving motion, and a stationary airfoil with a harmonic vertical gust superimposed on the steady stream. These solutions are identical with the results of the velocity potential formulation. This is to be expected since the velocity and acceleration potential approaches are completely equivalent under the assumption of small disturbances. However, the exercise presented in Appendix F does verify the expressions and procedure used for the unsteady problem.

The method was also applied to the problem of a straight, rectangular wing with oscillatory downwash, as described in Appendix G. The result of the analysis is an integral equation for the spanwise variation of the sectional lift distribution, correct to $O(1/A)$. An equivalent analysis has been presented by Reissner (ref. 19), based on a vorticity distribution, the result of which is an integral equation for the bound circulation. Numerically calculated lift distributions from the asymptotic method are compared with Reissner's results for the harmonically pitching wings presented in reference 20. There is good agreement between the two sets of results.

These two exercises represent an extension of Van Holten's analysis to the case of oscillatory downwash, and the results confirm the validity of the formulation and the detailed expressions used. It must be mentioned that, in the case of the finite wing, the reduced frequency of oscillation is assumed to be of $O(1)$. Van Holten further applies the pressure method to the case of a harmonically pitching wing in yawed flow and points out the approximation involved in using a simple cosine sweep correction.

The formulation of reference 17 for a rotor blade would therefore seem to be applicable to the unsteady, three-dimensional, yawed flow environment of a helicopter rotor blade in forward flight, correct to $O(1/A^2)$, under the restrictions of incompressible,

14

potential flow and small disturbances in flow velocity relative to forward speed. However, the results of such an analysis would be applicable to the rotor blade only to the extent that the blade flow environment is itself within the above restrictions. The assumption of small disturbances implies that the wake of the blade has a rigid helical shape with all its elements being convected with the stream velocity relative to the blade. For this to be acceptable, the freestream component of the rotor through-flow must be much greater than the rotor-induced component. Under conditions of low inflow, which occur at low forward speeds and low thrust, the wake is distorted from the helical shape by interaction with the reference blade and the following ones, and also by self-interaction between the wake elements. It may be expected that linearized theory will begin to break down when these conditions are approached.

The following factors can also have an influence on the rotor flow field.

(1)   The rapid roll-up of the vortex sheet near the blade tip can form a strong, concentrated vortex tube. While the wake of a fixed wing also rolls up at some distance behind the wing, the greater concentration of load near the tip of a helicopter blade causes the roll-up to be very rapid. In turn, the tip vortex influences the flow near the blade tip and also has an influence on the following blade, if it should pass close to it.

(2)   The combination of forward speed and rotational motion can lead to a region of reversed flow on the retreating side of the blade. It may be noted that this region grows with increasing forward speed.

(3)   Blade pitch angles are varied over the azimuth in such a way that they are larger on the retreating side, especially near the root for twisted blades. This can lead to conditions of dynamic stall which, like reversed flow, can only be accounted for empirically at present.

(4)   The superposition of forward and rotational motion also leads to a component of flow along the blade span, which can influence the sectional properties through its effect on the boundary layer. This radial flow is strongest along the fore-and-aft diameter of the disk and increases with advance ratio. It has been observed that linear theory computations, even under otherwise favorable conditions, are worst at the 0° and 180° azimuth positions (ref. 13), which may be at least partly due to this effect.

(5)   At high blade section Mach numbers, compressibility effects and the possibilities of local shock formation have to be considered.

In view of the above discussion, it would appear that any linear theory, such as the asymptotic approach, would be applicable only in a restricted range of flight conditions. This range of validity can be made more precise only by comparison with appropriate experimental measurements.

Comparison with Experiment and Other Methods

To evaluate the computational results obtained from the asymptotic method, conditions from the following experimental investigations were analyzed. (See Table I for specific geometric and flight conditions.)

Case 1: A two-bladed, teetering, model rotor of aspect ratio 5.4 with untwisted, constant chord blades was tested in a wind tunnel at advance ratios, μ, of 0.08, 0.15 and 0.29. Results for this experiment are presented in reference 21.

Case 2: A four-bladed, articulated, full-scale rotor of aspect ratio 17.2 with twisted blades was tested in flight at advance ratios of 0.06, 0.13 and 0.29. The experimental results are tabulated in reference 22.

Case 3: The four-bladed rotor of Case 2 was also tested in a wind tunnel at advance ratios of 0.29, 0.39 and 0.45. These results are presented in reference 23.

TABLE I. - GEOMETRIC AND FLIGHT CONDITIONS FOR THE
EXPERIMENTAL CASES

Case	Aspect ratio, A	Number of blades, B	Root Ratio, R_0/R_1	Linear twist, ϵ, deg.	Rotor angle, α_r, deg.	Thrust coefficient, C_T	Lock number, γ	Advance Ratio, μ	Wake Spacing, $\dfrac{2\pi w_r}{\Omega B R_1}$
1	5.4	2	0.17	0	0	0.00367	-	0.08	0.069
(ref.21)					2.0	0.00482	-	0.15	0.067
					6.7	0.00394	-	0.29	0.128
2	17.2	4	0.16	8	0	0.00499	11.4	0.06	0.055
(ref. 22)					0.6	0.00501	11.4	0.13	0.032
					6.1	0.00571	9.6	0.29	0.064
3	17.2	4	0.16	8	5.0	0.00357	10.0	0.29	0.049
(ref. 23)					4.0	0.00366	9.9	0.39	0.050
					4.8	0.00334	10.1	0.45	0.065

These cases were also analyzed using Willmer's method, the actuator disk method and the segmented vortex wake (SVW) method. In all of the computations, it was assumed that a fluid element is convected normal to the disk with the sum of the freestream inflow component and a constant thrust-induced velocity, determined from simple momentum relations. It was also assumed that the rigid blade motion parameters (collective pitch, coning angle and cyclic pitch) are unknown. The results presented here include the azimuthwise variation of total blade lift, spanwise variation of sectional lift and chordwise variation of surface pressure differential.

Results for the two-bladed, teetering, model rotor (Case 1) are presented in figures 5 to 11. The total blade lift (see fig. 5) for advance ratios of 0.08 and 0.15 from the asymptotic and SVW methods are quite similar and agree fairly well with the measured data. For the advance ratio of 0.29 the two methods yield different results and neither compares well with the experimental lift. The actuator disk method yields fair agreement with the measured data at the higher advance ratios of 0.15 and 0.29 but shows marked deviations at 0.08. Willmer's method shows the poorest correlation with the measured values. This disagreement appears to increase as the advance ratio is decreased. In summary, the asymptotic method provides the most consistent results for Case 1 except for the advancing blade ($0^\circ \leq \Psi_b \leq 180^\circ$) at an advance ratio of 0.29. This deviation has been reduced by decreasing the number of azimuthal harmonics and will be discussed later.

The spanwise distributions of sectional lift are shown in figures 6 to 8 for all three advance ratios at intervals of 30° in azimuth. For clarity, only the results of the asymptotic method are shown for comparison. Whenever the experimental curves are smooth, the computed values have nearly the same shape, except near the tip. At some azimuth locations, the measured curves exhibit sharp variations that are not illustrated by the computed load. These kinks are probably due to a close encounter with the tip vortex from the preceding blade, especially since they generally occur near the extreme advancing and retreating blade positions and are most predominant at the lowest advance ratio of 0.08.

The chordwise variation of surface pressure differential is shown in figures 9 to 11 for the advance ratio of 0.29 at radial stations, $r/R_1 = 0.75, 0.85, 0.95$, and azimuthal intervals of 45°. The measured variations are seen to be fairly smooth throughout, with the same general shape as a two-dimensional distribution of the asymptotic method. Computed results are not corrected for the leading edge singularity but agree with the measured data.

Flight-test results for the four-bladed, articulated, full-scale rotor (Case 2) are presented in figures 12 to 18. None of the Case 2 results from Willmer's method are presented, because they differed from the measured data by nearly an order of magnitude. The total blade lift for the advance ratio of 0.06 (see fig. 12(a)) as predicted by the other three methods shows significant disagreement with the experimental results. This can be attributed to the low advance ratio for which the actuator disk method loses its validity and the small value of wake spacing. The wake spacing as listed in Table I was computed from the total inflow velocity, w_r, which is the sum of the freestream inflow and the thrust-induced inflow. At this condition of small wake spacing it can be anticipated that the effects of wake distortion have caused the asymptotic and SVW methods to yield poor results. These effects could also be the reason for the complete failure of Willmer's method. As the advance ratio is increased to 0.13 (see fig. 12(b)) both the disk and SVW methods yield better correlation except for the downstream portion of the rotor disk from 300° to 360° and 0° to 90°. To obtain the asymptotic results for this case of very small wake spacing it was necessary to reduce the integration interval from $\Delta\Psi = 0.3$ (as used for the preceding test conditions) to $\Delta\Psi = 0.1$. Even with this refinement it is apparent that the correlation with the measured data is unacceptable. It can therefore be concluded that the

asymptotic method yields unreliable results when the successive wake spacing is less than five percent of the blade radius. At the highest advance ratio of 0.29 (see fig. 12(c)) all three methods provide consistent results for the retreating blade portion of the rotor disk, and their correlation with experiment may be considered fair. For the advancing blade all methods yield different results and none is close to the measured lift. As previously mentioned for Case 1, the asymptotic results for the advancing blade can be improved by decreasing the number of azimuthal harmonics and will be discussed later.

The results for the spanwise lift distributions which are presented in figures 13 to 15 show the same trends as for the two-bladed configuration of Case 1. The experimental curves show sharp variations in the neighborhood of 90° and 270° azimuth. As before, these are probably due to tip vortex encounters, which have been discussed in detail by Scheiman and Ludi in reference 24.

The measured chordwise distributions of figures 16 to 18 for the advance ratio of 0.29 have an approximately normal appearance at $r/R_1 = 0.75$ and 0.85, and correlation with the computed values is about the same as for the two-bladed rotor of Case 1. At $r/R_1 = 0.95$, however, the measured data show abrupt variations, again around the 90° azimuth position, which are not apparent in the computed points. It may be mentioned here that measured chordwise distributions have been compared with static two-dimensional data (from wind tunnel tests) for this rotor in reference 25. That comparison indicates that the measured data have a two-dimensional appearance over most of the disk.

Wind-tunnel results for the four-bladed, articulated, full-scale rotor (Case 3) are presented in figure 19. As for Case 2 none of the results from Willmer's method are included due to the poor correlation with test data. Both the actuator disk and SVW methods yield comparable results and agree fairly well with the experimental data at all three advance ratios except for the downstream portion of the rotor disk (320° to 360° and 0° to 90°) at $\mu = 0.45$. All asymptotic results are based on the reduced integration interval of 0.1. This method shows acceptable agreement for the advance ratios of 0.29 and 0.45 except again for the downstream portion of the disk at $\mu = 0.45$. For the advance ratio of 0.39 the asymptotic method yields unacceptable results. It will be seen later that the correlation for this condition is significantly improved by decreasing the number of azimuthal harmonics.

In summary it may be noted that all methods of analysis provide less than desirable comparisons for all three Cases at the highest advance ratios for the downstream portion of the rotor disk. It is likely that at high advance ratios the downstream portion of the disk can be affected by blade root vorticies and the wake of the hub and other fittings. Since none of these methods include these effects, such discrepancies should be anticipated. It can also be noted that the asymptotic method acknowledges a continuous wake, while the SVW and actuator disk methods correspond to lumped and averaged wake representations respectively. For this reason the sensitivity of each method to wake distortions may be expected to be different.

It is seen that Willmer's method is most sensitive to low inflow conditions. For wake spacing less than approximately 0.06 the results are unacceptable. The segmented vortex wake method seems to be less sensitive to these conditions than the asymptotic method and this feature could be a consequence of the discretized nature of the method. The actuator disk method is not sensitive to inflow conditions since instantaneous wake effects are averaged out; however, the results indicate a limit of acceptability in terms of advance ratio, below which the total lift is unsatisfactory. This lower limit appears to be approximately 0.1. Ormiston (ref. 27) observed a similar limit for the actuator disk method to be around 0.15.

In the context of these comparisons, it should be noted that a similar study was made by Hille in reference 26 for Case 2 at an advance ratio 0.13. The blade was represented by a lifting line along the quarter chord, and the boundary condition was satisfied along the three-quarter chord line. The method used a continuous vortex wake trailed from the instantaneous flapped position of the blade. In spite of refinements such as using a linear variation across the disk for the thrust-induced component of the total inflow velocity, it is noted that the comparison is not satisfactory.

Use of Measured Section Characteristics

The possibility of using measured airfoil section properties in the asymptotic method is discussed by Van Holten in reference 28. Since the near field asymptotic solution, to lowest order, is that for the pressure field of a two-dimensional airfoil, it would seem possible to introduce measured characteristics in this part of the solution, to achieve better correlation with measurements. However, a part of the near field solution, the function $g(z_b, \Psi_b)$ is undetermined by itself. It is determined only by combining the near field, far field and common part to form a composite solution. It is then made determinate by applying an essentially three-dimensional boundary condition, namely, integrating the pressure gradient on a fluid particle as it travels along a helical trajectory. For a complete two-dimensional correspondence, the path relative to the blade should be a straight line from an infinite distance upstream, as in flow past a fixed wing.

Section characteristics are measured on a two-dimensional airfoil in a wind tunnel, with the airfoil being given a pitching and/or heaving transverse motion. The form of the boundary condition for a rotor blade section (Appendix B) shows that not all of the terms can be simulated in this way. The direct use of wind tunnel data in the form of empirical factors in the asymptotic approach requires careful consideration of these boundary conditions.

Computational Study

As previously discussed, the unknown function in the pressure solution, $g(z_b, \Psi_b)$, is determined by using a collocation technique which includes a sum of functions, each being the product of a radial mode and an azimuthal harmonic, multiplied by a constant coefficient. With this representation, the solution requires the determination of these coefficients by forming a system of linear equations to be solved simultaneously. If five radial modes and five azimuthal harmonics are used, as was the case for all the computations previously discussed, there are a total of 55 unknown coefficients and the system of equations has a matrix of size (55 x 55). Since the determination of each coefficient matrix element involves an azimuthwise numerical integration, the total computational time is determined primarily by the time required to set up each coefficient element and the number of such elements involved. The collocation form determines the latter while the efficiency of numerical integration decides the former. To study the efficiency of the computational scheme, it was decided to vary both of these factors.

The numerical integration uses a five-point Gaussian formula over an azimuthal sub-interval, $\Delta \Psi$. For the previous computations this interval size was chosen to be 0.3 (rad) for all of Case 1 and for advance ratios of 0.06 and 0.29 for Case 2. The other conditions all required $\Delta \Psi = 0.1$. The computation time increases threefold with a reduction in $\Delta \Psi$ by the same factor. Other conditions studied with $\Delta \Psi = 0.1$ were Cases 1 and 2 at an advance ratio of 0.29. The results are illustrated in figures 20 and 21 from which it can be seen that the

refinement makes no significant difference in the total lift at these conditions. In an effort to improve the poor correlation of the asymptotic method for Case 3 at the advance ratio of 0.39, the integration interval was reduced from 0.1 to 0.05. The resulting lift as a function of azimuth angle showed no significant improvement as illustrated in figure 22.

The number of radial modes was increased from 5 to 10. This doubles the number of unknown coefficients and approximately quadruples the computation time. This modification was also only applied to Cases 1 and 2 with $\mu = 0.29$. For Case 1 the results were only marginally different. However, for Case 2, the results were unacceptable which may be an indication that, when the method is applied near its limit of validity, an increase in the number of radial modes may make the computational scheme unstable. Reducing the number of modes to four led to unsatisfactory results in some cases where the five mode computation had yielded acceptable results. It would therefore seem advisable to set the number of radial modes at five.

Varying the number of azimuthal harmonics does not seem to affect the solution as much as the number of radial modes. Computation with five modes and three harmonics for the conditions of Cases 1 and 2 showed that in most cases there was no significant difference from the five and five computation. In fact, for the advance ratio of 0.29 in Cases 1 and 2, the five and three computation led to significantly better results, as can be seen in figures 20 and 21. The correlation with the measured data is greatly improved for the advancing blade with the five and three computation. The reason for this improvement is not clear. It is possible that a method based on linear theory is not well suited to the calculation of higher harmonic variations so that it is better to neglect them altogether than to include them and miscalculate their contributions. The five mode and three harmonic representation was also used for Case 3 at the advance ratio of 0.39. This resulted in a most dramatic improvement as illustrated in figure 22. Based on this limited study, a computational scheme based on five radial modes and three azimuthal harmonics would appear to be an optimum compromise between accuracy and computational expense.

The computer program has been checked out and found to be free from programming errors although it could possibly be made more efficient with respect to computer time. As it stands, for the two-bladed rotor at an advance ratio of 0.29, with the five and three scheme, the program requires about 1.5 minutes to execute on the CDC Cyber 70 Model 74-28 computer. For different conditions, this time would scale approximately in direct proportion to the number of blades and in inverse proportion to the advance ratio. As a comparison of computation times, it may be noted that the asymptotic computation scheme with five radial modes and three azimuthal harmonics required approximately six times as much execution time as the segmented vortex wake scheme with five spanwise and twelve azimuthwise segments. The accuracy of the results was comparable for these two schemes. However, the computation time depends strongly on the size of the system of equations involved in the method. As an example, the computation times for these two schemes would be about the same if the vortex wake method used nine spanwise and sixteen azimuthwise segments.

CONCLUDING REMARKS

The combination of the acceleration potential formulation with the matched asymptotic expansion technique leads to a systematic determination of airloads on a helicopter rotor in forward flight. For a straight wing in steady flow, the method reduces to the simple lifting line solution of Prandtl or the extended lifting line solution of Weissinger, depending on the asymptotic order of terms retained. Numerical results for a straight wing in oscillatory motion compare well with results from Reissner's unsteady lifting line theory.

Under the assumptions of incompressible, potential flow with small disturbances, the asymptotic method appears valid for application to a helicopter rotor blade in forward flight. However, the rotor flow field is significantly influenced by nonlinear and real fluid effects such as wake distortion, vortex sheet roll-up, reverse flow, dynamic stall, radial flow, finite vortex core radius etc. In any linear, potential flow analysis, these factors are beyond the scope of the basic assumptions and may be expected to cause deviations between computed results and measurements.

The asymptotic scheme was used to compute airloads for comparison with experimental results corresponding to a two-bladed, teetering model rotor of medium aspect ratio and a four-bladed, articulated full-scale rotor of large aspect ratio. In general, the computed results were acceptable for those cases involving a successive wake spacing greater than five percent of the blade radius. Discrepancies at closer wake spacings (lower inflow) are to be expected from any linear, potential flow analysis.

A collocation scheme for the asymptotic method of five radial modes and three azimuthal harmonics appears to be an optimum compromise between accuracy and computational expense.

For further comparison, the same cases were also computed using other approximate methods. Willmer's method was unacceptable for all cases involving the four-bladed rotor. The actuator disk approximation showed no sensitivity to inflow and led to fairly acceptable results except at advance ratios below 0.1. A method based on a lifting line with a rigid, segmented vortex wake compared well with the asymptotic method and showed lesser sensitivity to low inflow conditions.

The near field solution for the rotor blade, to lowest order, involves the solution of a two-dimensional Laplace equation and therefore has the capability of using measured airfoil characteristics. However, the form of the boundary condition on the blade is essentially three-dimensional, and the use of measurements made on two-dimensional wind tunnel models requires careful consideration of these boundary conditions.

A comparison of computational times between the asymptotic method and the segmented vortex wake model indicated that the asymptotic approach required approximately six times as much execution time as the vortex model. This comparison was for comparable accuracies. It should be noted that for both techniques the execution time is highly dependent on the number of radial and azimuthal collocation parameters.

APPENDIX A

ROTOR BLADE BOUNDARY CONDITION

Each blade of the rotor is presumed to be rigid, uncambered and rectangular in planform with linear twist. Coordinate systems which are used to describe the rotor configuration are illustrated in figure 1. The "rotor-axes" coordinates, x_r, y_r, z_r, are oriented such that the x_r-y_r plane is the tip-path plane and the freestream direction is parallel to the x_r-z_r plane. The "flow-axes", x, y, z, are inclined to the rotor-axes by the angle α_r, which is a rotation about y_r, such that the freestream velocity is in the negative x direction. A third system which is fixed to the blade has its origin at the quarter-chord of the mid-span. These "blade-axes", x_b, y_b, z_b, are inclined to the tip-path plane by the coning angle, a_o, such that z_b coincides with the quarter-chord line. The rotor angular velocity is assumed constant. In the blade axes system a general point on the blade is given by

$$y_b = \{\theta_r - \epsilon(r_b - R_0)/(R_1 - R_0)\} \, x_b$$

where θ_r is the pitch angle at the root, relative to the x_b-z_b plane. The total twist, ϵ, is positive for section incidence decreasing toward the blade tip. The flapping angle is

$$\beta = a_o - a_1 \cos \Psi_b - b_1 \sin \Psi_b$$

so that the root pitch angle is given by

$$\theta_r = \theta_o + b_1 \cos \Psi_b - a_1 \sin \Psi_b$$

Consistent with linearized theory, small angle assumptions are made so that a point on the blade surface is given by

$$x = -r_b \cos \Psi_b - x_b \sin \Psi_b$$

$$y = -x_b \cos \Psi_b + r_b \sin \Psi_b$$

$$z = \{\theta_o - \epsilon(r_b - R_0)/(R_1 - R_0)\} \, x_b - (r_b - R_1) a_o$$

$$+ x \alpha_r + (b_1 x_b) \cos \Psi_b - (a_1 x_b) \sin \Psi_b$$

The velocity components at this point are given by

$$u = \frac{Dx}{Dt} = -(\Omega x_b + \dot{r}_b) \cos \Psi_b + (\Omega r_b - \dot{x}_b) \sin \Psi_b$$

22

$$v = \frac{Dy}{Dt} = (\Omega r_b - \dot{x}_b) \cos \Psi_b + (\Omega x_b + \dot{r}_b) \sin \Psi_b$$

$$w = \frac{Dz}{Dt} = -\Omega b_1 x_b \sin \Psi_b - \Omega a_1 x_b \cos \Psi_b + \dot{x}_b \{\theta_o - \epsilon(r_b - R_0)/(R_1 - R_0)$$

$$+ b_1 \cos \Psi_b - a_1 \sin \Psi_b\} + \dot{r}_b \{-\epsilon x_b/(R_1 - R_0) - a_o\} - U \alpha_r$$

Assuming $u = U + u'$, $v = v'$, $w = w'$, the quantities $\dot{x}_b$ and $\dot{r}_b$ can be determined as

$$\dot{x}_b = \Omega r_b + U \sin \Psi_b - v' \cos \Psi_b - u' \sin \Psi_b$$

$$\dot{r}_b = U \cos \Psi_b - \Omega x_b - u' \cos \Psi_b + v' \sin \Psi_b$$

Substituting these values into the expression for w, linearizing and setting $\mu = U/\Omega R_1$, the normal velocity of a point on the quarter-chord line is obtained as

$$(w_b/\Omega R_1)_{x_b = o} = \left[\{\theta_o - \epsilon(r_b - R_0)/(R_1 - R_0)\} r_b/R_1 - \mu\alpha_r - \mu a_1/2\right]$$

$$+ \left[b_1 r_b/R_1 - \mu a_o\right] \cos \Psi_b + \left[-a_1 r_b/R_1\right.$$

$$+ \mu\{\theta_o - \epsilon(r_b - R_0)/(R_1 - R_0)\}\bigg] \sin \Psi_b$$

$$+ \left[\mu a_1/2\right] \cos 2\Psi_b + \left[\mu b_1/2\right] \sin 2\Psi_b \tag{A1}$$

It has been assumed in the foregoing that the rotor incidence, α_r, and the coning angle, a_o, are small.

It can similarly be shown that the normal acceleration of a fluid particle on the blade is given by

$$\frac{1}{\Omega^2 R_1} \frac{Dw_b}{Dt} = F_1(\Psi_b, r_b/R_1) x_b/R_1 + F_2(\Psi_b) + F_3(\Psi_b) \dot{r}_b/R_1 \tag{A2}$$

where

$$F_1(\Psi_b, r_b/R_1) = -\theta_o - \epsilon\, R_0/(R_1 - R_0) + 4\epsilon\,(r_b/R_1)\left[R_1/(R_1 - R_0)\right]$$

$$-2b_1 \cos\,\Psi_b + \left[2a_1 + 4\,\mu\epsilon\,R_1/(R_1 - R_0)\right]\sin\,\Psi_b$$

$$F_2(\Psi_b) = \left[2\mu\theta_o + 2\,\mu\epsilon R_0/(R_1 - R_0)\right]\cos\,\Psi_b + 2\,\mu a_o \sin\,\Psi_b$$

$$+ 2\,\mu b_1 \cos 2\,\Psi_b + \left[-2\,\mu a_1 - \mu^2\epsilon\,R_1/(R_1 - R_0)\right]\sin 2\,\Psi_b$$

$$F_3(\Psi_b) = a_o + \left[-2a_1 - 4\,\mu\epsilon\,R_1/(R_1 - R_0)\right]\cos\,\Psi_b - 2b_1 \sin\,\Psi_b$$

With $\dfrac{\partial}{\partial y_b} \approx \dfrac{\partial}{\partial z}$, the solution for the pressure field must be obtained such that the normal pressure gradient on the blade surface balances the normal fluid acceleration. This yields

$$-\frac{1}{\rho\Omega^2 R_1}\,\frac{\partial p'}{\partial z} = F_1(\Psi_b, r_b/R_1)\,x_b/R_1 + F_2(\Psi_b) + F_3(\Psi_b)\,r_b/R_1 \qquad (A3)$$

Further, the normal velocity boundary condition at the quarter chord must be satisfied by integrating the normal pressure gradient along the linearized trajectory up to the reference point. A point (x_o, y_o, z_o) on the quarter-chord of the blade at time $t_o = \Psi_{bo}/\Omega$ is given by

$$x_o/R_1 = -(r_{bo}/R_1)\cos\,\Psi_{bo}$$

$$y_o/R_1 = (r_{bo}/R_1)\sin\,\Psi_{bo}$$

$$z_o/R_1 = a_o(1 - r_{bo}/R_1) - \alpha_r(r_{bo}/R_1)\cos\,\Psi_{bo}$$

The linearized trajectory in the flow axes system is given by

$$x(t) = x_o - U(t - t_o)$$

$$y(t) = y_o$$

$$z(t) = z_o$$

24

and, in the blade axes system, by

$$x_b/R_1 = (r_{bo}/R_1) \sin(\Psi_b - \Psi_{bo}) + \mu(\Psi_b - \Psi_{bo}) \sin \Psi_b$$

$$y_b/R_1 = \mu(\alpha_r + a_o \cos \Psi_b)(\Psi_b - \Psi_{bo}) + a_o(r_{bo}/R_1)\left[\cos(\Psi_b - \Psi_{bo}) - 1\right]$$

$$z_b/R_1 = -(R_0 + R_1)/(2R_1) + \mu(\Psi_b - \Psi_{bo}) \cos \Psi_b + (r_{bo}/R_1) \cos(\Psi_b - \Psi_{bo})$$

The normal velocity boundary condition at the quarter-chord of the blade is then written as

$$\frac{w_b}{\Omega R_1}(r_{bo}, \Psi_{bo}) = -\int_{-\infty}^{\Psi_{bo}} \frac{\partial}{\partial\left(\frac{y_b}{R_1}\right)}\left(\frac{p}{\rho\Omega^2 R_1^2}\right) d\Psi_b \qquad (A4)$$

25

APPENDIX B

LIFTING LINE OF PRESSURE DIPOLES

The pressure field must satisfy the Laplace equation which can be written in cylindrical coordinates (r, χ, z) as

$$\frac{\partial^2 p}{\partial r^2} + \frac{1}{r}\frac{\partial p}{\partial r} + \frac{1}{r^2}\frac{\partial^2 p}{\partial \chi^2} + \frac{\partial^2 p}{\partial z^2} = 0 \qquad (B1)$$

To apply a separation of variables, let

$$p = R(r)\, X(\chi)\, Z(z)$$

This leads to the ordinary differential equations

$$Z'' + q^2 Z = 0$$

$$X'' + n^2 X = 0$$

$$r^2 R'' + r R' - (n^2 + q^2 r^2) R = 0$$

The first two equations have sines and cosines as elementary solutions, while the third has modified Bessel functions of the first and second kind, $I_n(qr)$ and $K_n(qr)$, as solutions.

For the solution to represent a lifting line, it must tend to zero as $r \to \infty$ and become singular as $r \to 0$, which excludes the use of $I_n(qr)$. A field point can be represented by a given value of χ or with any multiple of 2π added to it, which requires that the solution be periodic in χ and that n be an integer. Since the solution must be antisymmetric about $\chi = 0$ or π, only sine solutions can be allowed for $X(\chi)$. Further, for the lifting line to be built up of dipoles, n=1, since $K_n(x) \sim x^{-n}$, $x \to 0$, n=1, 2...

The general solution for a dipole line is then of the form, $p(r, \chi, z) = \sin \chi \; K_1(qr)$ $\{A(q) \cos qz + B(q) \sin qt\}$. To obtain a line of strength $f_1(z)$, $-s \le z \le x$, the functions A and B are chosen as

$$A(q) = q \int_{-s}^{s} f_1(\zeta) \cos q\zeta \; d\zeta$$

$$B(q) = q \int_{-s}^{s} f_1(\zeta) \sin q\zeta \; d\zeta$$

Since all positive values of q are allowed, the dipole line has the solution

$$P_{dip}(r,\chi,z) = \frac{\sin\chi}{2\pi} \frac{1}{\pi} \int_{-s}^{s} f_1(\zeta)\,d\zeta \int_{0}^{\infty} q\,K_1(qr)\cos\{q(\zeta-z)\}\,dq \qquad (B2)$$

Integrating by parts and making use of $f_1(\pm s) = 0$, this expression can be alternately written as

$$P_{dip}(r,\chi,z) = -\frac{\sin\chi}{4\pi r} \int_{-s}^{s} f_1'(\zeta)\frac{(\zeta-z)\,d\zeta}{\left[r^2 + (\zeta-z)^2\right]^{1/2}}$$

It can be seen that a field for the lifting line of this form involves numerical integration along the span. An alternate approach is to obtain the field in prolate spheroidal coordinates (Ψ,θ,χ) which are related to cylindrical coordinates through (see fig. 3)

$$r = s\sinh\Psi\sin\theta$$

$$z = s\cosh\Psi\cos\theta$$

$$\chi = \chi$$

The Laplace equation becomes

$$\frac{1}{\sinh^2\Psi + \sin^2\theta}\left(\frac{\partial^2 p}{\partial\Psi^2} + \coth\Psi\frac{\partial p}{\partial\Psi} + \frac{\partial^2 p}{\partial\theta^2} + \cot\theta\frac{\partial p}{\partial\theta}\right) + \frac{1}{\sinh^2\Psi\sin^2\theta}\frac{\partial^2 p}{\partial\chi^2} = 0 \qquad (B3)$$

Separation of variables as

$$p = \psi(\Psi)\Theta(\theta)X(\chi)$$

leads to

$$\psi'' + (\coth\Psi)\psi' - \left\{n(n+1) + \frac{m^2}{\sinh^2\psi}\right\}\psi = 0$$

$$\Theta'' + (\cot\theta)\Theta' + \left\{n(n+1) - \frac{m^2}{\sin^2\theta}\right\}\Theta = 0$$

$$X'' + m^2 X = 0$$

27

The solution for $X(\chi)$ is as before. The first two equations have, as elementary solutions, the associated Legendre functions, $P_n^m(\cosh \Psi)$, $Q_n^m(\cosh \Psi)$, $P_n^m(\cos \theta)$, $Q_n^m(\cos \theta)$. For the solution to represent a dipole line it is necessary that $m=1$. For it to vanish as $r \to \infty$ ($\Psi \to \infty$) and be singular along the lifting line ($\Psi=0$), only $Q_n^1(\cosh \Psi)$ can be considered for ψ. To avoid any other singularities in the field, only $P_n^1(\cos \theta)$ can be considered for Θ. The solution for a lifting line of dipoles is then of the form

$$P_{dip}(\Psi, \theta, \chi) = \frac{\sin \chi}{2 \pi} \sum_{n=1}^{\infty} A_n P_n^1(\cos \theta) Q_n^1(\cosh \Psi) \tag{B4}$$

It can be seen that such an expression for the field of a lifting line, conveniently truncated, involves no numerical integration along the span.

APPENDIX C

INTEGRAL COEFFICIENTS FOR INDUCED VELOCITY

In order to simplify the final form of the integral terms in equation (11), the following derivatives will first be defined.

$$D_1 = \frac{\partial}{\partial\left(\frac{y_b}{R_1}\right)} \left[\frac{\sin\chi\,\cosh\Psi\,\sin\theta}{\sinh\Psi\,(\sinh^2\Psi + \sin^2\theta)}\right]$$

$$= \frac{2R_1}{(R_1-R_0)} \left[\frac{\sin^2\chi}{\sinh^2\Psi + \sin^2\theta} \left\{\frac{\cosh\Psi}{\sinh^2\Psi + \sin^2\theta} - \frac{\cosh^3\Psi\,\sin^2\theta}{\sinh^2\Psi\,(\sinh^2\Psi + \sin^2\theta)}\right.\right.$$

$$\left.\left. - \frac{2\cosh\Psi\,\sin^2\theta\,(\cosh^2\Psi + \cos^2\theta)}{(\sinh^2\Psi + \sin^2\theta)^2}\right\} + \frac{\cos^2\chi\,\cosh\Psi}{\sinh^2\Psi\,(\sinh^2\Psi + \sin^2\theta)}\right]$$

$$D_2 = \frac{\partial}{\partial\left(\frac{y_b}{R_1}\right)} \left[\frac{\sin\chi\,\sin\theta}{\sinh\Psi\,(\cosh\Psi - \cos\theta)}\right]$$

$$= \frac{2R_1}{(R_1-R_0)} \left[\frac{\sin^2\chi}{\cosh^2\Psi - \cos^2\theta} \left\{\frac{\sinh^2\Psi\,\cos^2\theta - \cosh^2\Psi\,\sin^2\theta}{\sinh^2\Psi\,(\cosh\Psi - \cos\theta)}\right.\right.$$

$$\left.\left. - \frac{\sin^2\theta\,(\cosh\Psi + \cos\theta)}{(\cosh\Psi - \cos\theta)^2}\right\} + \frac{\cos^2\chi}{\sinh^2\Psi\,(\cosh\Psi - \cos\theta)}\right]$$

$$D_3 = \frac{\partial}{\partial\left(\frac{y_b}{R_1}\right)} \left[\frac{\sin\chi}{r/(R_1-R_0)}\right] = \frac{(R_1-R_0)}{R_1}\,\frac{\cos 2\chi}{(r/R_1)^2}$$

$$D_4 = \frac{\partial}{\partial\left(\frac{y_b}{R_1}\right)} \left[\frac{\sin\phi}{\cosh\eta + \cos\phi}\right]$$

$$= \frac{2AR_1}{(R_1-R_0)} \left[\frac{\sinh\eta\ \cos\phi + \sinh\eta\ \cosh\eta\ \cos 2\phi}{(\sinh^2\eta\ \cos^2\phi + \cosh^2\eta\ \sin^2\phi)(\cosh\eta + \cos\phi)^2}\right]$$

$$D_5 = \frac{\partial}{\partial\left(\frac{y_b}{R_1}\right)} \left[\frac{\sin\chi}{2\pi}\ P_n^1(\cos\theta)\ Q_n^1(\cosh\Psi)\right]$$

$$= \frac{R_1}{(R_1-R_0)} \left[\frac{1}{\pi\ \sin\theta\ \sinh\Psi}\ P_n^1(\cos\theta)\ Q_n^1(\cosh\Psi)\right.$$

$$+ \frac{\tan\chi\ \sin 2\chi}{2\pi\ (\sinh^2\Psi + \sin^2\theta)}\ \left\{\sin\theta\ \cosh\Psi\ P_n^1(\cos\theta) Q_n^2(\cosh\Psi)\right.$$

$$\left.\left. - \cos\theta\ \sinh\Psi\ P_n^2(\cos\theta)\ Q_n^1(\cosh\Psi)\right\}\right]$$

$$D_6 = \frac{\partial}{\partial\left(\frac{y_b}{R_1}\right)} \left[e^{-\eta}\ \sin\phi\right]$$

$$= \frac{2AR_1}{(R_1-R_0)} \left[\frac{e^{-\eta}\ (\sinh\eta\ \cos^2\phi - \cosh\eta\ \sin^2\phi)}{\sinh^2\eta\ \cos^2\phi + \cosh^2\eta\ \sin^2\phi}\right]$$

It must be noted that the complete expression for the pressure field is valid only for a field point with a spanwise coordinate within the blade span. For a field point outside the blade span, it is assumed that only the far field exists. In the expressions that follow, that part of the pressure field that is valid only within the blade span is multiplied by the factor $\{H(z_b^*+1)-H(z_b^*-1)\}$. The Heaviside function, $H(x)$, that is unity for $x>0$ and zero for $x<0$ will

be denoted by H, so that

$$H = \begin{cases} 1, & |z_b^*| < 1 \\ \\ 0, & |z_b^*| > 1 \end{cases}$$

In terms of the derivatives (D_1 to D_6), the integral coefficients are as below

$$w_{rs,oo}^* = \int_{-\infty}^{\Psi_{bs}} \left[D_2 - \frac{1}{2} H(1 + z_b^*) D_3 \right] d\Psi_b$$

$$+ \int_{-\infty}^{\Psi_{bs}-\Delta\Psi_b} HA(1 + z_b^*) D_4 \, d\Psi_b$$

$$- \frac{A(1 + z_{br}^*)}{\left(\dfrac{r_{br}}{R_1} + \mu \sin \Psi_{bs} \right)} \coth(\eta_1/2)$$

$$+ \frac{\mu \cos \Psi_{bs}}{\left(\dfrac{r_{br}}{R_1} + \mu \sin \Psi_{bs} \right)^2} \left(\frac{1}{2} \coth(\eta_1/2) - \eta_1 \right)$$

where

$$\cosh \eta_1 = \frac{R_1}{b} \Delta\Psi_b \left(\frac{r_{br}}{R_1} + \mu \sin \Psi_{bs} \right) + \frac{1}{2}$$

$$w^*_{rs,okc} = \int_{-\infty}^{\Psi_{bs}} \left[D_2 - \frac{1}{2}H(1 + z^*_b) D_3 \right] \cos k\, \Psi_b \, d\Psi_b$$

$$+ \int_{-\infty}^{\Psi_{bs} - \Delta\Psi_b} HA(1 + z^*_b) D_4 \cos k\Psi_b \, d\Psi_b$$

$$- \frac{A(1 + z^*_{br})}{\left(\dfrac{r_{br}}{R_1} + \mu \sin \Psi_{bs}\right)} \cos k\, \Psi_{bs} \coth(\eta_1/2)$$

$$+ \left\{ \frac{\mu \cos k \Psi_{bs} \cos \Psi_{bs} - \dfrac{k}{2}\left(1 - \dfrac{R_0}{R_1}\right)\left(1 + z^*_{br}\right) \sin k\Psi_{bs}}{\left(\dfrac{r_{br}}{R_1} + \mu \sin \Psi_{bs}\right)^2} \right\} \left(\frac{1}{2} \coth \frac{\eta_1}{2} - \eta_1 \right)$$

$$+ \left\{ \frac{\dfrac{k}{2A}\left(1 - \dfrac{R_0}{R_1}\right)\mu \cos \Psi_{bs} \sin k\Psi_{bs} + \dfrac{k^2}{8A}\left(1 - \dfrac{R_0}{R_1}\right)^2\left(1 + z^*_{br}\right) \cos k\Psi_{bs}}{\left(\dfrac{r_{br}}{R_1} + \mu \sin \Psi_{bs}\right)^3} \right\} \times$$

$$\left(\frac{1}{4} \coth \frac{\eta_1}{2} - \sinh \eta_1 \right)$$

$$+ \frac{\cos k\, \Psi_{bs}}{\left(\dfrac{r_{br}}{R_1} + \mu \sin \Psi_{bs}\right)} \left[\frac{\sin \chi' \sin \theta'}{\sinh \Psi'(\cosh \Psi' - \cos \theta')} - 2A(1 + z^*_{br}) \right]$$

where (Ψ', θ', χ') corresponds to $r = \dfrac{b}{2}$, $x = \dfrac{\pi}{2}$, $z^*_b = z^*_{br}$

$w^*_{rs,oks}$ same as for $w^*_{rs,okc}$ except replace $\cos k \, \Psi_{bs}$ with $\sin k \, \Psi_{bs}$ and $\sin k \Psi_{bs}$ with $-\cos k \, \Psi_{bs}$

$$w^*_{rs,no} = \int_{-\infty}^{\Psi_{bs}} \left[-D_5 - H\frac{1}{4\pi} \sqrt{1 - z_b^{*2}} \; P_n^1(z_b^*) D_3 \right] d\Psi_b$$

$$+ \int_{-\infty}^{\Psi_{bs} - \Delta\Psi_b} H \frac{A}{2\pi} \sqrt{1 - z_b^{*2}} \; P_n^1(z_b^*) D_4 \, d\Psi_b$$

$$- \frac{A}{2\pi} \sqrt{1 - z_{br}^{*2}} \; P_n^1(z_{br}^*) \frac{\coth(\eta_1/2)}{\left(\dfrac{r_{br}}{R_1} + \mu \sin \Psi_{bs}\right)}$$

$$- \frac{\mu \cos \Psi_{bs}}{2\pi} \frac{n(n+1) P_n^0(z_{br}^*)}{\left(\dfrac{r_{br}}{R_1} + \mu \sin \Psi_{bs}\right)^2} \left(\frac{1}{2} \coth \frac{\eta_1}{2} - \eta_1 \right)$$

$$+ \frac{\mu^2 \cos^2 \Psi_{bs}}{4\pi A \sqrt{1 - z_{br}^{*2}}} \frac{n(n+1) P_n^1(z_{br}^*)}{\left(\dfrac{r_{br}}{R_1} + \mu \sin \Psi_{bs}\right)^3} \left(\frac{1}{4} \coth \frac{\eta_1}{2} - \sinh \eta_1 \right)$$

$$- \frac{1}{\left(\dfrac{r_{br}}{R_1} + \mu \sin \Psi_{bs}\right)} \left[\frac{1}{2\pi} P_n^1(\cos \theta \, ') Q_n^1(\cosh \Psi \, ') + \frac{A}{2\pi} \sqrt{1 - z_{br}^{*2}} \, P_n^1(z_{br}^*) \right]$$

$$w^*_{rs,nkc} = \int_{-\infty}^{\Psi_{bs}} -\left[D_5 + H\frac{1}{4\pi}\sqrt{1-z_b^{*2}}\; P_n^1(z_b^*)\, D_3\right]\cos k\,\Psi_b\; d\,\Psi_b$$

$$+ \int_{-\infty}^{\Psi_{bs}-\Delta\Psi_b} H\frac{A}{2\pi}\sqrt{1-z_b^{*2}}\; P_n^1(z_b^*)\, D_4 \cos k\,\Psi_b\; d\,\Psi_b$$

$$- \frac{A}{2\pi}\sqrt{1-z_{br}^{*\,2}}\; P_n^1(z_{br}^*)\,\frac{\coth\left(\frac{\eta_1}{2}\right)\cos k\,\Psi_{bs}}{\left(\frac{r_{br}}{R_1}+\mu\sin\Psi_{bs}\right)}$$

$$-\left\{\frac{\left(1-\frac{R_0}{R_1}\right)}{4\pi}k\sqrt{1-z_{br}^{*\,2}}\; P_n^1(z_{br}^*)\sin k\,\Psi_{bs} - \frac{\mu\, n(n+1)}{2\pi}P_n^0(z_{br}^*)\cos\Psi_{bs}\cos k\,\Psi_{bs}\right\}$$

$$\times\;\left(\frac{1}{2}\coth\frac{\eta_1}{2}-\eta_1\right)\Big/\left(\frac{r_{br}}{R_1}+\mu\sin\Psi_{bs}\right)^2$$

$$+\left\{\frac{\mu^2\cos^2\Psi_{bs}\cos k\,\Psi_{bs}\, n(n+1)\, P_n^0(z_{br}^*)}{4\pi A\sqrt{1-z_{br}^{*2}}}\right.$$

$$-\frac{1}{4\pi A}\left(1-\frac{R_0}{R_1}\right)\mu\,\cos\Psi_{bs}\, n(n+1)\, P_n^0(z_{br}^*)\, k\sin k\,\Psi_{bs}$$

$$\left.+\frac{1}{16\pi A}\left(1-\frac{R_0}{R_1}\right)^2\sqrt{1-z_{br}^{*\,2}}\; P_n^1(z_{br}^*)\, k^2\cos k\,\Psi_{bs}\right\}\times$$

$$\left(\frac{1}{4}\coth\frac{\eta_1}{2}-\sinh\eta_1\right)\Big/\left(\frac{r_{br}}{R_1}+\mu\sin\Psi_{bs}\right)^3$$

$$-\frac{\cos k\,\Psi_{bs}}{\left(\frac{r_{br}}{R_1}+\mu\sin\Psi_{bs}\right)}\left[\frac{1}{2\pi}P_n^1(\cos\theta')\, Q_n^1(\cosh\Psi') + \frac{A}{2\pi}\sqrt{1-z_{br}^{*2}}\; P_n^1(z_{br}^*)\right]$$

$w^*_{rs,nks}$ same as $w^*_{rs,nkc}$ except replace $\cos k\,\Psi_{bs}$ with $\sin k\,\Psi_{bs}$ and $\sin k\,\Psi_{bs}$ with $-\cos k\,\Psi_{bs}$

$$
\begin{aligned}
w^*_{rs} = \int_{-\infty}^{\Psi_{bs}} \Bigg[&-\frac{\left(1-\frac{R_0}{R_1}\right)}{4A^2}\left(F_2+\frac{R_0}{R_1}F_3\right)D_1 \\[2mm]
&-\frac{\left(1-\frac{R_0}{R_1}\right)^2}{8A^2}F_3 D_2 + H\,\frac{\left(1-\frac{R_0}{R_1}\right)}{8A^2}\left(F_2+\frac{r_b}{R_1}F_3\right)D_3 \Bigg]d\Psi_b \\[4mm]
&-\int_{-\infty}^{\Psi_{bs}-\Delta\Psi_b} H\,\frac{\left(1-\frac{R_0}{R_1}\right)}{2A}\left(F_2+\frac{r_b}{R_1}F_3\right)D_6\,d\Psi_b \\[4mm]
&+\frac{\left(1-\frac{R_0}{R_1}\right)}{2A}\frac{\left[F_2(\Psi_{bs})+\frac{r_{br}}{R_1}F_3(\Psi_{bs})\right]}{\left(\frac{r_{br}}{R_1}+\mu\sin\Psi_{bs}\right)}\left(\frac{1}{2}-e^{-\eta_1}\right) \\[4mm]
&+\frac{\left(1-\frac{R_0}{R_1}\right)^2}{8A^2}\frac{\left[F'_2(\Psi_{bs})+\frac{r_{br}}{R_1}F'_3(\Psi_{bs})+\mu\cos\Psi_{bs}\,F_3(\Psi_{bs})\right]}{\left(\frac{r_{br}}{R_1}+\mu\sin\Psi_{bs}\right)^2} \times \\[4mm]
&\cdot\left(\frac{3}{4}-\eta_1-e^{-\eta_1}+\frac{1}{2}e^{-2\eta_1}\right) \\[4mm]
&+\frac{3\left(1-\frac{R_0}{R_1}\right)^2}{32\,A^2}F_1\left(\Psi_{bs},\frac{r_{br}}{R_1}\right)
\end{aligned}
$$

35

APPENDIX D

COMPUTATION OF ASSOCIATED LEGENDRE FUNCTIONS

These functions are independent solutions of the associated Legendre equation and obey the following recursive relations (ref. 29).

$$P_n^m(x) = \frac{1}{(n-m)} \left[(2n-1) \, x \, P_{n-1}^m(x) - (n+m-1) \, P_{n-2}^m(x) \right]$$

$$P_n^m(x) = 2(m-1) \frac{x}{\sqrt{1-x^2}} \, P_n^{m-1}(x) - (n-m+2)(n+m-1) \, P_n^{m-2}(x)$$

and likewise for $Q_n^m(x)$. The functions $P_n^m(x)$ can be computed without difficulty using the recursive relations, given the explicit expressions for the first few functions. However, the functions $Q_n^m(x)$ decrease rapidly with x for $x > 1$ and, beyond a certain range of x, use of the recursive relations leads to excessive loss of significant figures due to roundoff error. In such a case, these functions must be computed either by using asymptotic expansions in inverse powers of the argument or by using the definition of $Q_n^m(x)$ in terms of the hypergeometric function.

In the computations carried out here, it is necessary to compute many of these functions very frequently, which requires that each computation be done as quickly as possible. For this reason, explicit expressions were used for the range of n and m required, as indicated below

Functions $P_n^m(x)$
_____

    m = 0:

$$P_1^0 = x$$

$$P_2^0 = (3x^2-1)/2$$

$$P_3^0 = (5x^3-3x)/2$$

$$P_4^0 = (35x^4-30x^2+3)/8$$

m = 1:

$$P_1^1 = \sqrt{1-x^2}$$

$$P_2^1 = 3x\sqrt{1-x^2}$$

$$P_3^1 = (15x^2-3)\sqrt{1-x^2}\ /2$$

$$P_4^1 = (35x^3-15x)\sqrt{1-x^2}\ /2$$

m = 2:

$$P_1^2 = 0$$

$$P_2^2 = 3(1-x^2)$$

$$P_3^2 = 15x(1-x^2)$$

$$P_4^2 = (105x^2-15)(1-x^2)/2$$

m = 3:

$$P_1^3 = P_2^3 = 0$$

$$P_3^3 = 15(1-x^2)^{3/2}$$

$$P_4^3 = 105x(1-x^2)^{3/2}$$

Functions $Q_n^m(x)$, $1 < x < 3$:

m = 1:

$$Q_1^1 = \sqrt{x^2-1} \left[\frac{1}{2} \ln \frac{x+1}{x-1} - \frac{x}{x^2-1} \right]$$

$$Q_2^1 = \sqrt{x^2-1} \left[\frac{3}{2} x \ln \frac{x+1}{x-1} - \frac{3x^2-1}{2(x^2-1)} - \frac{3}{2} \right]$$

$$Q_3^1 = \sqrt{x^2-1} \left[\frac{(15x^2-3)}{4} \ln \frac{x+1}{x-1} - \frac{(5x^3-3x)}{2(x^2-1)} - 5x \right]$$

$$Q_4^1 = \sqrt{x^2-1} \left[\frac{(35x^3-15x)}{4} \ln \frac{x+1}{x-1} - \frac{(35x^4-30x^2+3)}{8(x^2-1)} - 105 \frac{x^2}{8} + \frac{55}{24} \right]$$

m = 2:

$$Q_1^2 = \frac{2}{x^2-1}$$

$$Q_2^2 = (x^2-1) \left[\frac{3}{2} \ln \frac{x+1}{x-1} - \frac{6x}{x^2-1} + \frac{x(3x^2-1)}{(x^2-1)^2} \right]$$

$$Q_3^2 = (x^2-1) \left[\frac{15x}{2} \ln \frac{x+1}{x-1} - \frac{(15x^2-3)}{(x^2-1)} + \frac{x(5x^3-3x)}{(x^2-1)^2} - 5 \right]$$

$$Q_4^2 = (x^2-1) \left[\frac{(105x^2-15)}{4} \ln \frac{x+1}{x-1} - \frac{(35x^3-15x)}{(x^2-1)} + \frac{x(35x^4-30x^2+3)}{4(x^2-1)^2} - 105 \frac{x}{4} \right]$$

Functions $Q_n^m(x)$, $x > 3$

m = 1:

$$Q_1^1 \simeq -(x^2-1)\left[\frac{2}{3}x^{-3} + \frac{4}{5}x^{-5} + \frac{6}{7}x^{-7} + \frac{8}{9}x^{-9}\right]$$

$$Q_2^1 \simeq -(x^2-1)\left[\frac{2}{5}x^{-4} + \frac{4}{7}x^{-6} + \frac{6}{9}x^{-8} + \frac{8}{11}x^{-10}\right]$$

$$Q_3^1 \simeq -(x^2-1)\left[\frac{8}{35}x^{-5} + \frac{8}{21}x^{-7} + \frac{16}{33}x^{-9}\right]$$

$$Q_4^1 \simeq -(x^2-1)\left[\frac{8}{63}x^{-6} + \frac{8}{33}x^{-8} + \frac{48}{143}x^{-10}\right]$$

m = 2:

$$Q_1^2 = \frac{2}{x^2-1}$$

$$Q_2^2 \simeq (x^2-1)\left[\frac{8}{5}x^{-5} + \frac{24}{7}x^{-7} + \frac{16}{3}x^{-9}\right]$$

$$Q_3^2 \simeq (x^2-1)\left[\frac{8}{7}x^{-6} + \frac{8}{3}x^{-8} + \frac{48}{11}x^{-10}\right]$$

$$Q_4^2 \simeq (x^2-1)\left[\frac{16}{21}x^{-7} + \frac{64}{33}x^{-9}\right]$$

For some of the computational cases, when the functions were required for greater order and degree, the recursive relations were used with $Q_n^m(x)$ being defined in terms of the hypergeometric function beyond a certain value of x. $P_n^m(x)$ was computed recursively starting with $P_0^1, P_0^2, P_1^1, P_1^2$. The functions $Q_n^m(x)$ were computed as

x > 3:

$$Q_n^m = f_1 \left[1 + \sum_{k=1}^{\infty} f_2 \frac{1}{k!} \left(\frac{\sqrt{x^2-1} - x}{2\sqrt{x^2-1}} \right)^k \right]$$

where

$$f_1 = (-1)^m \left(\frac{2}{\sqrt{x^2-1}} \right)^{1/2} \frac{1}{\left(x + \sqrt{x^2-1} \right)^{n + \frac{1}{2}}} \frac{(n+m)!}{n!} \prod_{j=1}^{n} \left(1 + \frac{1}{2j} \right)$$

$$f_2 = \frac{\left\{ \left(k - \frac{1}{2} \right)^2 - m^2 \right\} \left\{ \left(k - \frac{3}{2} \right)^2 - m^2 \right\} \cdots \left\{ \frac{1}{4} - m^2 \right\}}{\left(n + k + \frac{1}{2} \right) \left(n + k - \frac{1}{2} \right) \cdots \left(n + \frac{3}{2} \right)}$$

x < 3:

$$Q_n^m = \frac{(2n-1)}{n} P_{n-1}^m(x) - \sum_{k=1}^{(n-1)/2} \frac{(2n-1-4k)}{(1+2k)(n-k)} P_{n-1-2k}^m(x)$$

$$+ \frac{1}{2} \ln \frac{x+1}{x-1} P_n^m(x) - \frac{m}{\sqrt{x^2-1}} P_n^{m-1}(x) + \frac{m(m-1)x}{\sqrt{x^2-1}} P_n^{m-2}(x)$$

$$- \frac{m(m-1)(m-2)(3x^2+1)}{3(x^2-1)^{3/2}} P_n^{m-3}(x)$$

$$+ \frac{m(m-1)(m-2)(m-3) x (x^2+1)}{(x^2-1)^2} P_n^{m-4}(x)$$

This expression is valid for $m \leq 4$.

OUTPUT PARAMETERS AND EQUILIBRIUM EQUATIONS

The perturbation pressure on the surface of the blade can be obtained by considering only the near field solution and setting $\eta'=0$.

$$\frac{1}{\rho\Omega^2 R_1^2} P_b(\phi) = -g^*(z_b^*, \Psi_b) \frac{\sin\phi}{1+\cos\phi}$$

$$+ 2\sin\phi \left[p_{dip}^*(\Psi', \theta', \chi', \Psi_b) + 2g^*(z_b^*, \Psi_b) \right]$$

$$+ \frac{1}{8A^2} \frac{d^2 g^*}{dz_b^{*2}} \sin 2\phi + \frac{1}{2A}\left(1-\frac{R_0}{R_1}\right)\left[F_2(\Psi_b) + \frac{r_b}{R_1} F_3(\Psi_b) \right] \sin\phi$$

$$+ \frac{1}{8A^2}\left(1-\frac{R_0}{R_1}\right)^2 F_1\left(\Psi_b, \frac{r_b}{R_1}\right) \left[\sin\phi + \frac{1}{2}\sin 2\phi \right] \qquad (E1)$$

By integration with respect to the chord, sectional quantities such as lift and pitching moment can be derived.
Section Lift:

$$\ell^*(z_b^*, \Psi_b) \equiv \frac{\ell}{\rho\Omega^2 R_1^3} = \frac{\pi}{A}\left(1-\frac{R_0}{R_1}\right)\left[p_{dip}^*(\Psi', \theta', \chi', \Psi_b) + g^*(z_b^*, \Psi_b) \right]$$

$$+ \frac{\pi}{4A^2}\left(1-\frac{R_0}{R_1}\right)^2 \left[F_2(\Psi_b) + \frac{r_b}{R_1} F_3(\Psi_b) \right]$$

$$+ \frac{\pi}{16A^3}\left(1-\frac{R_0}{R_1}\right)^3 F_1\left(\Psi_b, \frac{r_b}{R_1}\right) \qquad (E2)$$

Pitching moment about a point x = a (positive nose-down):

$$m^*(z_b^*, \Psi_b) \equiv \frac{m}{\rho \Omega^2 R_1^4}$$

$$= \frac{\pi}{4A^2} \left(1 - \frac{R_0}{R_1}\right)^2 \left[g^*(z_b^*, \Psi_b) + \frac{1}{32A^2} \left\{ 2 \frac{d^2 g^*}{dz_b^{*2}} \right. \right.$$

$$\left. \left. + \left(1 - \frac{R_0}{R_1}\right)^2 F_1\left(\Psi_b, \frac{r_b}{R_1}\right) \right\} \right] - \frac{1}{2A} \left(1 - \frac{R_0}{R_1}\right) \, a \, \ell^* \quad (E3)$$

Position of center of pressure from the leading edge:

$$\frac{x_{cp}}{b} = \frac{1}{2}(1+a) + \frac{A}{\left(1 - \frac{R_0}{R_1}\right)} \frac{m^*}{\ell^*} \quad (E4)$$

The sectional lift can be integrated along the span to give the total blade lift and the aerodynamic moment about the hub.

Let

$$\left\{ \begin{array}{c} I_0^1 \\ \\ I_0^2 \end{array} \right\} = \int_{R_0/R_1}^{1} \frac{\sin \theta'}{\sinh \Psi'(\cosh \Psi' - \cos \theta')} \left\{ \begin{array}{c} 1 \\ \\ r_b/R_1 \end{array} \right\} d\left(\frac{r_b}{R_1}\right)$$

$$\left\{ \begin{array}{c} I_n^1 \\ \\ I_n^2 \end{array} \right\} = \int_{R_0/R_1}^{1} P_n^1(\cos \theta') Q_n^1(\cosh \Psi') \left\{ \begin{array}{c} 1 \\ \\ r_b/R_1 \end{array} \right\} d\left(\frac{r_b}{R_1}\right)$$

42

Total blade lift:

$$L^* \equiv \frac{L}{\rho \Omega^2 R_1^4}$$

$$= \pi \left(1 - \frac{R_0}{R_1}\right) \left[\left(1 - \frac{R_0}{R_1}\right) - \frac{I_0^1}{A}\right] \left[A_{00} + \sum_{k=1}^{K} (A_{0k} \cos k \Psi_b + B_{0k} \sin k \Psi_b)\right]$$

$$+ \frac{1}{3} \left(1 - \frac{R_0}{R_1}\right)^2 \left[A_{10} + \sum_{k=1}^{K} (A_{1k} \cos k \Psi_b + B_{1k} \sin k \Psi_b)\right]$$

$$+ \frac{1}{2A} \left(1 - \frac{R_0}{R_1}\right) \sum_{n=1}^{N} I_n^1 \left[A_{n0} + \sum_{k=1}^{K} (A_{nk} \cos k \Psi_b + B_{nk} \sin k \Psi_b)\right]$$

$$+ \frac{\pi}{4A^2} \left(1 - \frac{R_0}{R_1}\right)^3 F_2(\Psi_b) + \frac{\pi}{8A^2} \left(1 - \frac{R_0}{R_1}\right)^3 F_3(\Psi_b) \left(1 + \frac{R_0}{R_1}\right)$$

$$+ \frac{\pi}{16A^3} \left(1 - \frac{R_0}{R_1}\right)^3 \left[\left\{-\theta_o + \epsilon \left(2 + \frac{R_0}{R_1}\right) \middle/ \left(1 - \frac{R_0}{R_1}\right)\right\}\right.$$

$$\left. - 2b_1 \cos \Psi_b + \left\{2a_1 + 4 \mu \epsilon \frac{1}{\left(1 - \frac{R_0}{R_1}\right)}\right\} \sin \Psi_b\right] \qquad (E5)$$

Moment of lift about the hub:

$$M^* \equiv \frac{M}{\rho \Omega^2 R_1^{\,5}}$$

$$= \pi\left(1 - \frac{R_0}{R_1}\right)\left[\frac{1}{2}\left(1 - \frac{R_0}{R_1}\right)\left(1 + \frac{R_0}{R_1}\right) + \frac{1}{6}\left(1 - \frac{R_0}{R_1}\right)^2 - \frac{I_0^{\,2}}{A}\right] \times$$

$$\left[A_{00} + \sum_{k=1}^{K}(A_{0k}\cos k\,\Psi_b + B_{0k}\sin k\,\Psi_b)\right]$$

$$+ \frac{1}{6}\left(1 - \frac{R_0}{R_1}\right)^2\left(1 + \frac{R_0}{R_1}\right)\left[A_{10} + \sum_{k=1}^{K}(A_{k}\cos k\,\Psi_b + B_{1k}\sin k\,\Psi_b)\right]$$

$$+ \frac{1}{10}\left(1 - \frac{R_0}{R_1}\right)^3\left[A_{20} + \sum_{k=1}^{K}(A_{2k}\cos k\,\Psi_b + B_{2k}\sin k\,\Psi_b)\right]$$

$$+ \frac{1}{2A}\left(1 - \frac{R_0}{R_1}\right)\sum_{n=1}^{N}I_n^2\left[A_{n0} + \sum_{k=1}^{K}(A_{nk}\cos k\,\Psi_b + B_{nk}\sin k\,\Psi_b)\right]$$

$$+ \frac{\pi}{8A^2}\left(1 - \frac{R_0}{R_1}\right)^2\left[\left(1 - \frac{R_0^{\,2}}{R_1^{\,2}}\right)F_2(\Psi_b) + \left(1 - \frac{R_0^{\,3}}{R_1^{\,3}}\right)F_3(\Psi_b)\right]$$

$$+ \frac{\pi}{32A^3}\left(1 - \frac{R_0}{R_1}\right)^3\left(1 - \frac{R_0^{\,2}}{R_1^{\,2}}\right)\left[\left\{-\theta_0 - \epsilon\,\frac{R_0/R_1}{\left(1 - \frac{R_0}{R_1}\right)}\right\} - 2b_1\cos\Psi_b\right.$$

$$\left. + \left\{2a_1 + 4\,\mu\epsilon\,\frac{1}{\left(1 - \frac{R_0}{R_1}\right)}\right\}\sin\Psi_b\right] + \frac{\pi}{12A^3}\epsilon\left(1 - \frac{R_0}{R_1}\right)^2\left(1 - \frac{R_0^{\,3}}{R_1^{\,3}}\right) \qquad (E6)$$

Radial position of lift center:

$$\frac{r_L^*}{R_1} = \frac{M^*}{L^*}$$

The additional equations needed to solve for the blade motion parameters are

1)
$$\frac{1}{2\pi} \int_0^{2\pi} L^*(\Psi_b) \, d\Psi_b = \frac{\pi C_T}{B}$$

where B is the number of blades.
Substituting for L^*

$$\left[-\frac{1}{A}\left(1-\frac{R_0}{R_1}\right) I_0^1 + \left(1-\frac{R_0}{R_1}\right)^2 \right] A_{00} + \frac{1}{3\pi}\left(1-\frac{R_0}{R_1}\right)^2 A_{10}$$

$$+\frac{1}{2\pi A}\left(1-\frac{R_0}{R_1}\right)\sum_{n=1}^{N} I_n^1 A_{n0} - \frac{1}{16A^3}\left(1-\frac{R_0}{R_1}\right)^4 \theta_o$$

$$+\frac{1}{8A^2}\left(1-\frac{R_0}{R_1}\right)^3\left(1+\frac{R_0}{R_1}\right) a_o = C_T - \frac{1}{16A^3}\left(1-\frac{R_0}{R_1}\right)^3\left(2+\frac{R_0}{R_1}\right)\epsilon \qquad (E8)$$

2)
$$\frac{1}{2\pi}\int_0^{2\pi} M^*(\Psi_b)\, d\Psi_b = \frac{I\Omega^2 a_o}{\rho\Omega^2 R_1^5}$$

Substituting for M^*

$$\left[-\frac{\pi}{A}\left(1-\frac{R_0}{R_1}\right) + \pi\left(1-\frac{R_0}{R_1}\right)\left\{\frac{1}{2}\left(1-\frac{R_0^2}{R_1^2}\right) + \frac{1}{6}\left(1-\frac{R_0}{R_1}\right)^2\right\}\right] A_{00}$$

$$+\frac{1}{6}\left(1-\frac{R_0^2}{R_1^2}\right)\left(1-\frac{R_0}{R_1}\right) A_{10} + \frac{1}{10}\left(1-\frac{R_0}{R_1}\right)^3 A_{20} + \frac{1}{2A}\left(1-\frac{R_0}{R_1}\right)\sum_{n=1}^{N} I_n^2 A_{n0}$$

$$+\left[\frac{\pi}{12A^2}\left(1-\frac{R_0}{R_1}\right)^2\left(1-\frac{R_0^3}{R_1^3}\right) - \frac{I\Omega^2}{\rho\Omega^2 R_1^5}\right] a_o - \frac{\pi}{32A^3}\left(1-\frac{R_0}{R_1}\right)^3\left(1-\frac{R_0^2}{R_1^2}\right)\theta_o$$

$$=\left[\frac{\pi}{32A^3}\left(1-\frac{R_0}{R_1}\right)^2\left(1-\frac{R_0^2}{R_1^2}\right)\frac{R_0}{R_1} - \frac{\pi}{12A^3}\left(1-\frac{R_0}{R_1}\right)^5\right]\epsilon \qquad (E9)$$

46

3)
$$\frac{1}{\pi} \int_0^{2\pi} M^*(\Psi_b) \cos \Psi_b \, d\Psi_b = 0$$

Substituting for M^*

$$\left[-I_0^2 + A \left\{ \frac{1}{2} \left(1 - \frac{R_0^2}{R_1^2} \right) + \frac{1}{6} \left(1 - \frac{R_0}{R_1} \right)^2 \right\} \right] A_{01}$$

$$+ \frac{A}{6\pi} \left(1 - \frac{R_0^2}{R_1^2} \right) A_{11} + \frac{A}{10\pi} \left(1 - \frac{R_0}{R_1} \right)^2 A_{21}$$

$$+ \frac{1}{2\pi} \sum_{n=1}^{N} I_n^2 A_{n1} - \frac{1}{6A} \left(1 - \frac{R_0}{R_1} \right) \left(1 - \frac{R_0^3}{R_1^3} \right) a_1$$

$$- \frac{1}{16A^2} \left(1 - \frac{R_0}{R_1} \right)^2 \left(1 - \frac{R_0^2}{R_1^2} \right) b_1 + \frac{1}{4A} \left(1 - \frac{R_0}{R_1} \right) \left(1 - \frac{R_0^2}{R_1^2} \right) \mu \theta_0$$

$$= \frac{1}{3A} \left(1 - \frac{R_0^3}{R_1^3} \right) \mu - \frac{1}{4A} \left(1 - \frac{R_0^2}{R_1^2} \right) \frac{R_0}{R_1} \mu \epsilon \qquad (E10)$$

47

4) $$\frac{1}{\pi} \int_{0}^{2\pi} M^*(\Psi_b) \sin \Psi_b \, d\Psi_b = 0$$

Substituting for M^*

$$\left[-I_o^2 + A \left\{ \frac{1}{2} \left(1 - \frac{R_0^2}{R_1^2} \right) + \frac{1}{6} \left(1 - \frac{R_0}{R_1} \right)^2 \right\} \right] B_{01}$$

$$+ \frac{A}{6\pi} \left(1 - \frac{R_0^2}{R_1^2} \right) B_{11} + \frac{A}{10\pi} \left(1 - \frac{R_0}{R_1} \right)^2 B_{21}$$

$$+ \frac{1}{2\pi} \sum_{n=1}^{N} I_n^2 B_{nl} + \frac{1}{4A} \left(1 - \frac{R_0}{R_1} \right) \left(1 - \frac{R_0^2}{R_1^2} \right) a_o$$

$$+ \frac{1}{16A^2} \left(1 - \frac{R_0}{R_1} \right)^2 \left(1 - \frac{R_0^2}{R_1^2} \right) a_1 - \frac{1}{6A} \left(1 - \frac{R_0}{R_1} \right) \left(1 - \frac{R_0^3}{R_1^3} \right) b_1$$

$$= -\frac{1}{8A^2} \left(1 - \frac{R_0}{R_1} \right) \left(1 - \frac{R_0^2}{R_1^2} \right) \mu \epsilon \tag{E11}$$

48

APPENDIX F

AIRFOIL WITH OSCILLATORY DOWNWASH

The coordinate system for the airfoil is shown in figure 2. Under the assumption of small disturbances, the perturbation pressure p satisfies the Laplace equation

$$\frac{\partial^2 p}{\partial x^2} + \frac{\partial^2 p}{\partial y^2} = 0$$

Since oscillatory downwash is considered, the complex exponential notation is adopted.

$$p(x,y,t) = \bar{p}(x,y) \, e^{i\omega t}$$

$$v_a(x,t) = \bar{v}_a(x) \, e^{i\omega t}$$

$$\frac{Dv_a}{Dt} = \left(i\omega \bar{v}_a + U \frac{d\bar{v}_a}{dx} \right) e^{i\omega t}$$

where ω is the frequency of oscillation and v_a the downwash on the airfoil surface. The boundary value problem is posed as follows.

$$\nabla^2 p = 0$$

$$-\frac{1}{\rho}\frac{\partial p}{\partial y} = \frac{Dv_a}{Dt} \quad \text{on the surface}$$

$$p \to 0 \quad \text{as } (x^2 + y^2) \to \infty \tag{F1}$$

p singular at the leading edge such that

$$v(x,t) = v_a(x,t) \quad \text{on the surface}$$

The pressure gradient condition ensures that the flow has the correct curvature on the surface. It is then sufficient to satisfy the normal velocity condition at any one point, such as the leading edge.

The complete solution can be separated into a singular part and a regular part

$$p = p_{sing} + p_{reg}$$

The singular part, p_{sing}, which satisfies the condition $-\frac{1}{\rho}\frac{\partial p}{\partial y} = 0$ on the surface, is singular at the leading edge. The regular part, p_{reg}, is continuous everywhere and satisfies $-\frac{1}{\rho}\frac{\partial p}{\partial y} = \frac{DV_a}{Dt}$ on the surface. For an airfoil at rest in steady flow, $\frac{DV_a}{Dt} = 0$, and the solution contains only a singular part. In terms of elliptic coordinates (η,ϕ), the singular solution can be shown to be (see ref. 17)

$$\bar{p}_{sing}(\eta,\phi) = \bar{g}\,\frac{\sin\phi}{\cosh\eta + \cos\phi} \qquad (F2)$$

where $\bar{g}$ is a constant to be determined. The elliptic coordinates are described by the relations

$$x = b\cosh\eta\cos\phi$$

$$y = b\sinh\eta\sin\phi$$

The regular solution can be obtained by separation of variables

$$\frac{1}{\rho U^2}\,\bar{p}_{reg} = H(\eta)\,\Phi(\phi)$$

Substitution into the Laplace equation yields the ordinary differential equations

$$H'' - n^2 H = 0$$

$$\Phi'' + n^2 \Phi = 0$$

50

for which the general solutions are

$$H = C_1 e^{n\eta} + C_2 e^{-n\eta}$$

$$\Phi = C_3 \sin n\phi + C_4 \cos n\phi$$

For the solution to be periodic in ϕ and antisymmetric about $\phi = 0, \pi$ the sine solutions above are admissible for ϕ and n must be an integer. For the solution to die out at infinity, only the negative exponential solution can be used for H. The regular solution is then of the form

$$\frac{1}{\rho U^2} \bar{P}_{reg} = \sum_{n=1}^{\infty} a_n e^{-n\eta} \sin n\phi \qquad (F3)$$

Applying the pressure gradient condition,

$$\frac{1}{\rho U^2} \frac{\partial \bar{P}_{reg}}{\partial \eta}\bigg|_{\eta=0} = -\sum_{n=1}^{\infty} n\, a_n \sin n\phi$$

$$= -\left[ik\, \frac{\bar{v}_a}{U} \sin\phi + \frac{\partial}{\partial\phi}\left(\frac{\bar{v}_a}{U}\right) \right]$$

from which the coefficients are obtained as

$$a_n = \frac{2}{n\pi} \int_0^{\pi} \left[ik\, \frac{\bar{v}_a}{U} \sin\phi - \frac{\partial}{\partial\phi}\left(\frac{\bar{v}_a}{U}\right) \right] \sin n\phi\, d\phi \qquad (F4)$$

where $k = \omega b/U$ is the reduced frequency.

It only remains to determine the constant $\bar{g}$ and this is done by applying the normal velocity condition

$$-\frac{1}{\rho} \int_{-\infty}^{t} \frac{\partial p}{\partial y_o}\bigg|_{y_o=0} \, dt_o = v_a(x,t)$$

The integration is conducted along the linearized trajectory of the fluid particle, given by

$$x_o = x + U(t_o - t)$$

$$y_o = 0$$

Hence,

$$\omega t_o = \omega t + \frac{\omega}{U}(x_o - x)$$

$$p(x_o, y_o, t_o) = \bar{p}(x_o, y_o) \, e^{i\omega t_o}$$

$$= \bar{p}(x_o, y_o) \, e^{i\omega t} \, e^{ik(x_o - x)/b}$$

Integrating up to the leading edge $\frac{x}{b} = -1$,

$$\frac{\bar{v}_a}{U}\bigg|_{\frac{x}{b} = -1} = -e^{ik} \int_{-\infty}^{-1} \frac{\partial}{\partial\left(\frac{y_o}{b}\right)}\left(\frac{\bar{p}}{\rho U^2}\right)\bigg|_{y_o = 0} e^{ikx_o/b} \, d\left(\frac{x_o}{b}\right)$$

Substituting for the pressure, and letting

$$f_n(k) \equiv \int_0^\infty e^{-ik \cosh \eta} e^{-n\eta} \, d\eta$$

the condition becomes

$$-\frac{\bar{v}_a(-b)}{U} e^{-ik} = \bar{g} \int_0^\infty \frac{e^{-ik \cosh \eta}}{(\cosh \eta - 1)} \, d\eta - \sum_{n=1}^\infty (-1)^n n a_n f_n$$

The integral on the right is divergent and it is shown in Appendix H that

$$\text{Finite Part} \left\{ \int_0^\infty \frac{e^{-ik \cosh \eta}}{(\cosh \eta - 1)} \, d\eta \right\} = \frac{i\pi k}{2} \left[H_1^{(2)}(k) + i H_0^{(2)}(k) \right]$$

which yields

$$\bar{g} = \frac{2}{i\pi k \left[H_1^{(2)}(k) + i H_0^{(2)}(k) \right]} \left[-\frac{\bar{v}_a(-b)}{U} e^{-ik} + \sum_{n=1}^\infty (-1)^n n a_n f_n \right] \qquad (F5)$$

The solution for the pressure field is complete and associated quantities can be derived, e.g. Sectional lift:

$$\frac{\bar{\ell}}{\rho U^2 b} = \int_0^{2\pi} \frac{\bar{p}}{\rho U^2} (-\sin\phi) \, d\phi = -2\pi(\bar{g} + \tfrac{1}{2} a_1) \qquad (F6)$$

The final expression for the surface pressure differential is

$$\frac{\Delta \bar{P}_a}{\rho U^2} = \frac{\bar{P}_{upper} - \bar{P}_{lower}}{U^2}$$

$$= \frac{4}{i\pi k \left[H_1^{(2)}(k) + i H_0^{(2)}(k) \right]} \left[-\frac{\bar{v}_a(-b)}{U} e^{-ik} + \sum_{n=1}^{\infty} (-1)^n n a_n f_n \right] \sqrt{\frac{1-x}{1+x}}$$

$$+ 2 \sum_{n=1}^{\infty} a_n \sin n\phi \qquad\qquad\qquad (F7)$$

where $x = \cos \phi$.

This formulation will now be applied to two specific cases of oscillatory downwash so that the results obtained may be compared with available results obtained using the velocity potential approach.

(1)   Harmonic pitching and heaving:
If $\bar{h}$ and $\bar{\alpha}$ denote the amplitudes of the heaving and pitching motions and a the pitch axis location,

$$\frac{\bar{v}_a(x)}{U}(x) = -\bar{\alpha} - ik \left[\bar{h} + (x-a) \bar{\alpha} \right]$$

It can be shown that

$$a_1 = -2 ik \bar{\alpha} + k^2 (\bar{h} + a \bar{\alpha})$$

$$a_2 = \frac{k^2 \bar{\alpha}}{4}$$

$$a_n = 0 \qquad (n \geq 3)$$

$$f_1 = -\frac{\pi}{2} H_1^{(2)}(k) - \frac{e^{-ik}}{ik}$$

$$f_2 = -\frac{2}{ik} e^{-ik} + \frac{2}{k^2} e^{-ik} - \frac{\pi}{2}\left[H_1^{(2)}(k) + iH_0^{(2)}(k)\right]$$

$$+ \pi\left(\frac{1}{2} - \frac{1}{ik}\right) H_1^{(2)}(k)$$

$$\frac{\bar{v}_a(-b)}{U} = -\bar{\alpha} - ik\left[\bar{h} - (1+a)\,\bar{\alpha}\right]$$

It follows that

$$\bar{g} = C(k)\left[-\bar{\alpha} - ik\bar{h} - ik\bar{\alpha}\left(\frac{1}{2} - a\right)\right] + \frac{ik\bar{\alpha}}{2}$$

$$\text{where} \quad C(k) \equiv \frac{H_1^{(2)}(k)}{H_1^{(2)}(k) + iH_0^{(2)}(k)}$$

$$\frac{\Delta\bar{P}_a}{\rho U^2} = \sqrt{\frac{1-x}{1+x}}\ \left[2C(k)\left\{-\bar{\alpha} - ik\bar{h} + ik\bar{\alpha}\left(a - \frac{1}{2}\right)\right\}\right.$$

$$\left. - 3ik\,\bar{\alpha} + 2k^2\left(\bar{h} - a\bar{\alpha}\right)\right]$$

$$+ x\sqrt{\frac{1-x}{1+x}}\ \left[-4\,ik\,\bar{\alpha} + 2k^2\left(\bar{h} - a\bar{\alpha}\right) + k^2\bar{\alpha}\right]$$

$$+ x^2\sqrt{\frac{1-x}{1+x}}\ \left[k^2\bar{\alpha}\right] \tag{F8}$$

This result can be shown to be identical with that calculated by the vortex approach (ref. 30, eq. 5-342).

(2) Stationary airfoil in a steady stream with a sinusoidal vertical gust:
If $\bar{v}_g$ denotes the amplitude of the gust, then

$$\frac{v_a(x,t)}{U} = - \bar{v}_g \, e^{-ikx} \, e^{i\omega t}$$

$$\frac{Dv_a}{Dt} = 0$$

Hence the problem contains only a singular solution and it can be shown that

$$\bar{g} = \frac{2\bar{v}_g}{i\pi k \left[H_1^{(2)}(k) + iH_0^{(2)}(k) \right]}$$

$$\frac{\bar{\ell}}{\rho U^2 b} = 2\pi \bar{g} = - \frac{4\bar{v}_g}{ik \left[H_1^{(2)}(k) + iH_0^{(2)}(k) \right]} \tag{F9}$$

The corresponding result from the velocity potential approach (ref. 30 eq. 5-376) is

$$\frac{\bar{\ell}}{\rho U^2 b} = 2\pi \bar{v}_g \left[C(k) \left\{ J_0(k) - iJ_1(k) \right\} + iJ_1(k) \right] \tag{F10}$$

The two results appear to be different, but the second can be reduced as follows.

$$C(k) \left[J_0(k) - iJ_1(k) \right] + iJ_1(k)$$

$$= \frac{i}{H_1^{(2)}(k) + iH_0^{(2)}(k)} \left[J_1(k) Y_0(k) - J_0(k) Y_1(k) \right]$$

Using the recurrence relations for cross products of Bessel functions (ref. 31, 9.1.32 and 9.1.34), the expression inside the square bracket can be shown to be equal to (2/ k). The result for the lift becomes

$$\frac{\bar{\ell}}{\rho U^2 b} = - \frac{4\bar{v}_g}{ik\left[H_1^{(2)}(k) + iH_0^{(2)}(k)\right]}$$

which is identical with the result of the pressure method.

APPENDIX G

HIGH ASPECT RATIO WING WITH OSCILLATORY DOWNWASH

The coordinate system used for the straight, rectangular wing is shown in figure 4. The linearized boundary value problem can be stated as

$$
\left.
\begin{aligned}
&\nabla^2 p = 0 \\[2em]
&p \to 0 \text{ as } (x^2 + y^2 + z^2) \to \infty \\[2em]
&\frac{\partial p}{\partial y} = -\frac{1}{\rho}\frac{Dv_a}{Dt} \quad \text{on the wing surface} \\[2em]
&p \to -\infty \text{ along the leading edge such that} \\[2em]
&-\frac{1}{\rho}\int_{-\infty}^{t} \frac{\partial p}{\partial y_a}\bigg|_{y_a=0} dt_o = v_a(x,z,t) \text{ on the wing}
\end{aligned}
\right\}
\tag{G1}
$$

A solution is required for wings of large aspect ratio, A. The aim of the analysis will be to obtain an approximate solution by neglecting all terms of order greater than $O(A^{-1})$.

The near field solution. - In the vicinity of the wing surface, excluding the tip regions, it is assumed that the characteristic length for spanwise variations is the span while the characteristic length for variations in the other two directions is the chord. The Laplace equation is then written as,

$$
\frac{\partial^2 p}{\partial\left(\frac{x}{b}\right)^2} + \frac{\partial^2 p}{\partial\left(\frac{y}{b}\right)^2} = -\frac{1}{A^2}\frac{\partial^2 p}{\partial\left(\frac{z}{s}\right)^2}
$$

where, by the above assumption, the partial derivatives are of the same order. In the limit $A \to \infty$, the near field is a solution of the two-dimensional Laplace equation. For the large aspect ratio wing, the asymptotic expansion

$$
p = p_0 + \frac{1}{A}p_1 + \cdots
$$

shows that, neglecting terms of order greater than $O(A^{-1})$, the near field is still described by the two-dimensional Laplace equation,

$$\frac{\partial^2 p_{near}}{\partial x^2} + \frac{\partial^2 p_{near}}{\partial y^2} = 0$$

with the conditions

$$\frac{\partial p_{near}}{\partial y} = -\rho \frac{D v_a}{Dt}$$

on the wing $p_{near} \rightarrow -\infty$ at the leading edge such that $v(x,z\ t) = v_a(x,z,t)$. As shown in Appendix F, the general solution is

$$\frac{1}{\rho U^2} p_{near} = g(z,t) \frac{\sin \phi}{\cosh \eta + \cos \phi}$$

(G2)

$$+ \sum_{n=1}^{\infty} \left[a_n(z,t) e^{-n\eta} + b_n(z,t) e^{n\eta} \right] \sin n\phi$$

the positive exponent being retained since there is no condition at infinity. The coefficients are given by

$$a_n - b_n = \frac{2}{n\pi} \int_0^{\pi} \frac{D}{D\left(\frac{Ut}{b}\right)} \left(\frac{v_a}{U}\right) \sin \phi \, \sin n \, \phi \, d\phi$$

It can be shown that the far-field behavior of the near field solution is described by

$$\underset{\frac{r}{b} \to \infty}{\text{Lim}} \quad \frac{P_{near}}{\rho U^2} = g(z,t) \frac{\sin \chi}{r/b}$$

$$+ \sum_{n=1}^{\infty} \left[a_n \left(\frac{r}{2b}\right)^{-n} + b_n \left(\frac{r}{2b}\right)^{n} \right] \sin n\chi$$

where r and χ are cylindrical coordinates.

The far field solution. - At large distances from the wing, the characteristic length can be taken to be the span for variations in all directions. The far field problem is p_{far} singular along the line, x = y = 0 (-s ≤ z ≤ s), and antisymmetric relative to the plane y = 0.

$$\nabla^2 P_{far} = 0$$

(G3)

$$P_{far} \to 0 \text{ as } (x^2 + y^2 + z^2) \to \infty$$

As shown in Appendix B, the far field solution to $O(A^{-1})$ is that of a line of dipoles along the mid-chord of the wing.

$$\frac{P_{far}}{\rho U^2} = \frac{\sin \chi}{2\pi} \frac{1}{\pi} \int_{-1}^{1} f_1(\zeta^*,t) \, d\zeta^* \int_{0}^{\infty} q K_1(qr^*) \cos \left\{ q(\zeta^* - z^*) \right\} dq$$

(G4)

where the starred variables are non-dimensional with respect to the semi-span, s.

$$\underset{r^* \to 0}{\text{Lim}} \quad K_1(qr^*) = \frac{1}{qr^*}$$

The near field behavior of the far field solution is described by

$$\lim_{r^* \to 0} \frac{P_{far}}{\rho U^2} = \frac{\sin \chi}{2\pi r^*} \frac{1}{\pi} \int_{-1}^{1} f_1(\zeta^*,t)\, d\zeta^* \int_{0}^{\infty} \cos\left\{q(\zeta^*-z^*)\right\} dq$$

$$= \frac{\sin \chi}{2\pi r^*} f_1(z^*,t)$$

The matching condition. - In order to construct a composite solution that tends correctly to the near and far field solutions in the respective regions, and varies smoothly from one to the other, it is required that

$$\lim_{\frac{r}{b} \to \infty} P_{near} = \lim_{\frac{r}{s} \to 0} P_{far}$$

By inspecting the limiting behavior of the solutions, it is seen that

$$f_1(z^*,t) = \frac{2\pi}{A}\left[g(z^*,t) + \frac{1}{2} a_1(z^*,t)\right]$$

$$b_n(z^*,t) = 0 \text{ for all } n$$

The composite solution is written as

$$p = p_{near} + p_{far} - p_{common}$$

where

$$P_{common} = \underset{\substack{r \to \infty \\ b}}{\text{Lim}} \; P_{near} = \underset{\substack{r \to 0 \\ s}}{\text{Lim}} \; P_{far}$$

The composite solution to $O(A^{-1})$ is

$$\frac{p}{\rho U^2} = g(z^*,t) \frac{\sin \phi}{\cosh \eta + \cos \phi} + \sum_{n=1}^{\infty} a_n(z^*,t) e^{-n\eta} \sin n\phi$$

$$+ \frac{\sin \chi}{2\pi} \frac{1}{\pi} \int_{-1}^{1} \left[g(\zeta^*,t^*) + \frac{1}{2} a_1(\zeta^*,t) \right] d\zeta^* \int_{0}^{\infty} q k_1 (qr^*) \cos \left\{ q(\zeta^* - z^*) \right\} dq$$

$$- \left[g(z^*,t) + \frac{1}{2} a_1(z^*,t) \right] \frac{\sin \chi}{Ar^*} \tag{G5}$$

Since the problem pertains to oscillatory downwash, all quantities will be assumed to have complex exponential time dependence. The sectional lift is given by

$$\frac{\bar{\ell}}{\rho U^2 b} (z^*) = -2 \int_{-1}^{1} \frac{\bar{p}}{\rho U^2} \Bigg|_{y=0} dx = -2\pi \left[\bar{g} + \frac{1}{2} a_1 \right]$$

which confirms the result of matching, viz that the dipole strength distribution is proportional to the sectional lift. The unknown function $\bar{g}$ (z*) is to be determined by applying the normal velocity boundary condition,

$$-\frac{1}{\rho} \int_{-\infty}^{t} \frac{\partial p}{\partial y_0} \Bigg|_{y_0=0} dt_0 = v_a(x,z,t)$$

62

where the integration is along the linearized trajectory

$$y_o = 0$$

$$z_o = z$$

$$x_o = x + U(t_o - t)$$

Integrating up to the midchord line, the condition becomes

$$\frac{\bar{v}_a(0, z^*)}{U} = -\int_{-\infty}^{0} \frac{\partial}{\partial\left(\frac{y_o}{b}\right)} \left(\frac{\bar{p}}{\rho U^2}\right)\Bigg|_{y_o = 0} e^{ikx_o/b} \, d\left(\frac{x_o}{b}\right)$$

Substituting for the pressure gradient, letting $\xi = -\dfrac{x_o}{b} = Ar^*$ and rearranging, the equation can be written as

$$\frac{-2}{i\pi k \left[H_1^{(2)}(k) + iH_0^{(2)}(k)\right]} \left[\frac{\bar{v}_a(0,z^*)}{U} - \sum_{n=1}^{\infty} (-1)^n n\bar{a}_n(z^*) f_n \right.$$

$$\left. - \sum_{n=1}^{\infty} n\bar{a}_n(z^*) \int_{\pi/2}^{\pi} e^{ik\cos\phi}\sin n\phi \, d\phi \right] + \frac{1}{2}\bar{a}_1(z^*)$$

$$= \bar{g}(z^*) + \frac{1}{2}\bar{a}_1(z^*)$$

$$+ \frac{2}{i\pi k \left[H_1^{(2)}(k) + iH_0^{(2)}(k)\right]} \frac{1}{2\pi} \left[\frac{\bar{\ell}(z^*)}{\rho U^2 b} \int_0^{\infty} \frac{e^{-ik\xi}}{\xi^2} \, d\xi \right.$$

$$\left. - \frac{1}{\pi A} \int_{-1}^{1} \frac{\bar{\ell}(\zeta^*)}{\rho U^2 b} \, d\zeta^* \int_0^{\infty} q\cos\left\{q(\zeta^* - z^*)\right\} dq \int_0^{\infty} \frac{K_1\left(\frac{q\xi}{A}\right)}{\xi} e^{-ik\xi} \, d\xi \right]$$

The left hand side, when multiplied by -2π, is seen to be the expression for sectional lift from two-dimensional theory (Appendix F), and will be denoted by $\dfrac{\bar{\ell}^{2D}}{\rho U^2 b}(z^*)$. The first term on the right is the actual sectional lift, to the order of approximation considered here, viz $O(A^{-1})$. The second term on the right can be put into a more convenient form, as shown in Appendix H. The result is the following integral equation for the sectional lift distribution.

$$
\frac{\bar{\ell}^{2D}(z^*)}{\rho U^2 b} = \frac{\bar{\ell}(z^*)}{\rho U^2 b}
$$

$$
- \frac{1}{i\pi k \left[H_1^{(2)}(k) + i H_0^{(2)}(k) \right]} \int_{-1}^{1} \frac{d}{d\zeta^*} \left(\frac{\bar{\ell}}{\rho U^2 b} \right) d\zeta^* \times
$$

$$
\int_0^\infty \frac{e^{-ik\xi}}{\xi^2} \left[\frac{A(\zeta^*-z^*)}{\sqrt{\xi^2 + A^2(\zeta^*-z^*)^2}} - \frac{(\zeta^*-z^*)}{|\zeta^*-z^*|} \right] d\xi \qquad (G6)
$$

The integral term represents the effect of finite span to $O(A^{-1})$. In kernel form,

$$
\frac{\bar{\ell}^{2D}(z^*)}{\rho U^2 b} = \frac{\bar{\ell}(z^*)}{\rho U^2 b} - \frac{1}{i\pi k \left[H_1^{(2)} + i H_0^{(2)} \right]} \int_{-1}^{1} \frac{d}{d\zeta^*} \left(\frac{\bar{\ell}}{\rho U^2 b} \right) K\left[kA(\zeta^*-z^*) \right] d\zeta^*
$$

where

$$
K(\tau) = k \int_0^\infty \frac{e^{-i\lambda}}{\lambda^2} \left[\frac{\tau}{\sqrt{\lambda^2 + \tau^2}} - \frac{\tau}{|\tau|} \right] d\lambda
$$

64

Integrating by parts,

$$K(\tau) = -ik \int_0^\infty \frac{e^{-i\lambda}}{\lambda} \left[\frac{\lambda}{\sqrt{\lambda^2 + \tau^2}} - \frac{|\tau|}{\tau} \right] d\lambda$$

$$-k\tau \int_0^\infty \frac{e^{-i\lambda} \, d\lambda}{(\lambda^2 + \tau^2)^{3/2}}$$

$$= -ik \, N_C(\tau) - k \, N_B(\tau) \tag{G7}$$

The functions N_B and N_C are the same as those discussed by Ashley, et al. in reference 32 and can be expressed in terms of special functions.

$$N_B(\tau) = \frac{1}{\tau} - i + i\frac{\pi}{2}\left[I_1(|\tau|) - L_1(|\tau|)\right]\frac{|\tau|}{\tau}$$

$$+ \left[\frac{|\tau|}{\tau} K_1(|\tau|) - \frac{1}{\tau}\right]$$

$$N_C(\tau) = \gamma + i\frac{\pi}{2} + \ln(2|\tau|)$$

$$- i\frac{|\tau|}{\tau} \int_0^{|\tau|} \left[K_0(x) + i\frac{\pi}{2}\left\{L_0(x) - I_0(x)\right\}\right] dx$$

where I_n and K_n are the modified Bessel functions of the first and second kind and L_n the modified Struve function.

Reduction to the case $k=0$. – In the limit $k \to 0$, the following limiting values are valid.

$$i \pi k \left[H_1^{(2)}(k) + i H_0^{(2)}(k) \right] \to -2$$

$$N_B(\tau) \to \frac{1}{\tau} - i$$

$$N_C(\tau) \to \gamma + \ln(2 |\tau|) + i \frac{\pi}{2}$$

$$K(\tau) \to -\frac{k}{\tau} = -\frac{1}{A(\zeta^* - z^*)}$$

The integral equation becomes

$$\frac{\bar{\ell}^{2D}(z^*)}{\rho U^2 b} = \frac{\bar{\ell}(z^*)}{\rho U^2 b} - \frac{1}{2A} \int_{-1}^{1} \frac{d}{d\zeta^*} \left(\frac{\bar{\ell}}{\rho U^2 b} \right) \frac{d\zeta^*}{\zeta^* - z^*}$$

which is the same as Prandtl's result for a high aspect ratio wing in steady flow.

Comparison with Reissner's result. – Reissner (ref. 19) represents the wing by a distribution of vorticity on the planform and in the wake, and then applies standard lifting-line approximations to the downwash integral. The basic result of this analysis is an integral equation for the spanwise variation of the reduced circulation.

$$\frac{\bar{\Omega}^{2D}(z^*)}{U} = \frac{\bar{\Omega}(z^*)}{U} \frac{J_0(k) - i J_1(k)}{i \pi k \left[H_1^{(2)}(k) + i H_0^{(2)}(k) \right]} \int_{-1}^{1} \frac{d}{d\zeta^*} \left(\frac{\bar{\Omega}}{U} \right) K \left[kA(\zeta^* - z^*) \right] d\zeta^* \quad (G8)$$

where $\bar{\Omega} = e^{ik} \bar{\Gamma}$ and $\bar{\Gamma}$ is the bound circulation. Unlike steady flow, the lift distribution in unsteady flow is not completely determined by the bound circulation. However, the result of the pressure method can be compared numerically with Reissner's result. Numerical results for the latter, for the case of a uniformly pitching rectangular wing, are presented in reference 20, and the comparison is tabulated as follows.

Reduced frequency, k	Spanwise coordinate, z^*	Asymptotic lift derivative, $\dfrac{\bar{\ell}/\bar{\alpha}}{\rho U^2 b}$	Reissner's lift derivative, $\dfrac{\bar{\ell}/\bar{\alpha}}{\rho U^2 b}$
Aspect ratio, A = 3			
0.167	0.0	4.087 + 0.355i	4.126 + 0.496i
0.167	0.4	3.899 + 0.362i	3.926 + 0.454i
0.167	0.8	2.961 + 0.324i	3.002 + 0.314i
0.333	0.0	3.848 + 0.993i	3.914 + 1.072i
0.333	0.4	3.693 + 0.986i	3.746 + 1.082i
0.333	0.8	2.894 + 0.835i	2.946 + 0.948i
0.667	0.0	3.625 + 2.537i	3.674 + 2.620i
0.667	0.4	3.533 + 2.490i	3.566 + 2.602i
0.667	0.8	3.049 + 2.091i	3.034 + 2.258i
Aspect ratio, A = 6			
0.167	0.0	4.659 + 0.083i	4.668 + 0.086i
0.167	0.4	4.533 + 0.129i	4.558 + 0.156i
0.167	0.8	3.712 + 0.244i	3.810 + 0.278i
0.333	0.0	4.203 + 0.792i	4.242 + 0.802i
0.333	0.4	4.120 + 0.833i	4.146 + 0.860i
0.333	0.8	3.479 + 0.872i	3.570 + 0.936i
0.667	0.0	3.809 + 2.508i	3.836 + 2.516i
0.667	0.4	3.766 + 2.517i	3.782 + 2.544i
0.667	0.8	3.389 + 2.353i	3.450 + 2.452i

It is seen that the two sets of results are quite close, although it is difficult to associate the observed deviations between the two possible causes, viz the numerical calculation process and actual differences in the two equations.

An unsteady lifting line theory has also been derived by James (ref. 33), using the acceleration potential approach. This result should be directly comparable to the one derived here. However, it has been pointed out recently (ref. 34) that James' results are in error and hence this comparison was not carried out.

APPENDIX H

MISCELLANEOUS INTEGRALS

Evaluation of the integral (see Appendix F). -

$$I = \int_0^\infty \frac{e^{-ik\cosh\eta}}{\cosh\eta - 1}\, d\eta$$

As it stands, the integral is divergent, but the divergent part can be isolated by writing

$$I = \int_0^\infty \frac{\left(e^{-ik\cosh\eta} - e^{-ik}\right)}{\cosh\eta - 1}\, d\eta + \int_0^\infty \frac{e^{-ik}\, d\eta}{\cosh\eta - 1}$$

$$= I_1 + I_2$$

where I_2 is divergent. The integrand in I_1 is indeterminate, of the 0/0 form at the lower limit, but application of L' Hospital's rule shows it to be finite.

$$I_1 = \int_1^\infty \frac{\left(e^{-ik\xi} - e^{-ik}\right) d\xi}{(\xi - 1)\sqrt{\xi^2 - 1}}$$

Using

$$\frac{d\xi}{(\xi - 1)\sqrt{\xi^2 - 1}} = -d\left(\sqrt{\frac{\xi+1}{\xi-1}}\right)$$

$$I_1 = -\int_1^\infty \left(e^{-ik\xi} - e^{-ik} \right) d\left(\sqrt{\frac{\xi+1}{\xi-1}} \right)$$

$$= \left[e^{-ik\xi} - e^{-ik} \right] \sqrt{\frac{\xi+1}{\xi-1}} \Bigg|_{\xi \to \infty} - ik \int_1^\infty \left(\sqrt{\frac{\xi+1}{\xi-1}} - 1 \right) e^{ik\xi} \, d\xi - ik \int_1^\infty e^{-ik\xi} \, d\xi$$

Since $\displaystyle \lim_{\xi \to \infty} \sqrt{\frac{\xi+1}{\xi-1}} = 1$

The first integral on the right can be expressed in terms of Hankel functions

$$I_1 = \frac{i\pi k}{2} \left[H_1^{(2)}(k) + iH_0^{(2)}(k) \right] + e^{-ik}$$

The finite part of I_2 can be extracted by recognizing it as the integral that would appear in the case of steady flow (ref. 17). This value of the finite part of I_2 is -1, thus

$$I = I_1 + e^{-ik}(-1)$$

$$= \frac{i\pi k}{2} \left[H_1^{(2)}(k) + iH_0^{(2)}(k) \right]$$

Simplification of the expression (see Appendix G). -

$$I_{fs} = -\frac{1}{\pi A} \int_{-1}^{1} \frac{\bar{\ell}(\zeta^*)}{\rho U^2 b} \, d\zeta^* \int_{0}^{\infty} q \cos\left\{ q(\zeta^* - z^*) \right\} dq \int_{0}^{\infty} \frac{K_1\left(\frac{q\xi}{A}\right)}{\xi} e^{-ik\xi} \, d\xi$$

$$+ \frac{\bar{\ell}(z^*)}{\rho U^2 b} \int_{0}^{\infty} \frac{e^{-ik\xi}}{\xi^2} \, d\xi$$

$$= (I_{fs})_1 + (I_{fs})_2$$

Letting $u \equiv \dfrac{q\xi}{A}$

$$(I_{fs})_1 = -\frac{A}{\pi} \int_{-1}^{1} \frac{\bar{\ell}(\zeta^*)}{\rho U^2 b} \, d\zeta^* \int_{0}^{\infty} \frac{e^{-ik\xi}}{\xi^3} \, d\xi \int_{0}^{\infty} u \cos\left\{ \frac{uA}{\xi} (\zeta^* - z^*) \right\} K_1(u) \, du$$

$$= -\frac{A}{\pi} \int_{-1}^{1} \frac{\bar{\ell}(\zeta^*)}{\rho U^2 b} \, d\zeta^* \int_{0}^{\infty} \frac{e^{-ik\xi}}{\xi^3} \, d\xi \int_{0}^{\infty} u \cos\left\{ \frac{uA}{\xi} (\zeta^* - z^*) \right\} d\left[-K_0(u) \right]$$

70

The integral with respect to u is to be interpreted as

$$\int_0^\infty f(u)\, du = \lim_{\beta \to 0} \int_0^\infty f(u)\, e^{-\beta u}\, du$$

$$(I_{fs})_1 = \frac{A}{\pi} \int_0^\infty \frac{e^{-ik\xi}}{\xi^3}\, d\xi \int_0^\infty \left[-K_0(u)\right] du \int_{-1}^1 \frac{\bar{\ell}(\zeta^*)}{\rho U^2 b}\left[\cos\left\{\frac{uA}{\xi}(\zeta^* - z^*)\right\} d\zeta^*\right.$$

$$\left. + (\zeta^* - z^*)\, d\left[\cos\left\{\frac{uA}{\xi}(\zeta^* - z^*)\right\}\right]\right]$$

Making use of $\bar{\ell}(\pm 1) = 0$,

$$(I_{fs})_1 = -\frac{A}{\pi} \int_{-1}^1 (\zeta^* - z^*) \frac{d}{d\zeta^*}\left(\frac{\bar{\ell}}{\rho U^2 b}\right) d\zeta^* \int_0^\infty \frac{e^{-ik\xi}}{\xi^3}\, d\xi \int_0^\infty \left[-K_0(u)\right] \cos\left\{\frac{uA}{\xi}(\zeta^* - z^*)\right\} du$$

The inner integral can be evaluated as (ref. 31)

$$\int_0^\infty K_0(u) \cos\left\{\frac{uA}{\xi}(\zeta^* - z^*)\right\} du = \frac{\pi}{2}\left[1 + \left(\frac{A}{\xi}\right)^2 (\zeta^* - z^*)^2\right]^{-1/2}$$

$$(I_{fs})_2 = \left[\int_0^\infty \frac{e^{-ik\xi}}{\xi^2}\, d\xi\right]\left[-\frac{1}{2}\int_{-1}^1 \frac{d}{d\zeta^*}\left(\frac{\bar{\ell}}{\rho U^2 b}\right)\frac{(\zeta^* - z^*)}{|\zeta^* - z^*|}\, d\zeta^*\right]$$

$$I_{fs} = \frac{1}{2}\int_{-1}^1 \frac{d}{d\zeta^*}\left(\frac{\bar{\ell}}{\rho U^2 b}\right) d\zeta^* \int_0^\infty \frac{e^{-ik\xi}}{\xi^2}\left[\frac{A(\zeta^* - z^*)}{\sqrt{\xi^2 + A^2(\zeta^* - z^*)^2}} - \frac{(\zeta^* - z^*)}{|\zeta^* - z^*|}\right] d\xi$$

REFERENCES

1. Stepniewski, W.Z.: Rotary-Wing Aerodynamics, Vol. I - Basic Theories of Rotor Aerodynamics (With Application to Helicopters). NASA CR-3082, January 1979.

2. Baskin, V.E.; Vil'dgrube, L.S.; Vozhdayev, Ye.S.; and Maykapar, G.I.: Theory of the Lifting Airscrew. NASA TT F-823, February 1976.

3. Theodorsen, T.: General Theory of Aerodynamic Instability and the Mechanism of Flutter. NACA Rep. 496, 1935.

4. Greenberg, J.M.: Airfoil in Sinusoidal Motion in a Pulsating Stream. NACA TN 1326, June 1947.

5. Gormont, R.E.: A Mathematical Model of Unsteady Aerodynamics and Radial Flow for Application to Helicopter Rotors. USAAMRDL-TR-72-67, May 1973.

6. Willmer, M.A.P.: The Loading of Helicopter Rotor Blades in Forward Flight. R.&M. 3318, British A.R.C., April 1959.

7. Piziali, R.A.: Method for the Solution of the Aeroelastic Response Problem for Rotary Wings. J. Sound & Vib., vol. 4, no. 3, 1966, pp. 445-489.

8. Daughaday, H.; and Piziali, R.A.: An Improved Computational Model for Predicting the Unsteady Aerodynamic Loads of Rotor Blades. J. American Helicopter Soc., vol. 11, October 1966, pp. 3-10.

9. Miller, R.H.: Theoretical Determination of Rotor Blade Harmonic Airloads. ASRL TR 107-2, M.I.T., August 1964.

10. Landgrebe, A.J.: An Analytical Method for Predicting Rotor Wake Geometry. J. American Helicopter Soc., October 1969, pp. 20-32.

11. Azuma, A.; and Kawachi, K.: Local Momentum Theory and its Application to the Rotary Wing. AIAA Paper 75-865, June 1975.

12. Dat, R.: Representation of a Lifting Line in an Arbitrary Motion by a Line of Acceleration Doublets. NASA TT F-12952, May 1970.

13. Costes, J-J.: Computation of Unsteady Aerodynamic Forces on Helicopter Rotor Blades. NASA TT F-15039, August 1973.

14. Landgrebe, A.J.; Moffitt, R.C.; and Clark, D.R.: Aerodynamic Technology for Advanced Rotorcraft, Parts I and II. J. American Helicopter Soc., vol. 22, nos. 2 & 3, April and July 1977, pp. 21-27 & pp. 2-9.

15. Johnson, W.: Comparison between Experimental Data and Helicopter Airloads Calculated Using a Lifting Surface Theory. ASRL TR-157-1, M.I.T., July 1970.

16. Johnson, W.: Comprehensive Helicopter Analysis a State of the Art Review. NASA TM–78539, November 1978.

17. Van Holten, Th.: The Computation of Aerodynamic Loads on Helicopter Blades in Forward Flight, Using the Method of the Acceleration Potential. Rep. VTH-189, Technische Hogeschool Delft, Netherlands, March 1975.

18. Weissinger, J.: The Lift Distribution on Swept-back Wings. NACA TM 1120, 1947. (Translated from ZWB Forschungsbericht Nr. 1553, Berlin-Adlershof, 1942.)

19. Reissner, E.: Effect of Finite Span on the Airload Distributions for Oscillating Wings, I – Aerodynamic Theory of Oscillating Wings of Finite Span. NACA TN 1194, March 1947.

20. Reissner, E.; and Stevens, J.E.: Effect of Finite Span on the Airload Distributions for Oscillating Wings, II – Methods of Calculation and Examples of Application. NACA TN 1195, October 1947.

21. Rabbott, J.P. Jr.; and Churchill, G.B.: Experimental Investigation of the Aerodynamic Loading on a Helicopter Rotor Blade in Forward Flight. NACA RM L56I07, October 1956.

22. Scheiman, J.: A Tabulation of Helicopter Rotor Blade Differential Pressures, Stresses and Motions as Measured in Flight. NASA TM X–952, March 1964.

23. Rabbott, J.P. Jr.; Lizak, A.A.; and Paglino, V.M.: A Presentation of Measured and Calculated Full-Scale Rotor Blade Aerodynamic and Structural Loads. USAAVLABS Tech. Rep. 66-31, July 1966.

24. Scheiman, J.; and Ludi, L.H.: Qualitative Evaluation of Effect of Helicopter Rotor Blade Tip Vortex on Blade Airloads. NASA TN D–1637, 1963.

25. Scheiman, J.; and Kelly, H.L.: Comparison of Flight-Measured Helicopter Rotor Blade Chordwise Pressure Distributions with Static Two-Dimensional Airfoil Characteristics. NASA TN D-3936, May 1967.

26. Hille, R.: Erweiterung des Traglinienmodells beim Hubschrauberrotors (Extension of the Lifting Line Model of Helicopter Rotors). Hamburg Universitaet, Fachbereich Physik, Doktor Dissertation, 1974.

27. Ormiston, Robert A.: An Actuator Disk Theory for Rotor Wake Induced Velocities. Aerodynamics of Rotary Wings. AGARD CP-111, Sept. 1972.

28. Van Holten, Th.: On the Validity of Lifting Line Concepts in Rotor Analysis. Vertica, vol. 1, 1977, pp. 239-254.

29. Tables of Associated Legendre Functions. Mathematical Tables Project, Nat. Bur. Stand., Columbia University Press, 1945.

30. Bisplinghoff, R.L.; Ashley, H.; and Halfman, R.L.: Aeroelasticity. Addison-Wesley Publishing Co., 1955.

31. Abramowitz, M.; and Stegun, I.A.: Handbook of Mathematical Functions. Dover Publications, Inc., December 1972.

32. Ashley, H.; Moser, H.H.; and Dugundji, J.: Investigation of Rotor Response to Vibratory Aerodynamic Inputs - Part III. Three-Dimensional Effects on Unsteady Flow through a Helicopter Rotor. WADC Tech. Rep. 58-87, October 1958.

33. James, E.C.: Lifting Line Theory for an Unsteady Wing as a Singular Perturbation Problem. J. Fluid Mech., vol. 70, part 4, 1975, pp. 753-771.

34. Ahmadi, A.R.: An Asymptotic Unsteady Lifting Line Theory with Energetics and Optimum Motion of Thrust-Producing Lifting Surfaces. Lab. Rep. 80–2, M.I.T., Fluid Dynamics Res. Lab., September 1980.
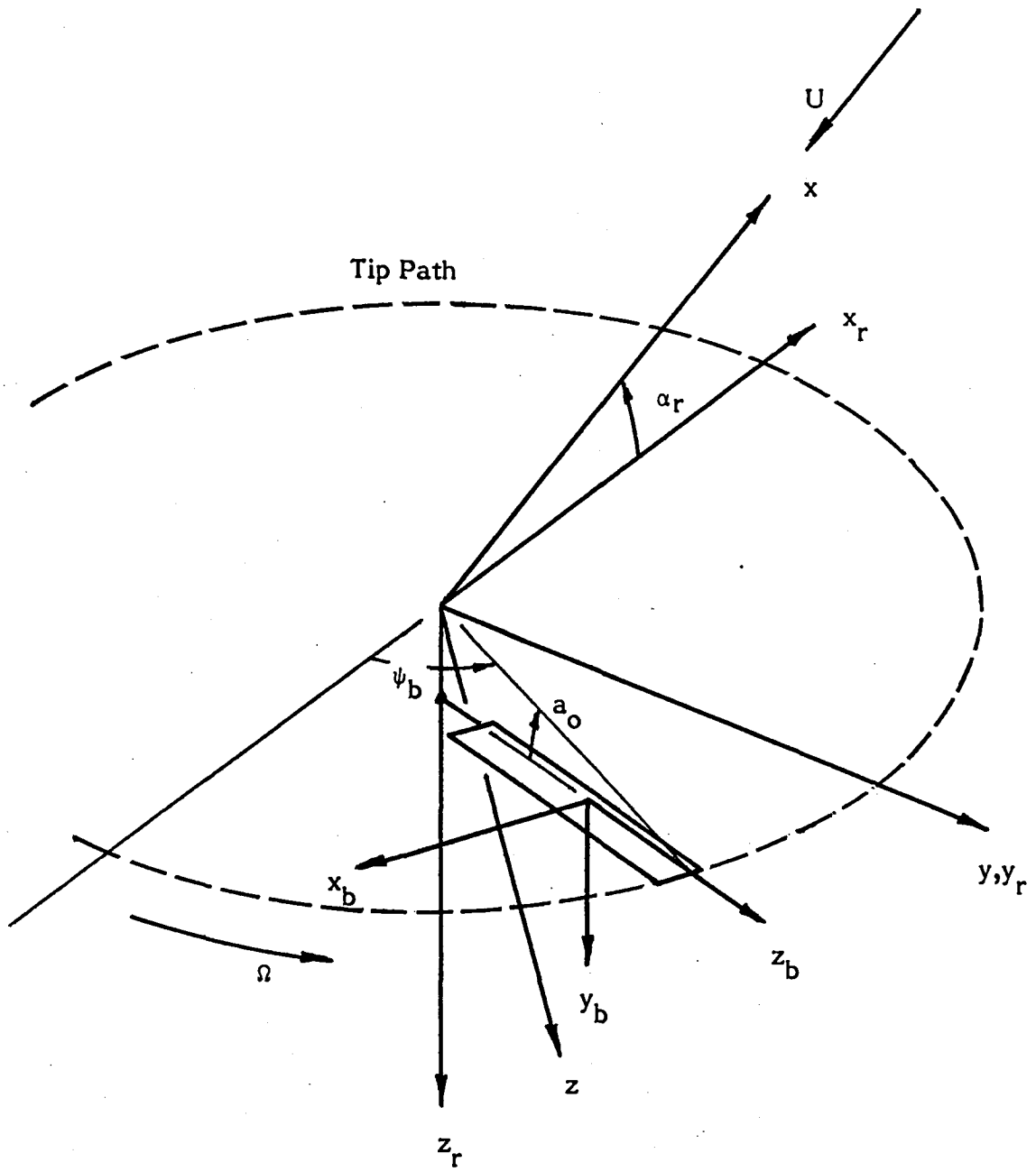
Figure 1. – Rotor coordinate systems.

Blade Section	Wing Section
$x_b = b \left(\frac{1}{2} + \cosh \eta \cos \phi\right)$	$x_a = b \cosh \eta \cos \phi$
$y_b = b \sinh \eta \sin \phi$	$y_a = b \sinh \eta \sin \phi$
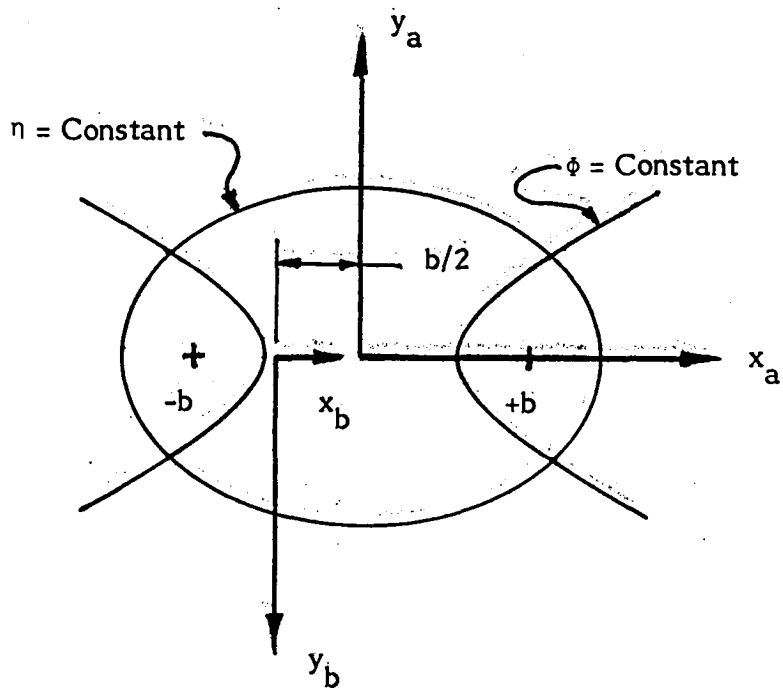
Figure 2. - Sectional Cartesian and elliptic coordinates.

Cylindrical
Coordinates

Prolate-sheroidal
Coordinates

$x_a = r \cos \chi$

$r = s \sinh \psi \sin \theta$

$y_a = r \sin \chi$

$z_a = s \cosh \psi \cos \theta$

$z_a = z_a$

$\chi = \chi$
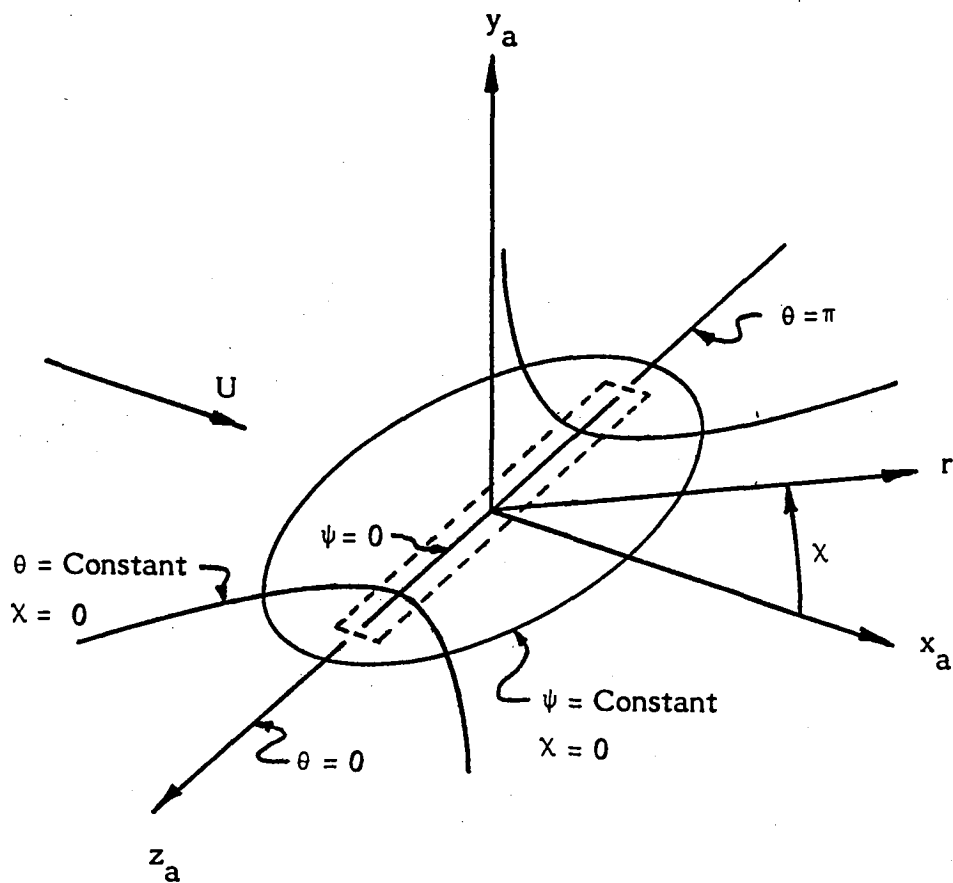
Figure 3. – Cylindrical and Prolate-spheroidal coordinates.

77
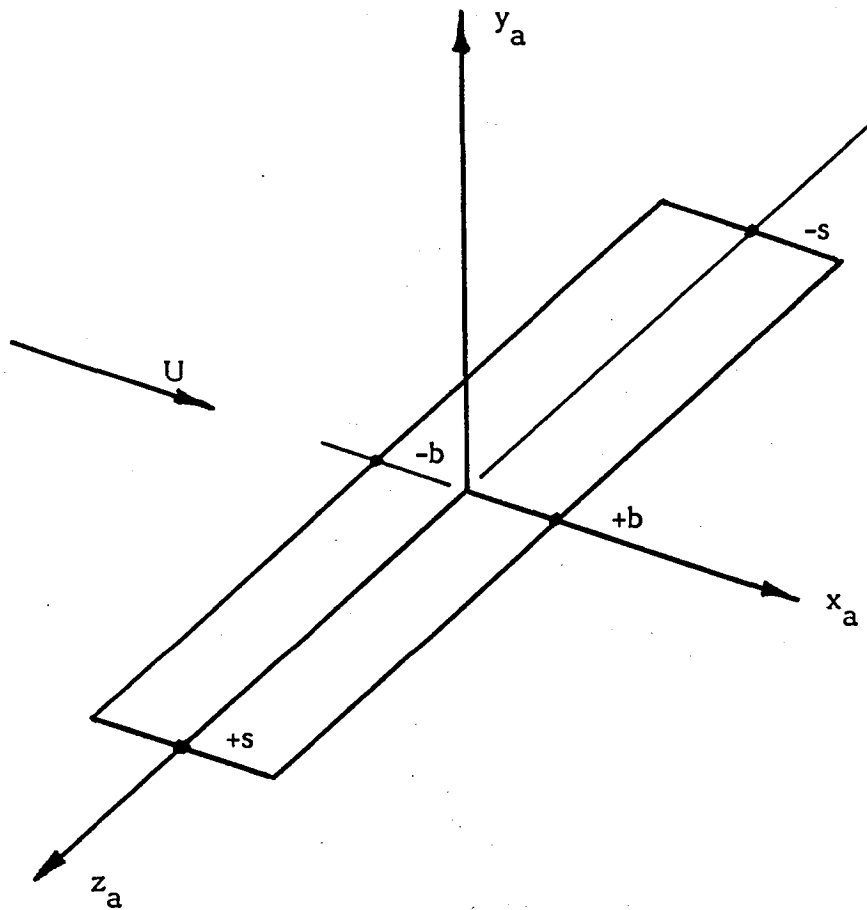
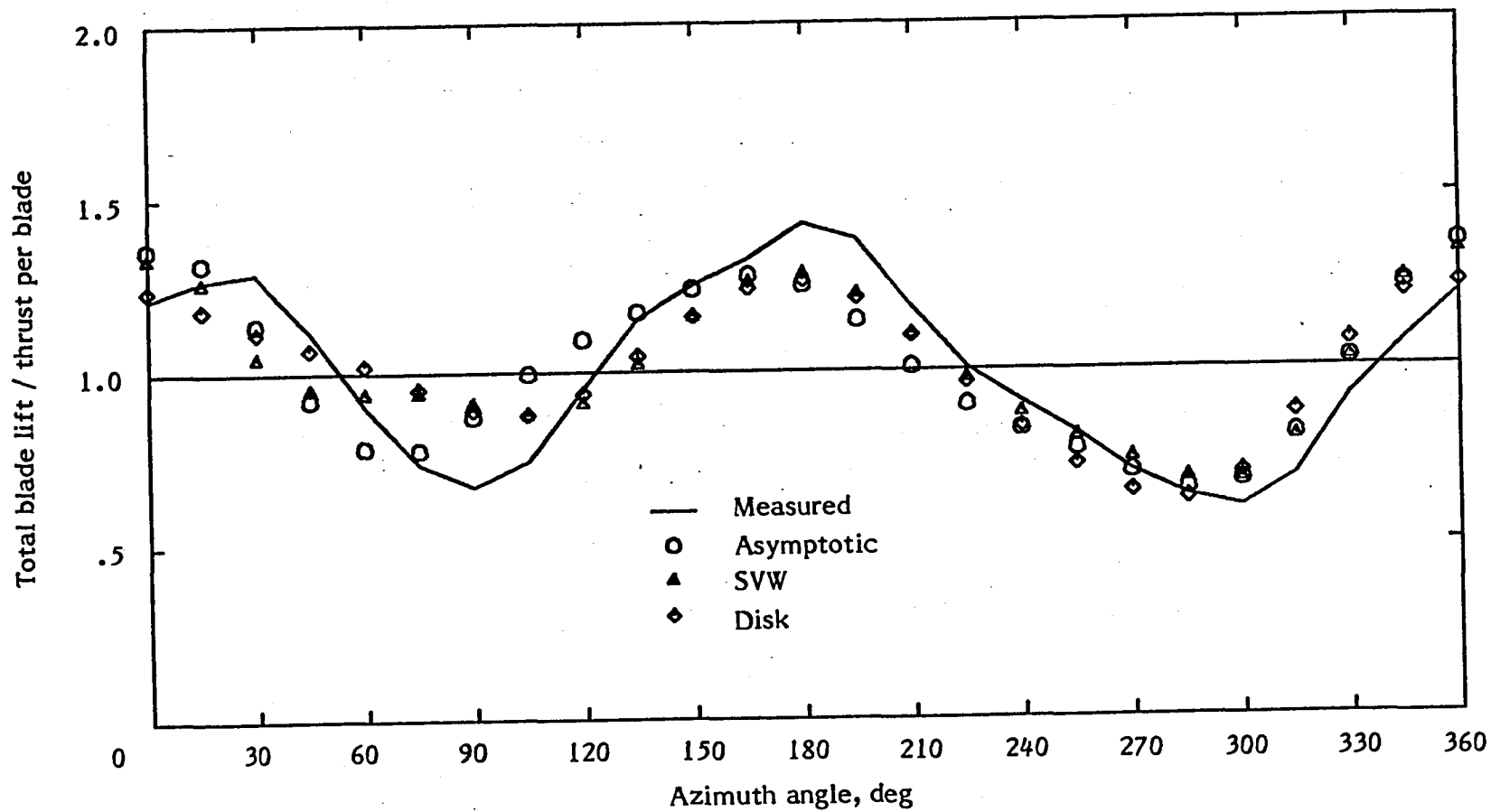Figure 4. – Coordinate system for a straight rectangular wing.
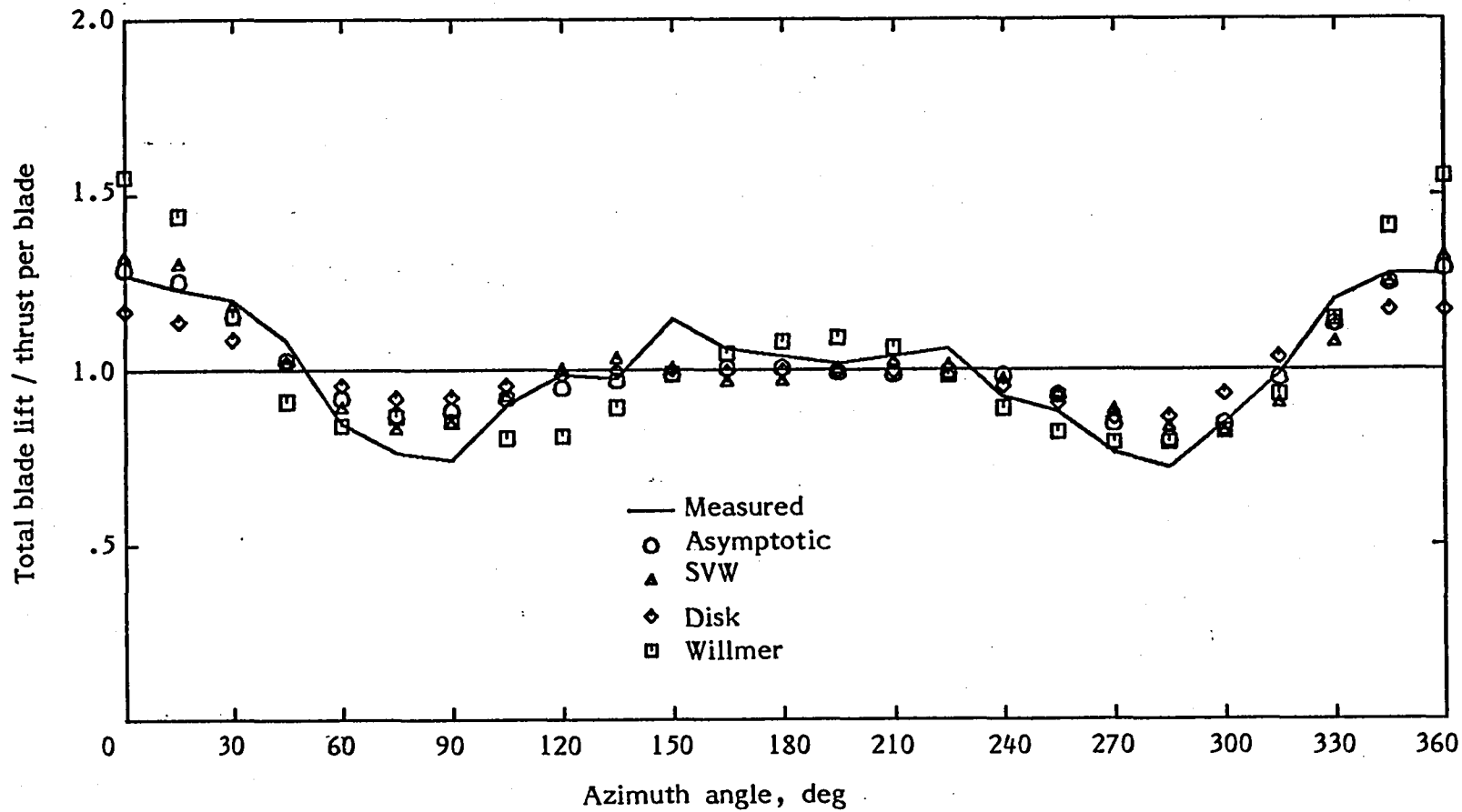
(a) Advance ratio, 0.08.

Figure 5. - Normalized total blade lift versus azimuth position for Case 1.
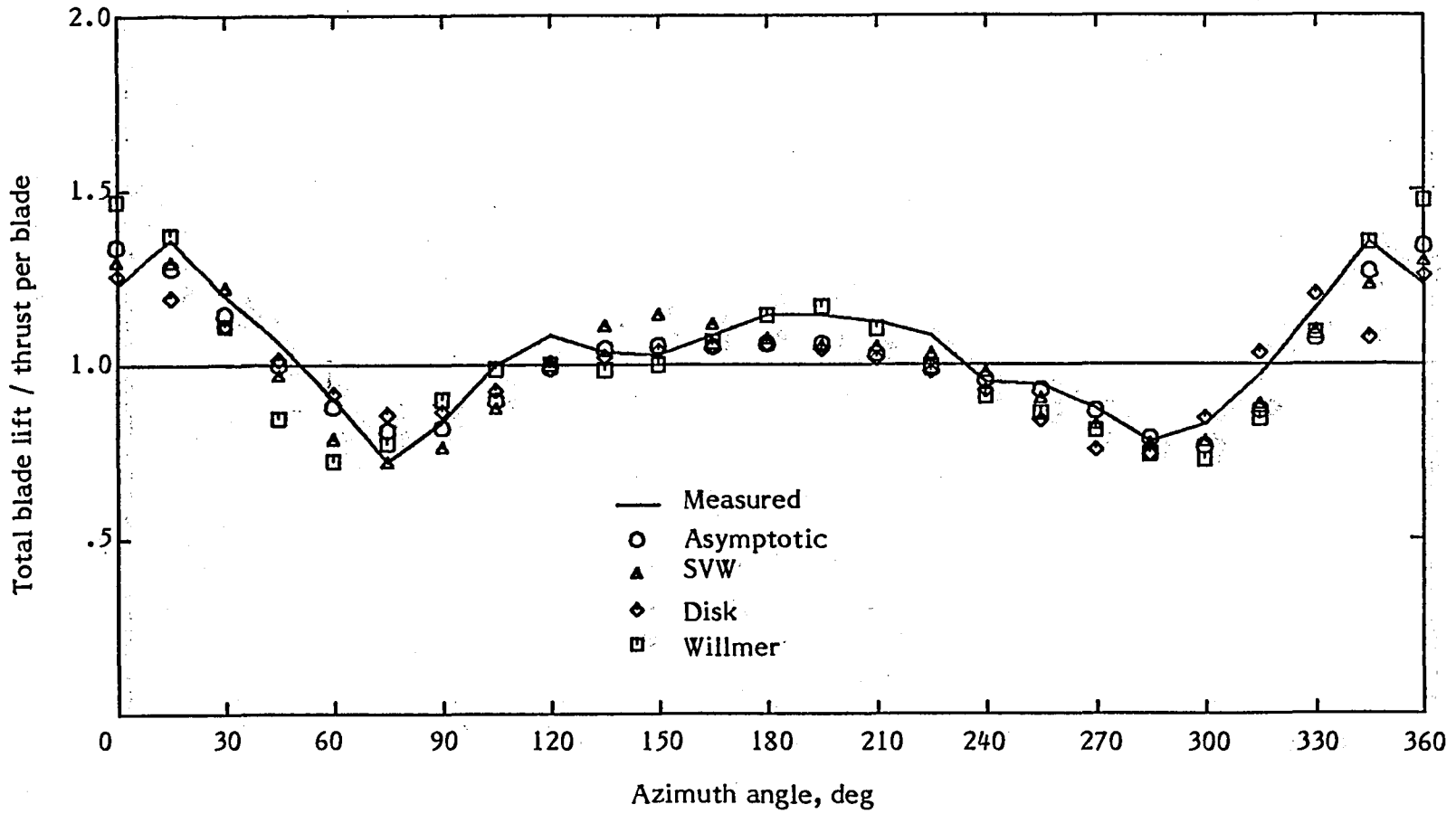
(b) Advance ratio, 0.15.

Figure 5. – Continued.
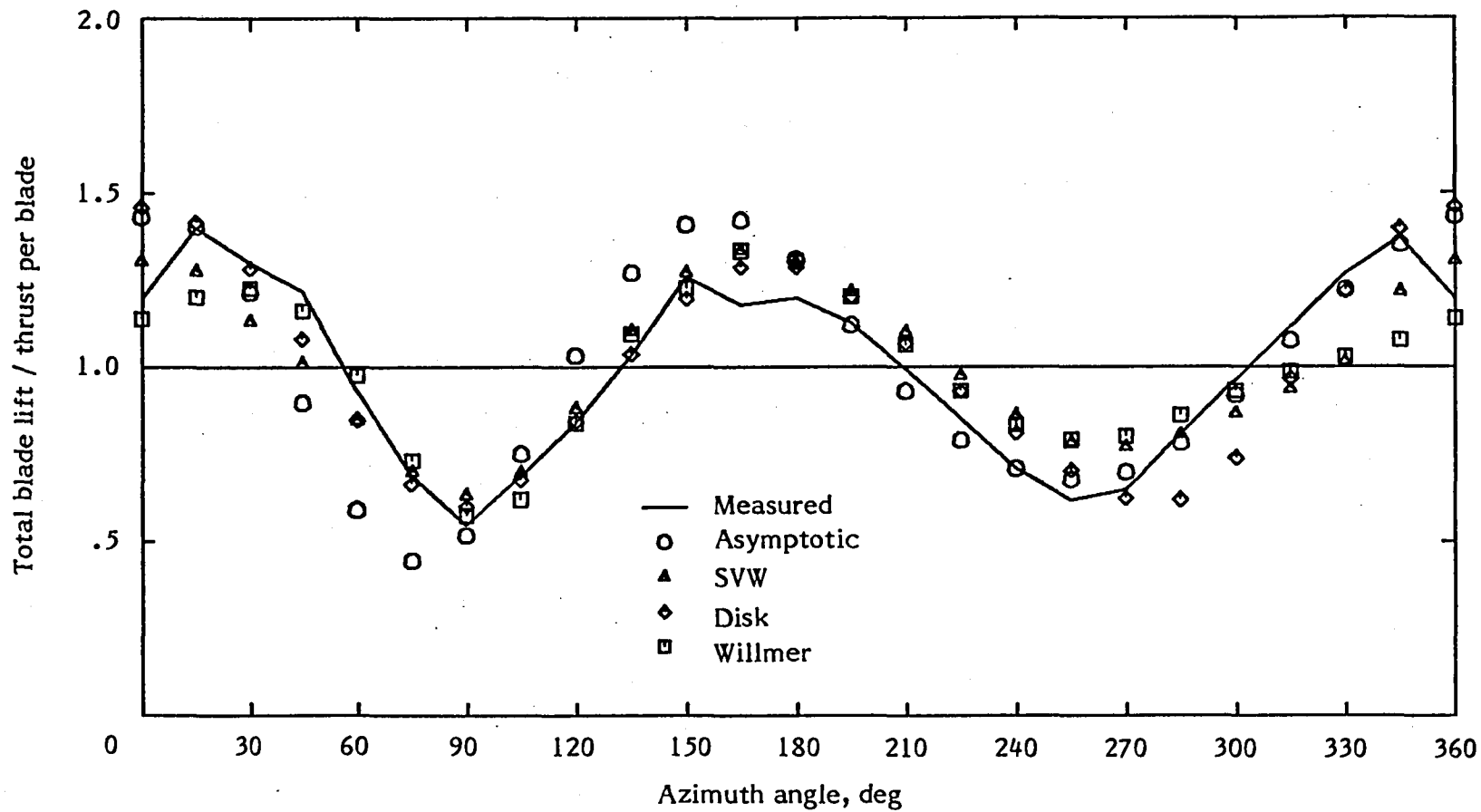
(c) Advance ratio, 0.29.

Figure 5. - Concluded.
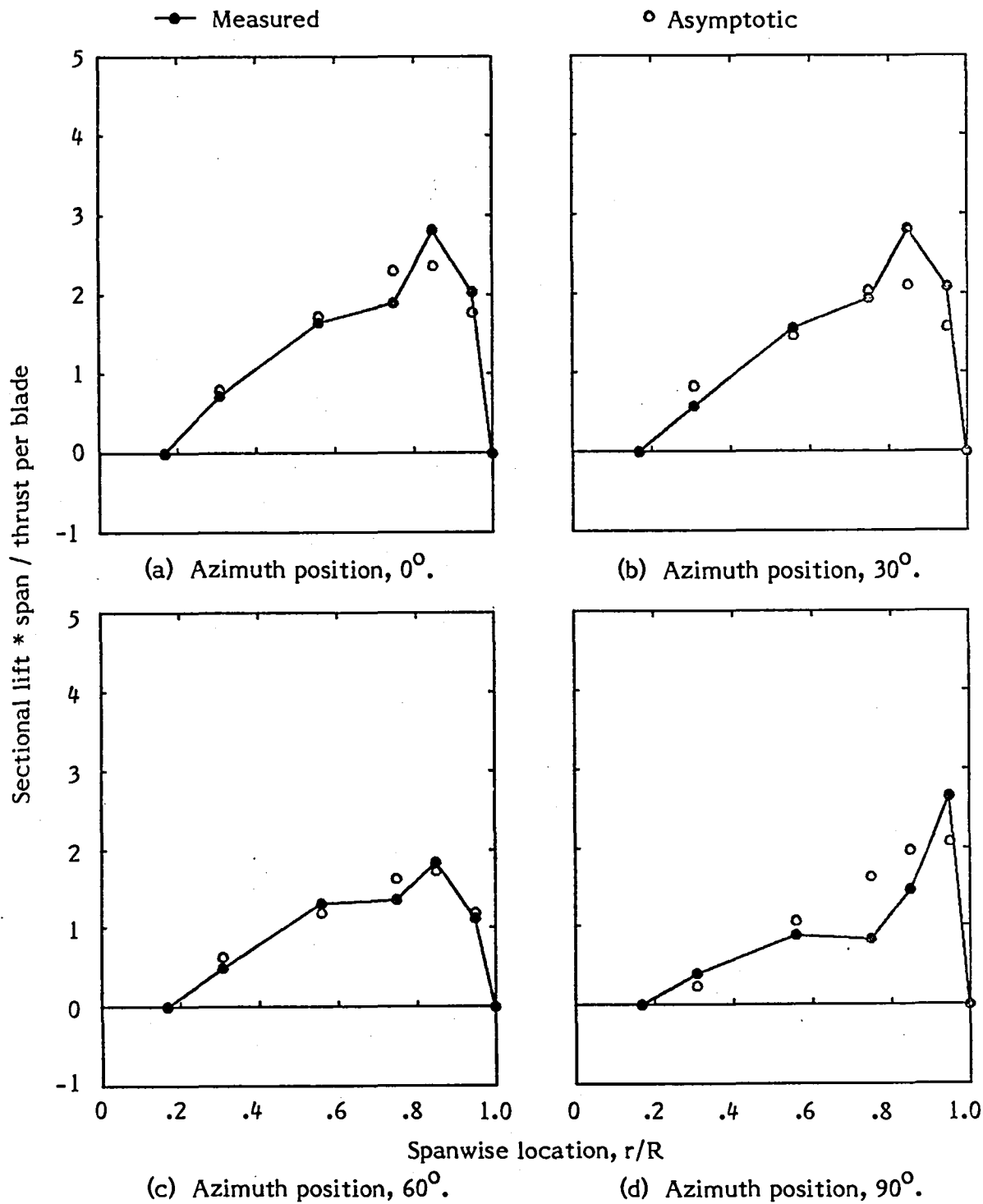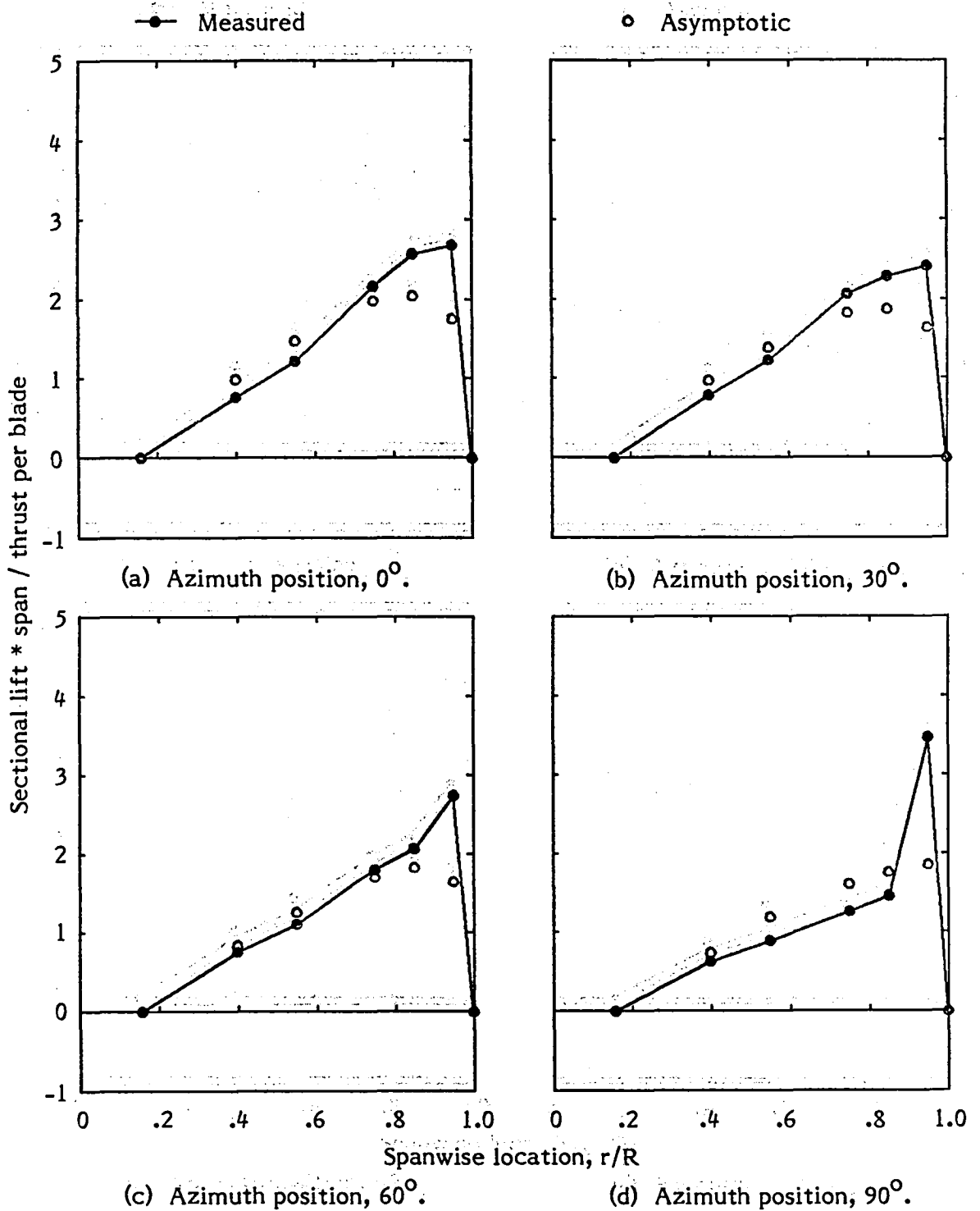
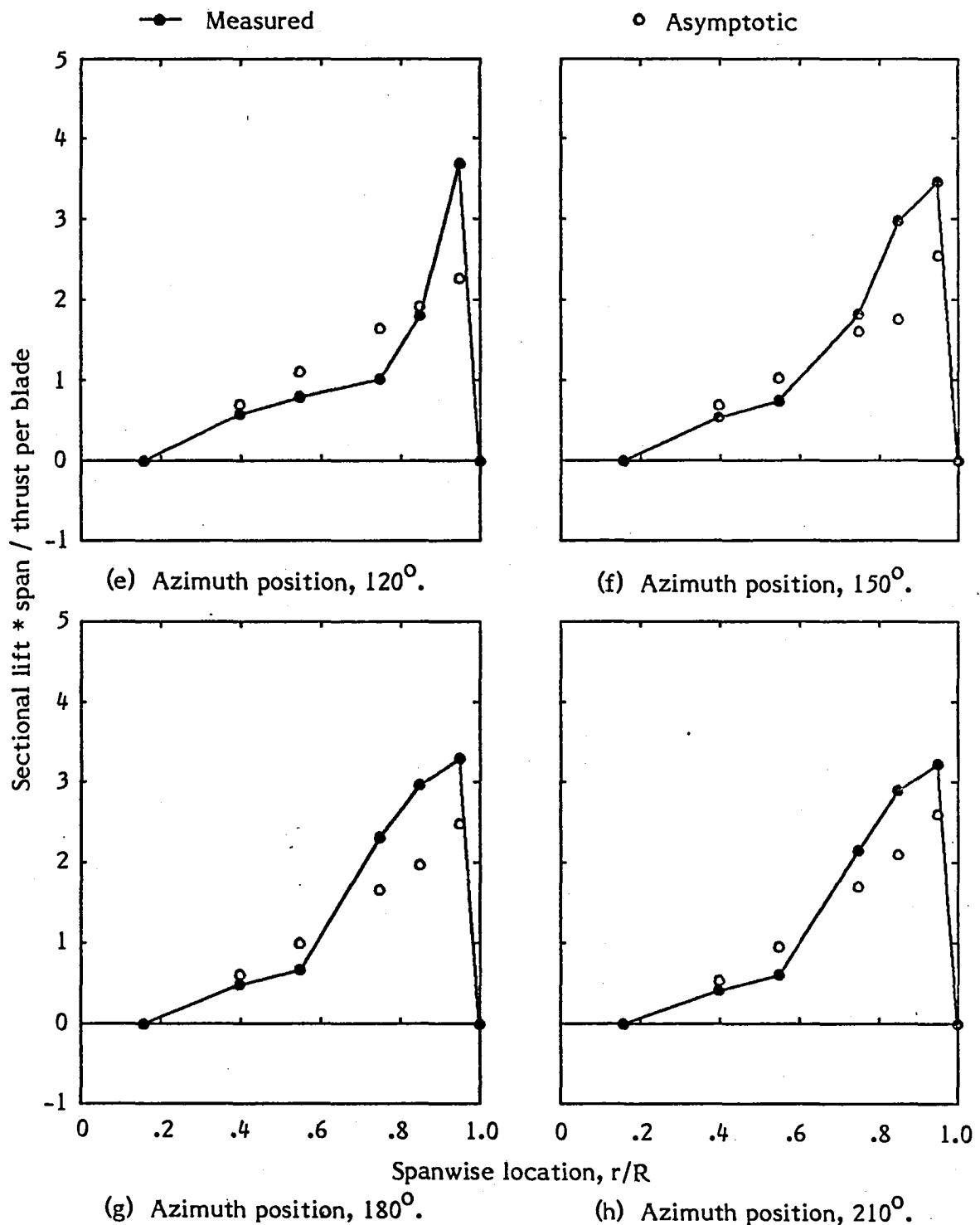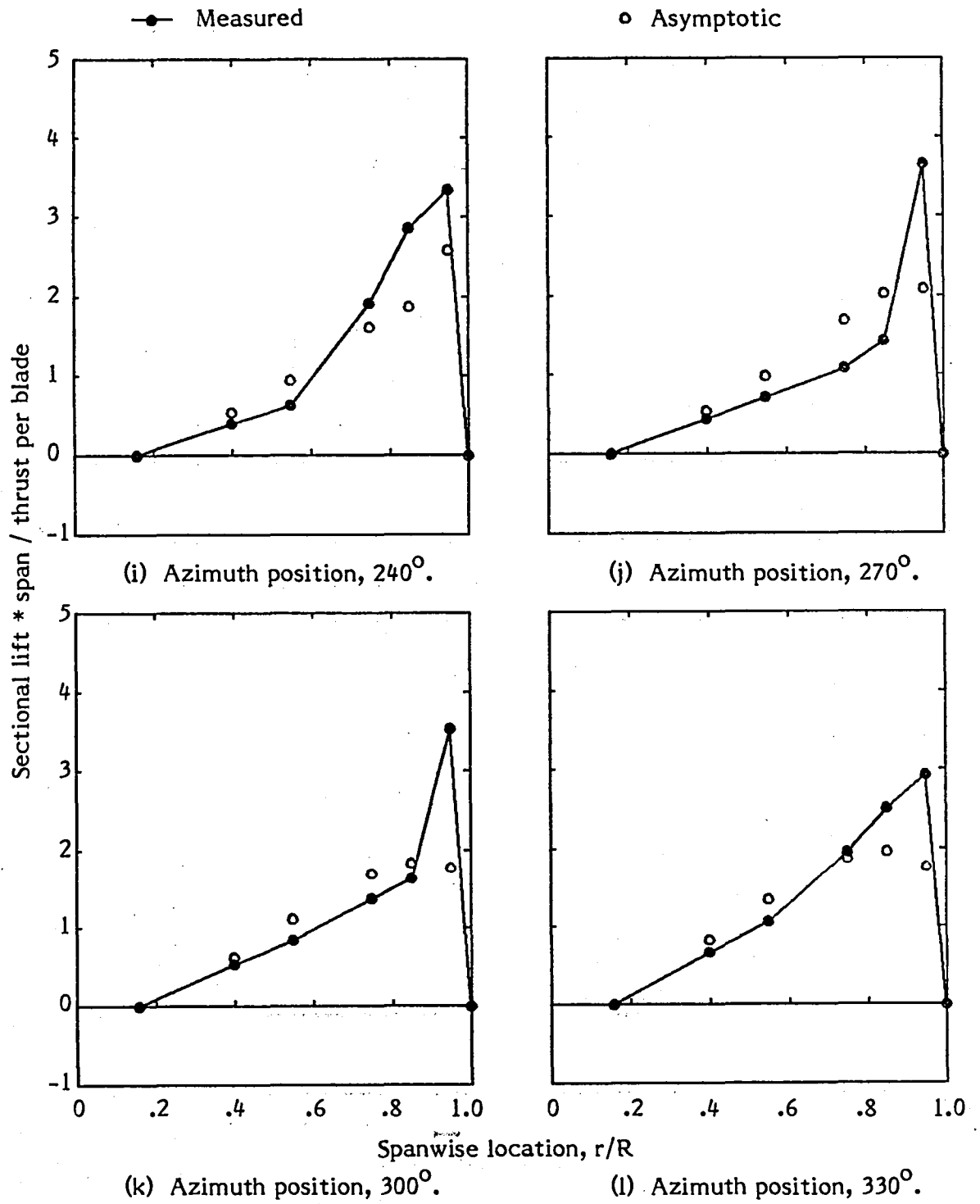Figure 6. – Normalized sectional lift versus spanwise location for Case 1 with advance ratio of 0.08.

Figure 6. - Continued.

- ● Measured   ○ Asymptotic

(i) Azimuth position, 240°.   (j) Azimuth position, 270°.

Spanwise location, r/R

(k) Azimuth position, 300°.   (l) Azimuth position, 330°.
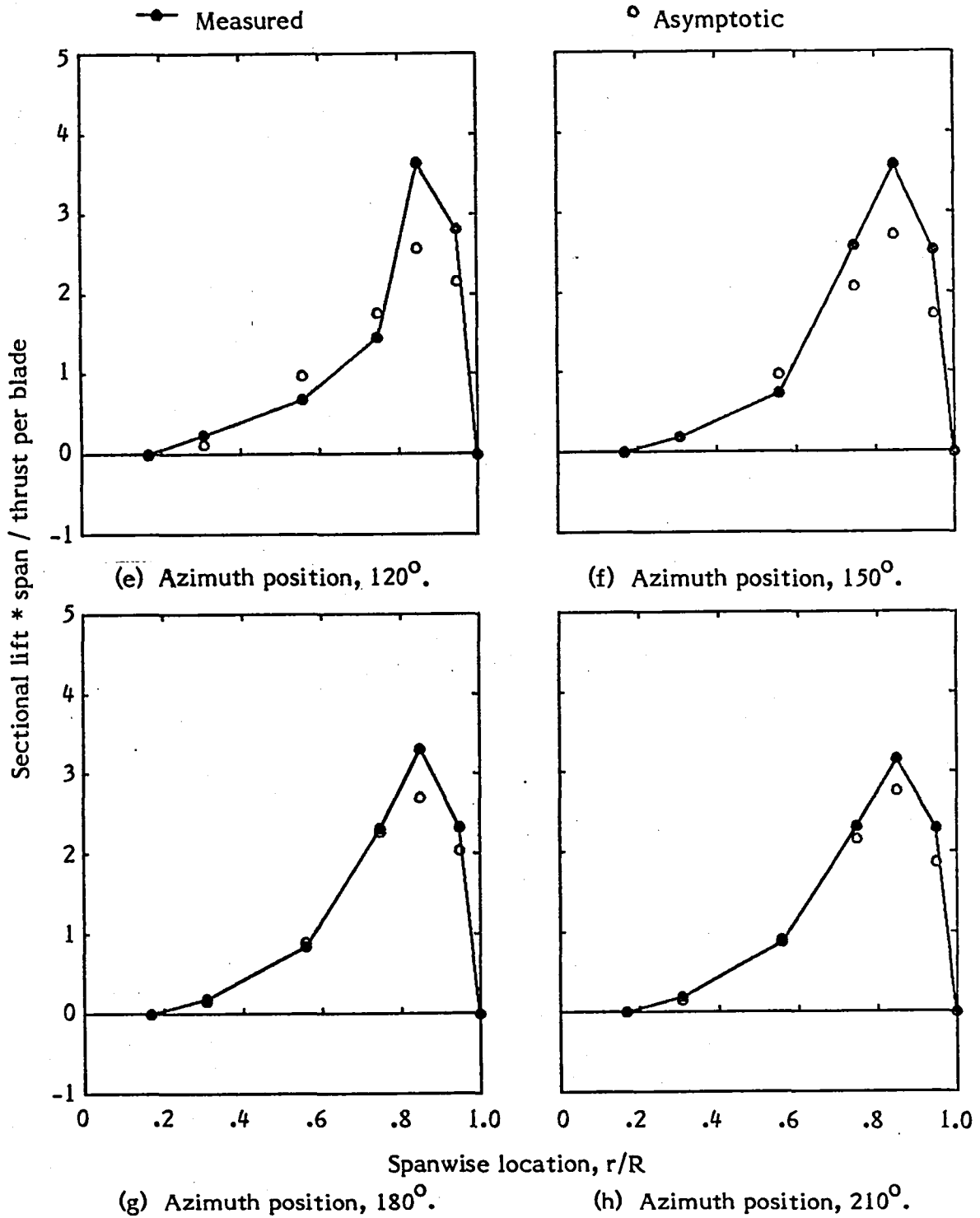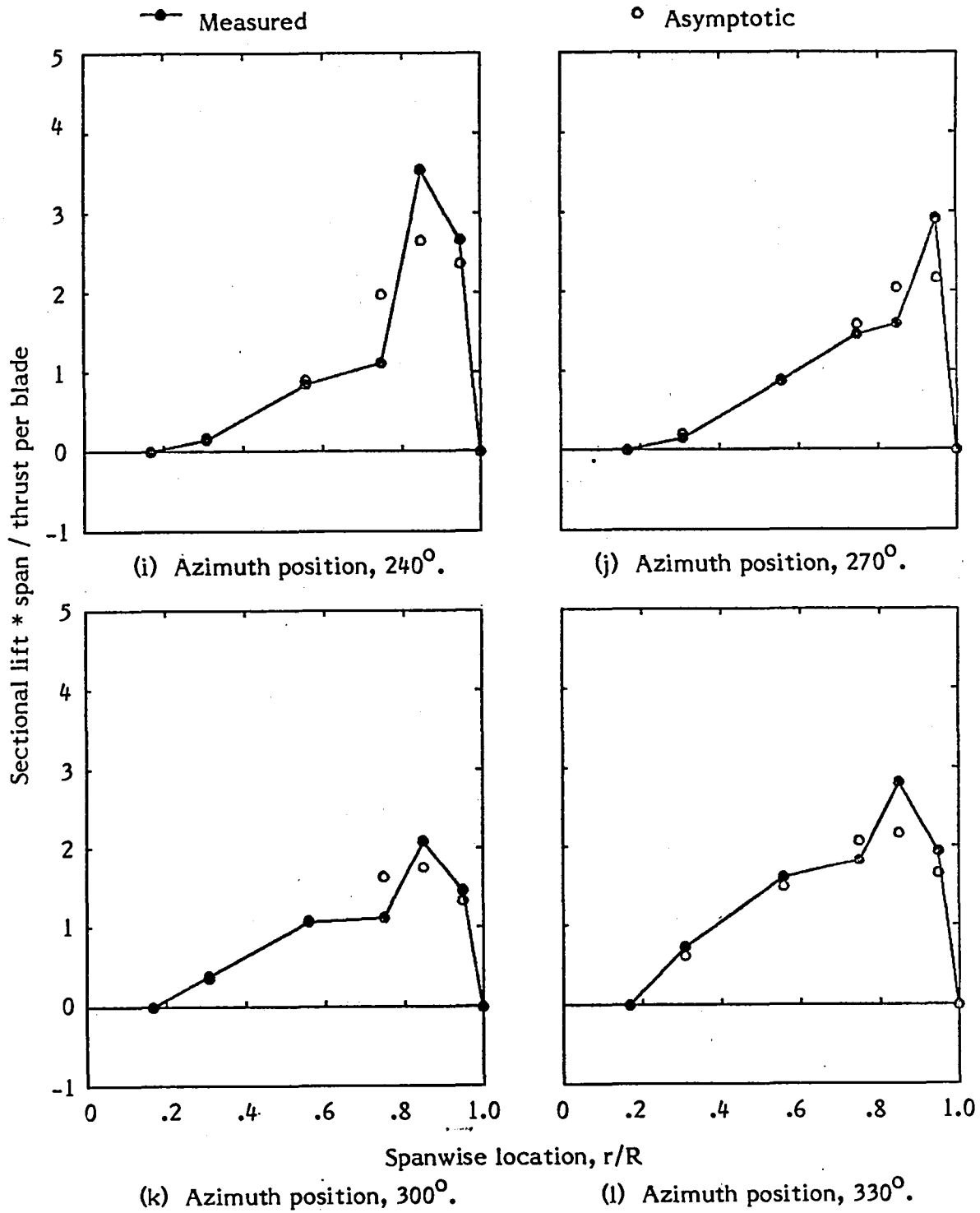
Figure 6. - Concluded.

84
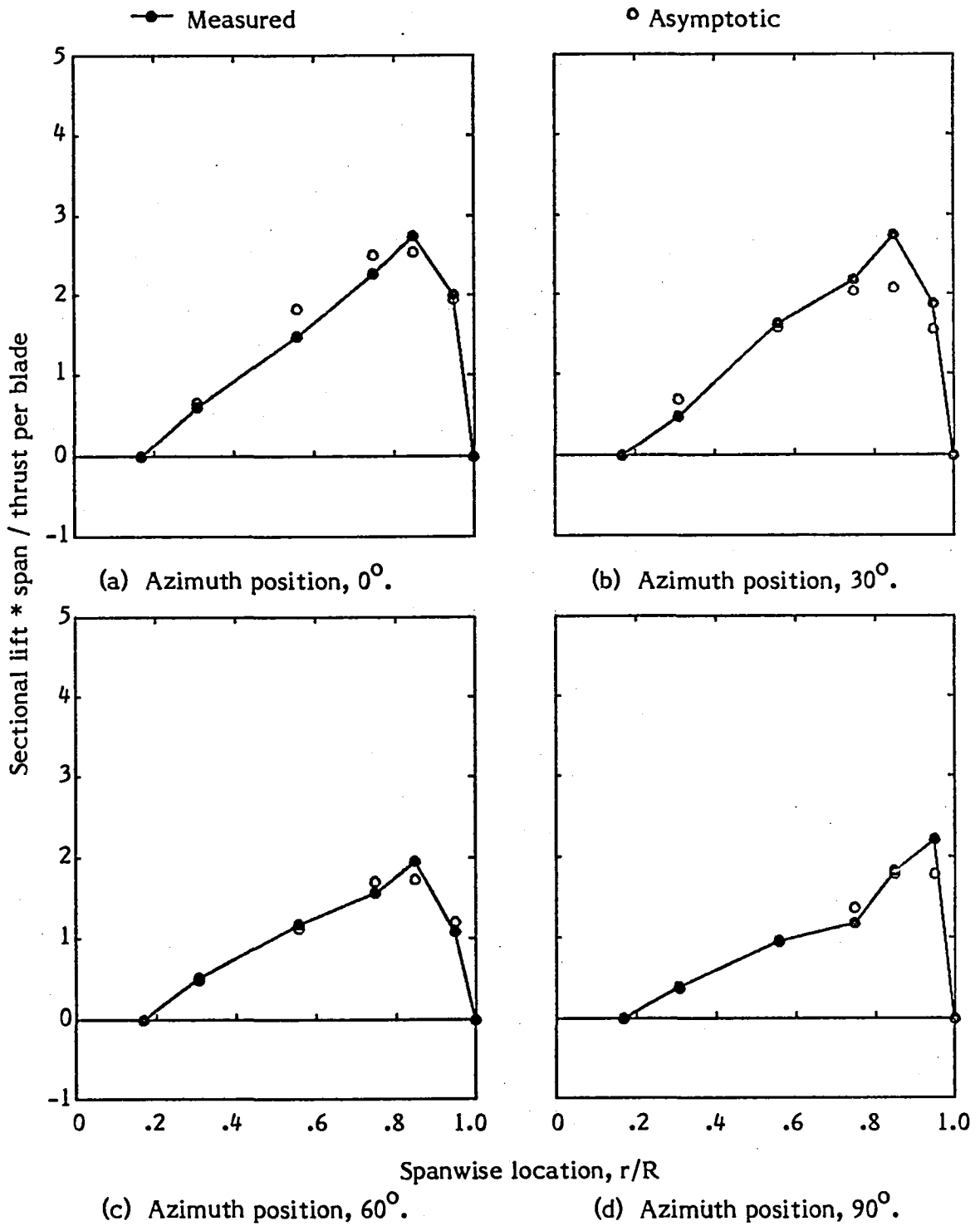
Figure 7. – Normalized sectional lift versus spanwise location for Case 1 with advance ratio of 0.15.

(e) Azimuth position, 120°.

(f) Azimuth position, 150°.

(g) Azimuth position, 180°.

(h) Azimuth position, 210°.

Figure 7. – Continued.

(i) Azimuth position, 240°.

(j) Azimuth position, 270°.

(k) Azimuth position, 300°.

(l) Azimuth position, 330°.
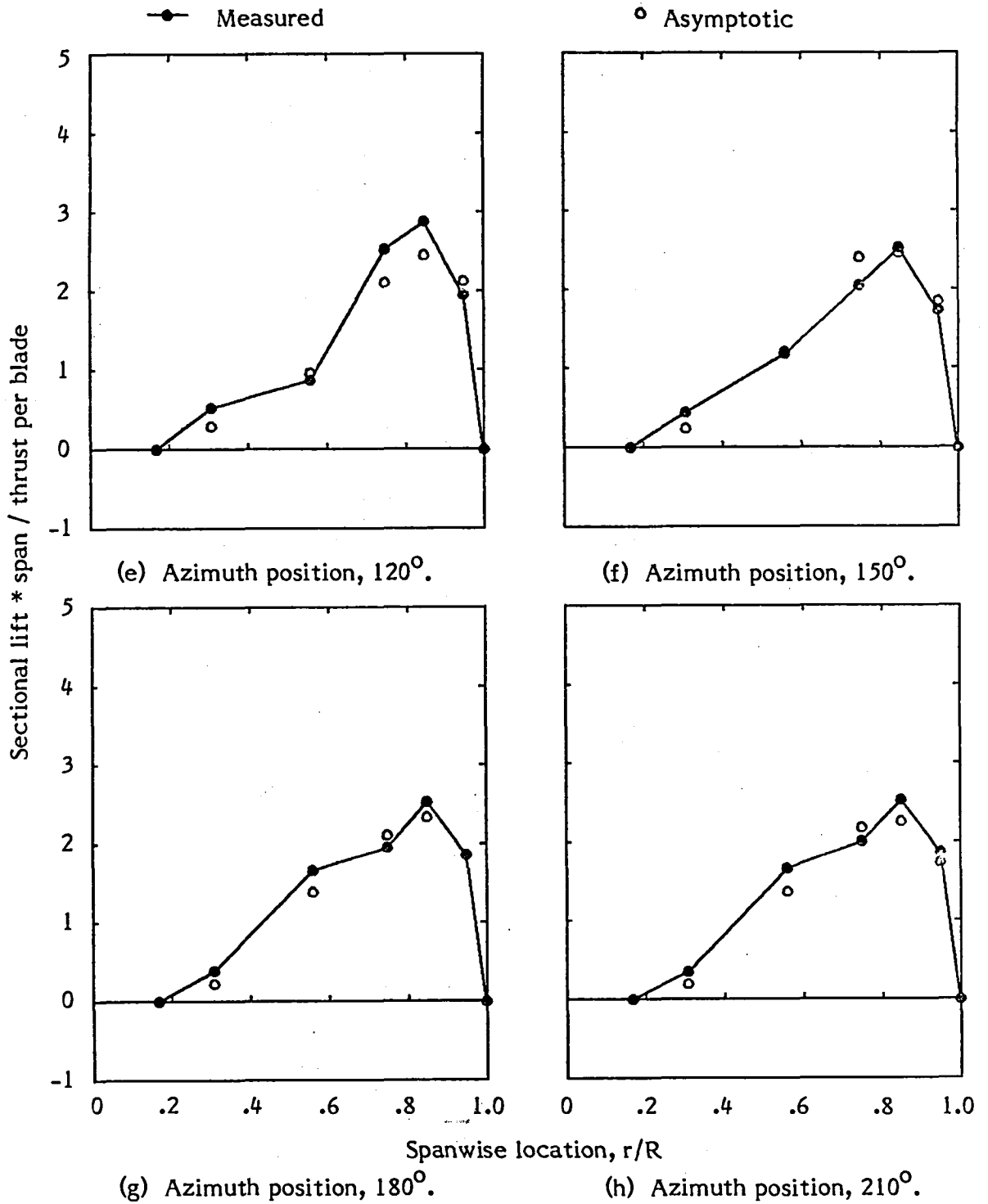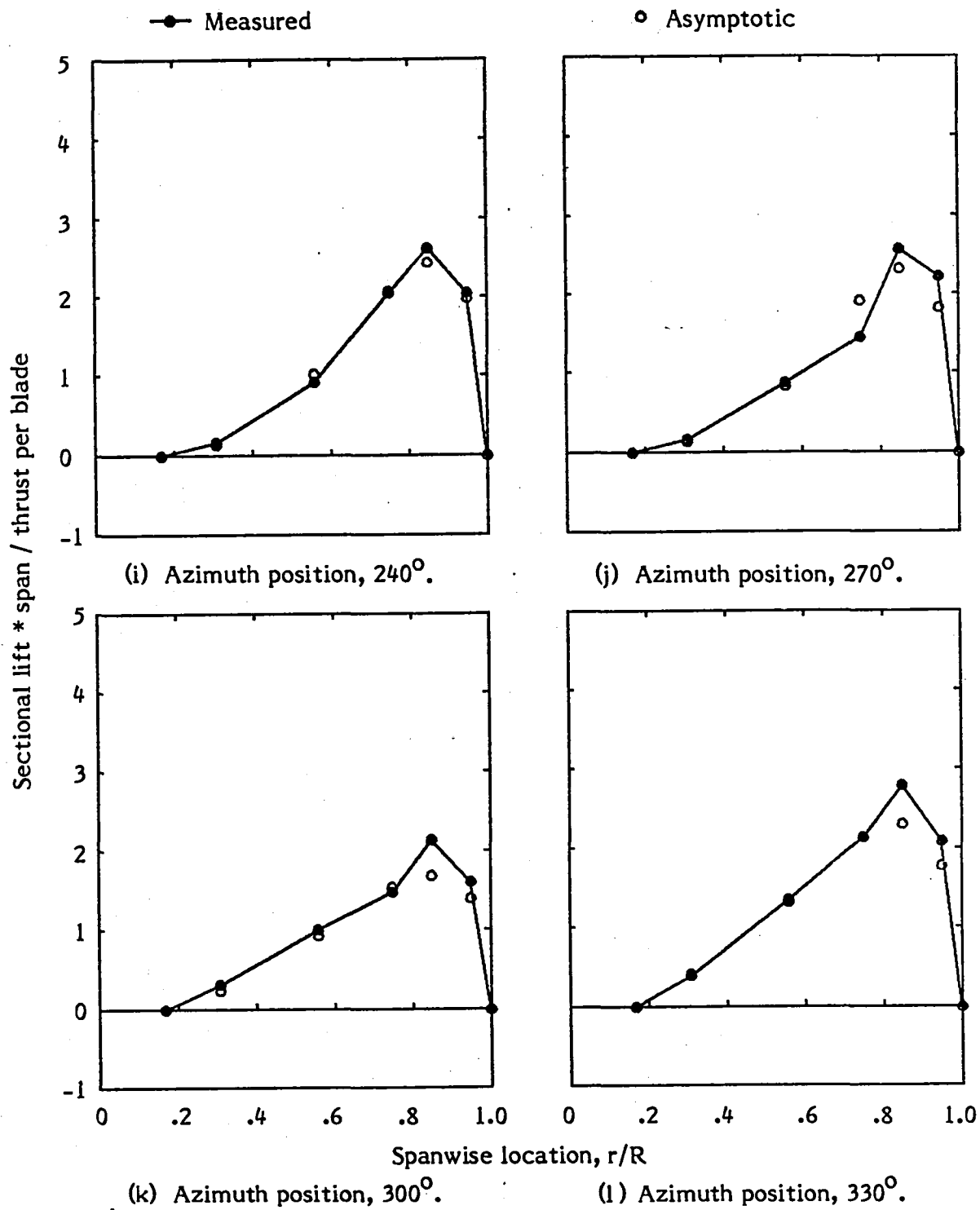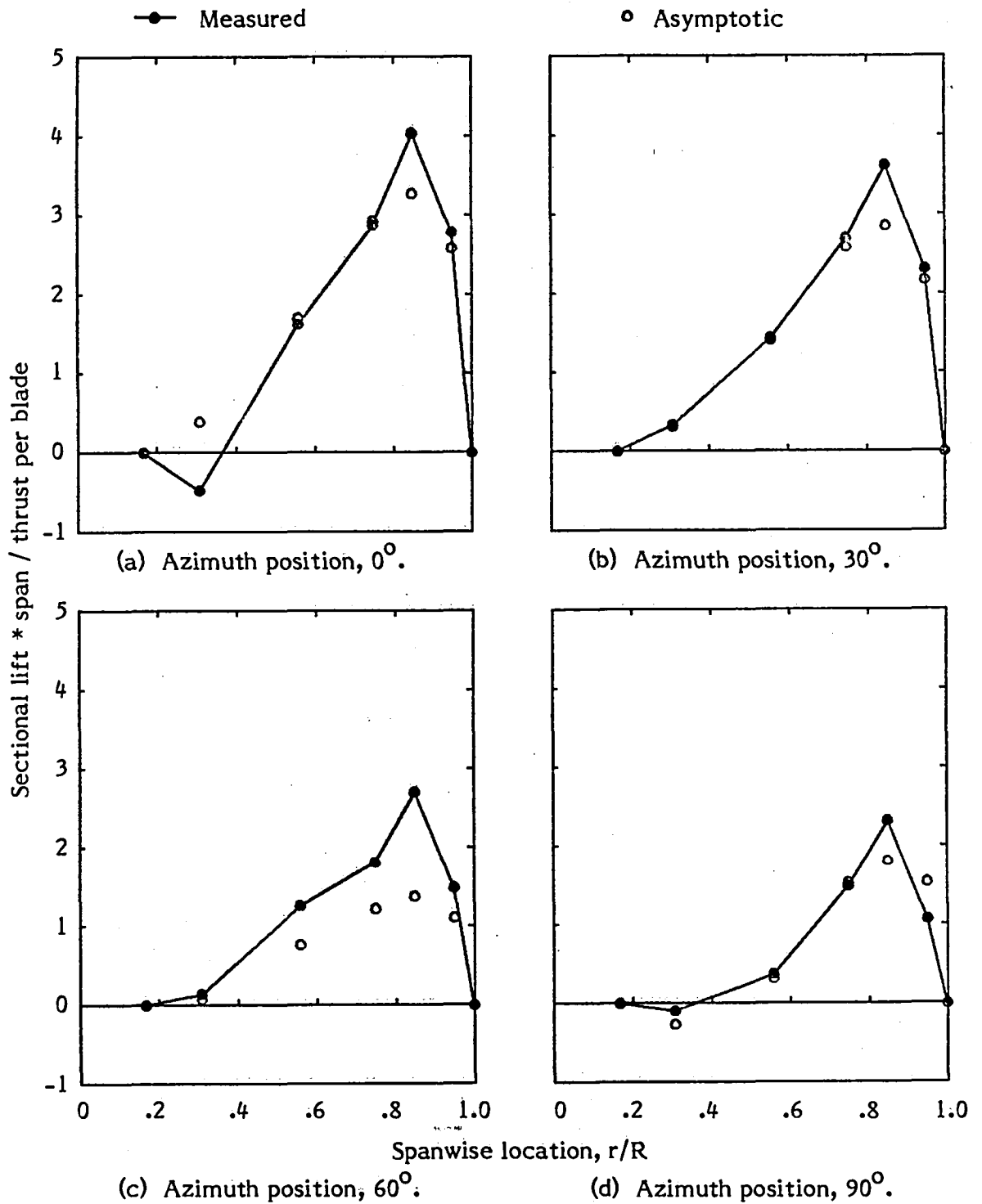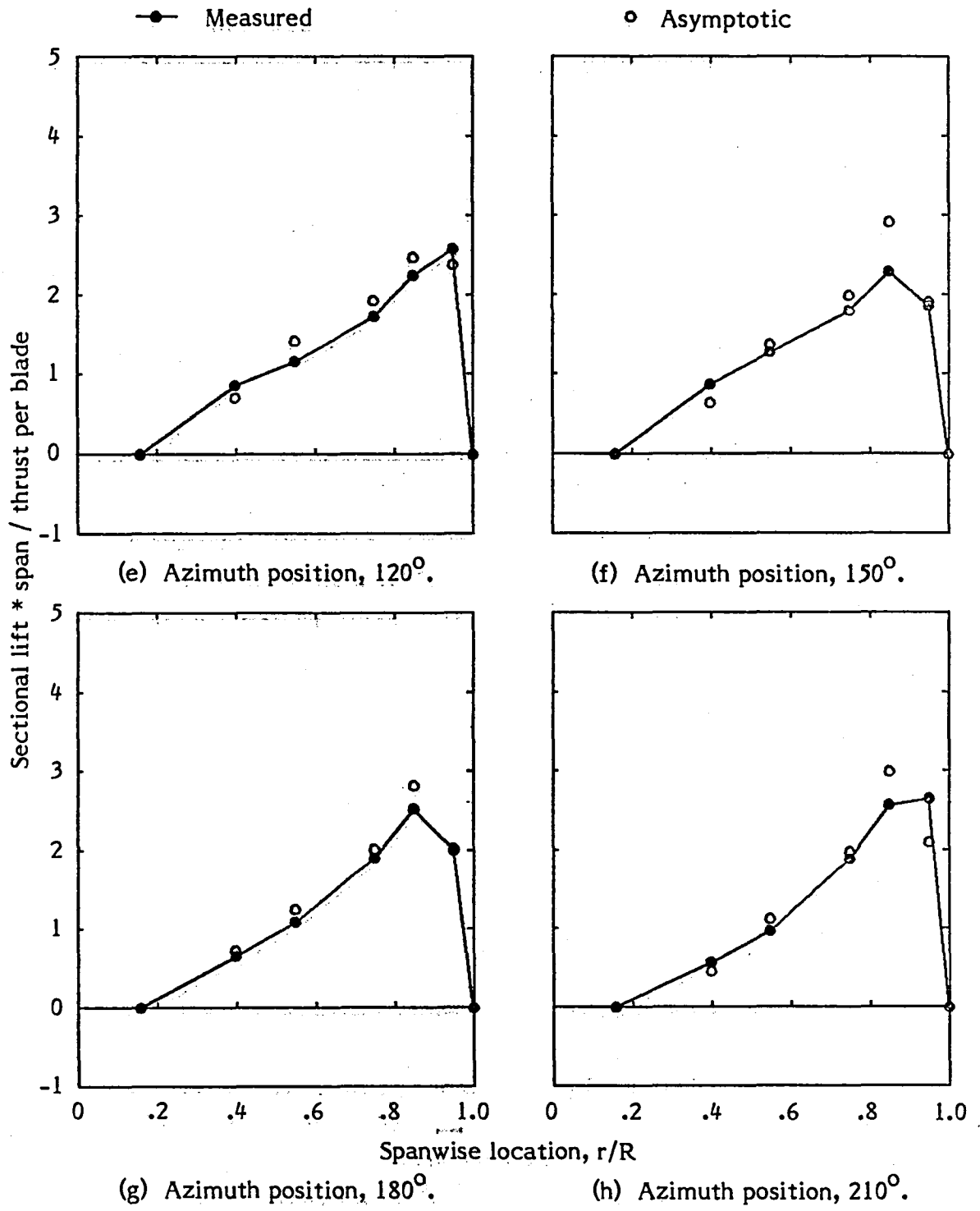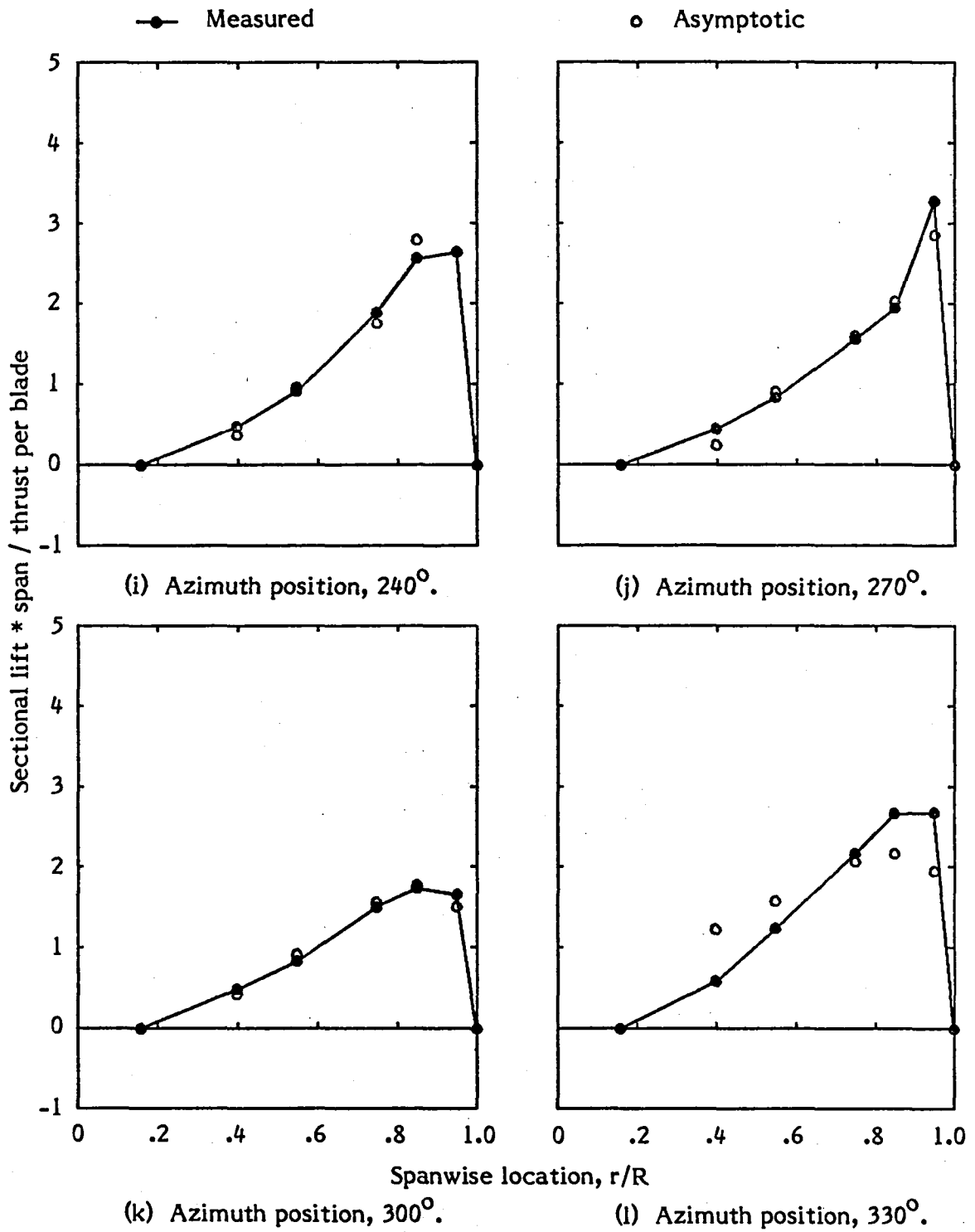
Figure 7. – Concluded.

Figure 8. – Normalized sectional lift versus spanwise location for Case 1 with advance ratio of 0.29.

(e) Azimuth position, 120°.

(f) Azimuth position, 150°.

(g) Azimuth position, 180°.

(h) Azimuth position, 210°.

Figure 8. - Continued.

(i) Azimuth position, 240°.

(j) Azimuth position, 270°.

(k) Azimuth position, 300°.

(l) Azimuth position, 330°.
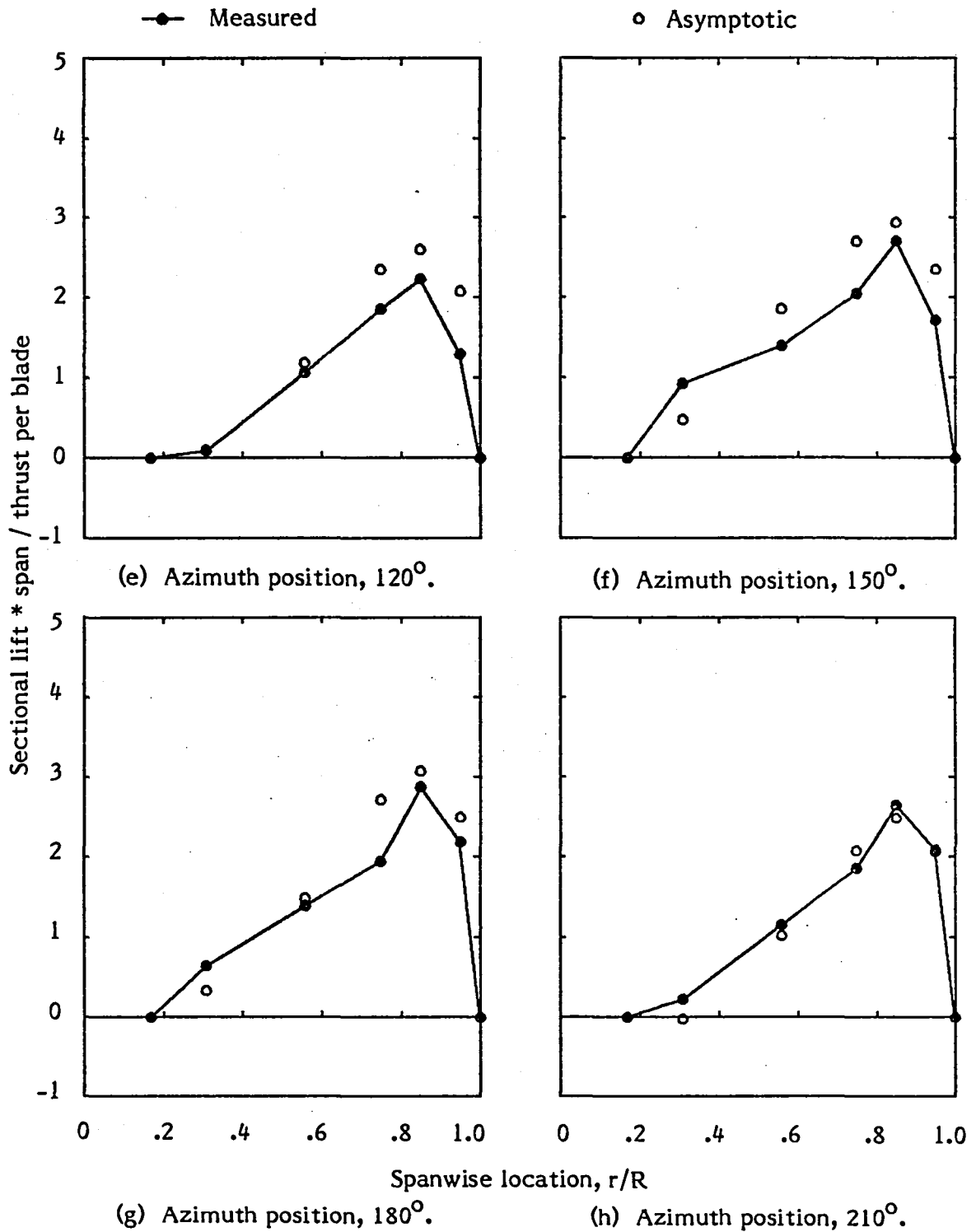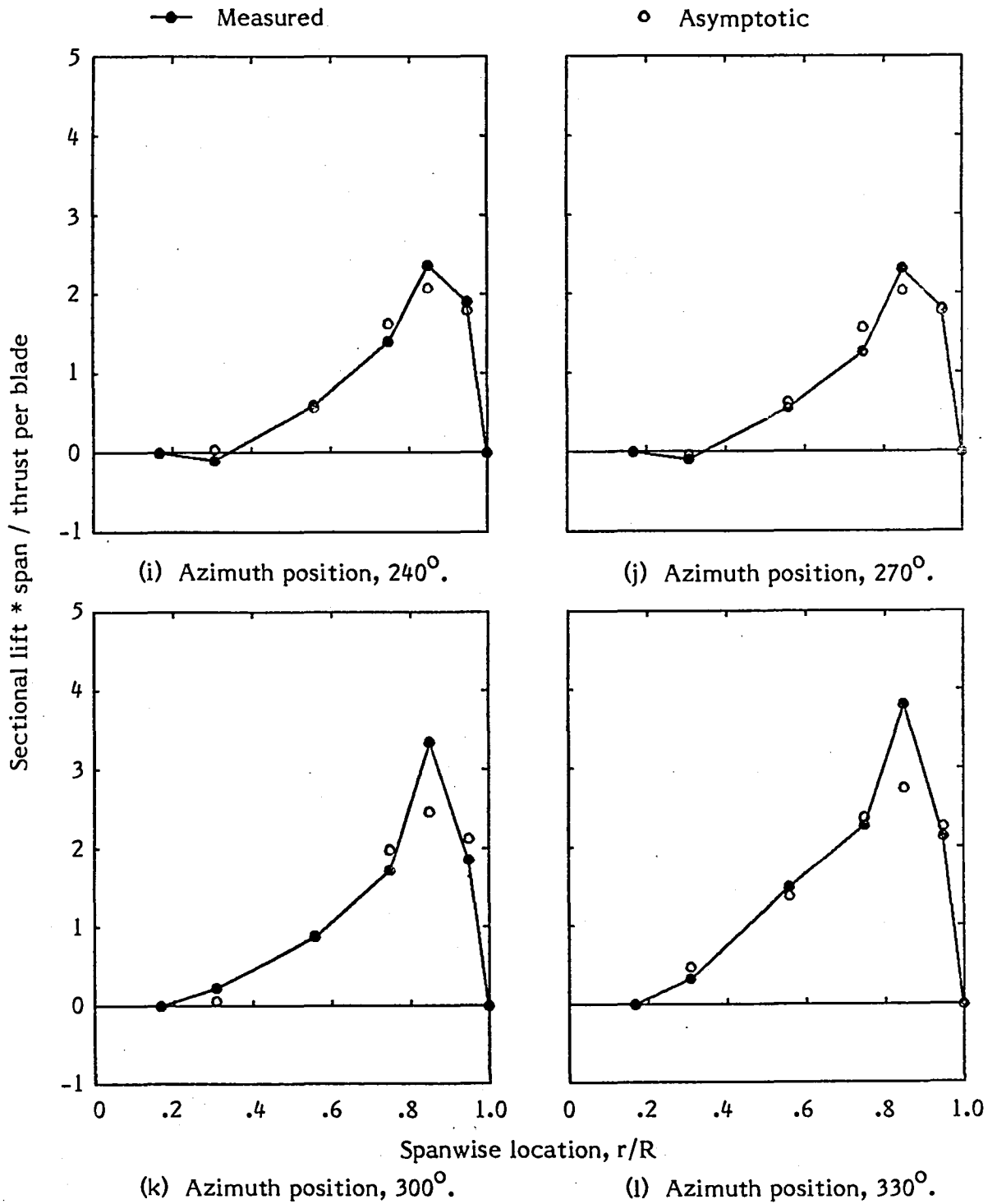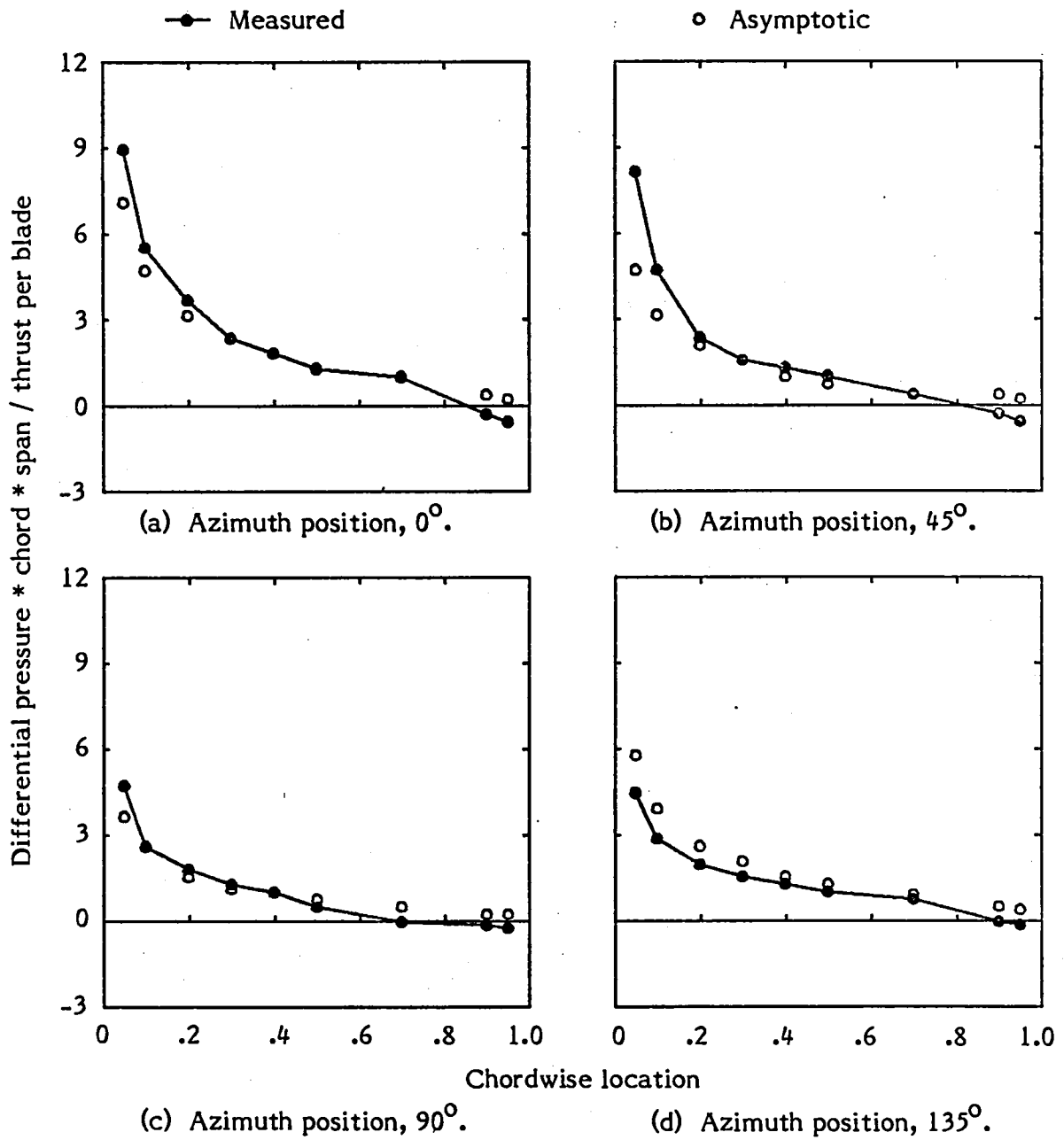
Figure 8. - Concluded.

Figure 9. - Differential pressure versus chordwise location for Case 1
with advance ratio of 0.29 at 75 percent span.

(e) Azimuth position, 180°.

(f) Azimuth position, 225°.

(g) Azimuth position, 270°.

(h) Azimuth position, 315°.
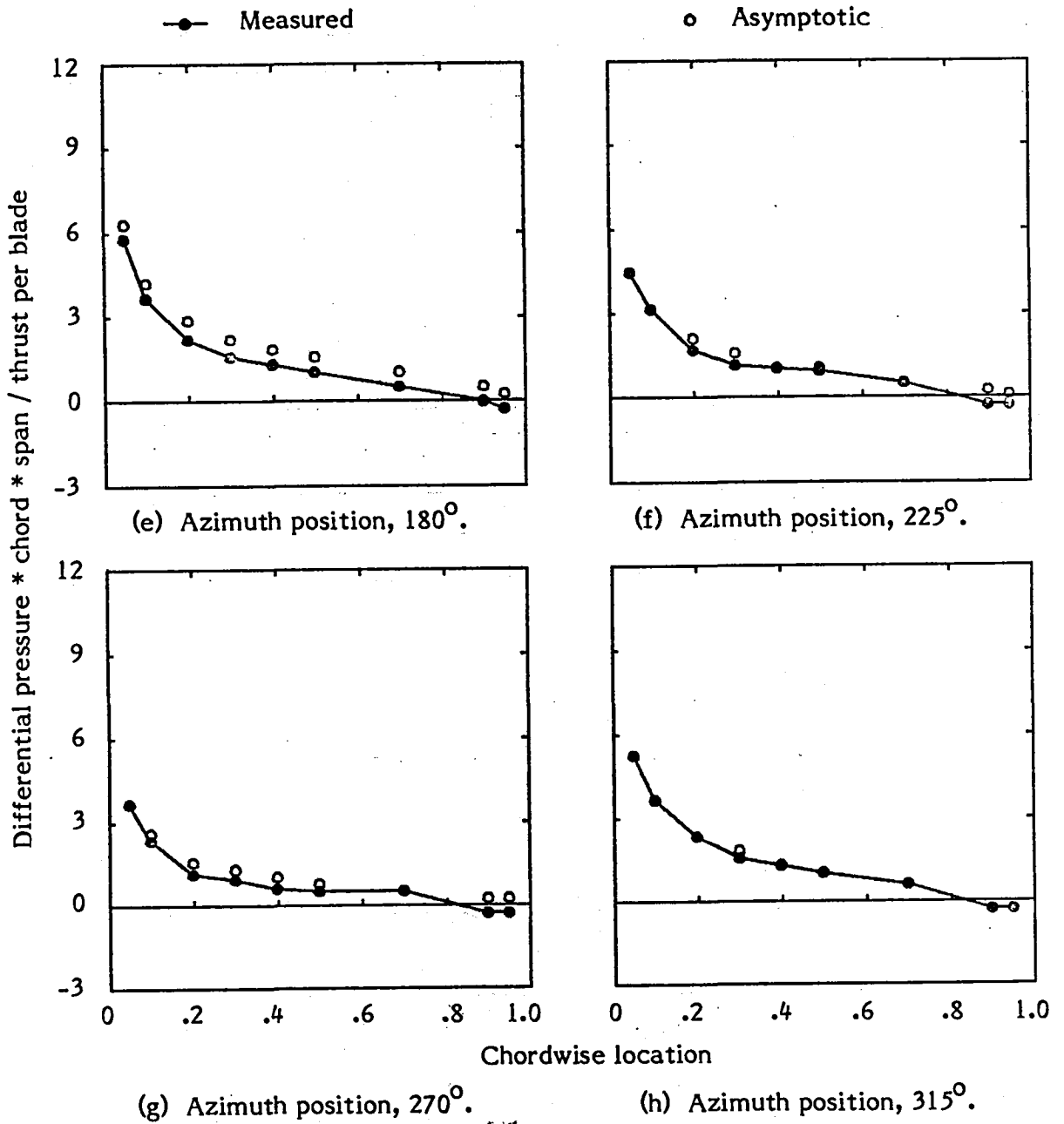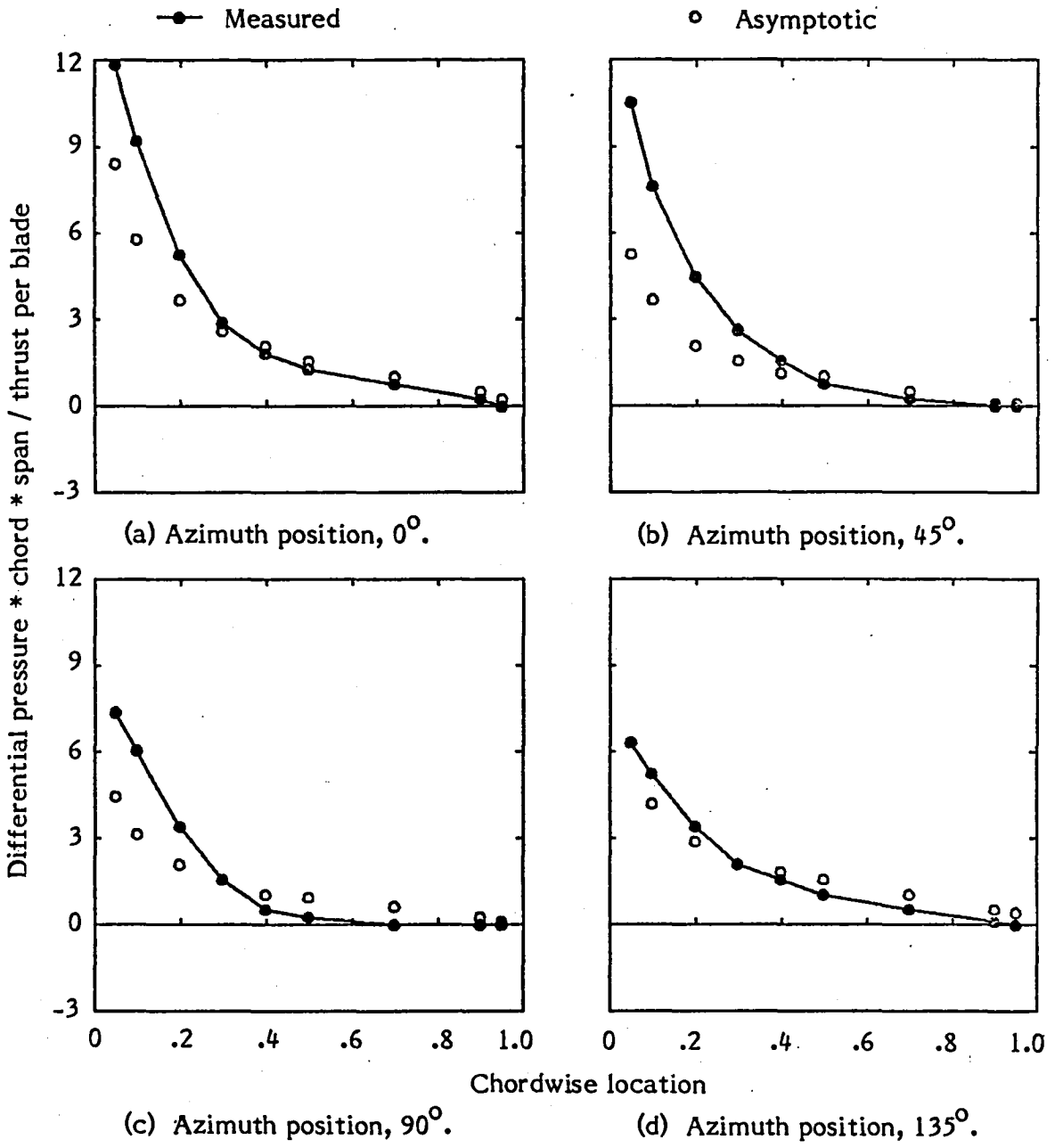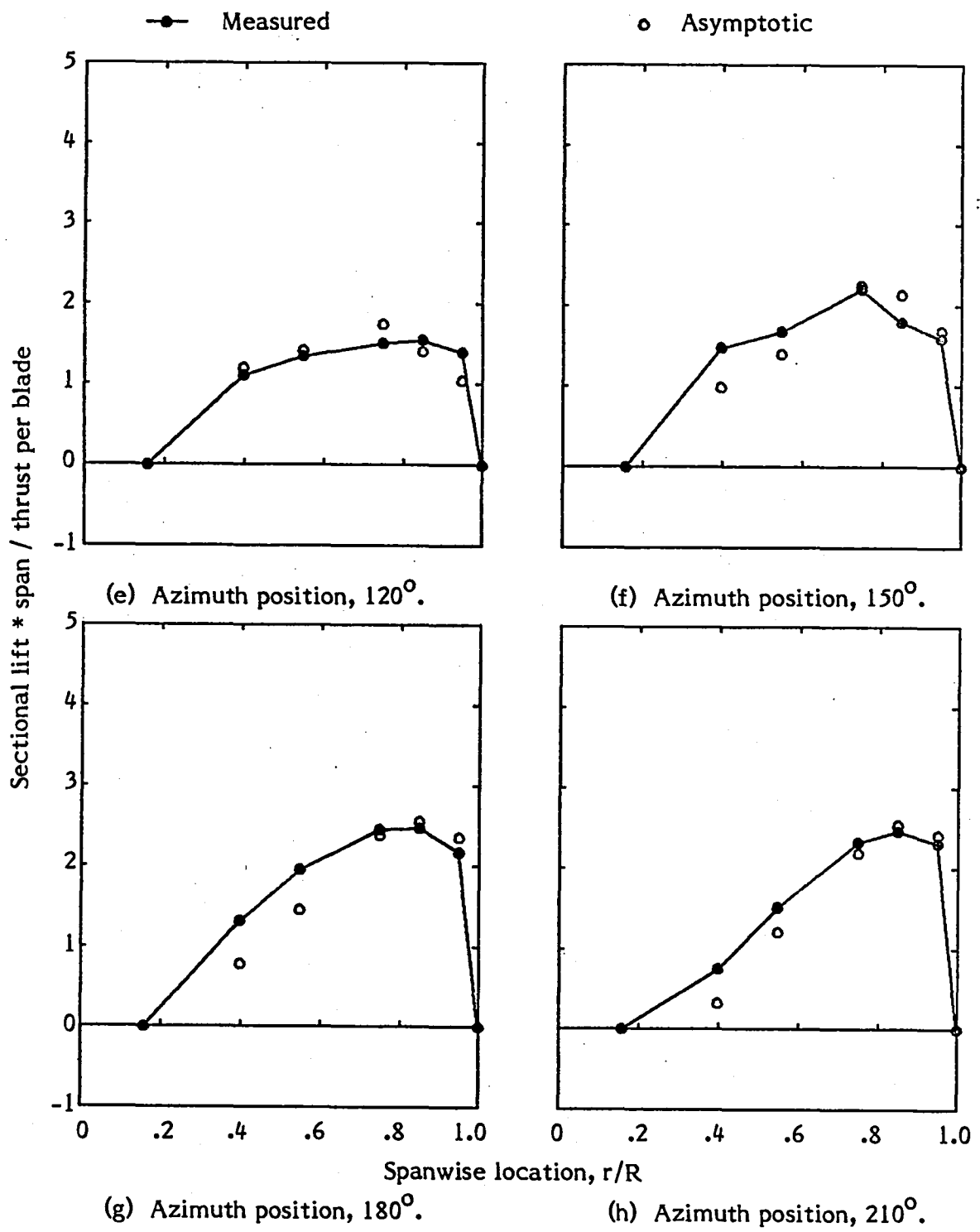
Figure 9. - Concluded.

Figure 10. - Differential pressure versus chordwise location for Case 1 with advance ratio of 0.29 at 85 percent span.

(e) Azimuth position, 180°.

(f) Azimuth position, 225°.
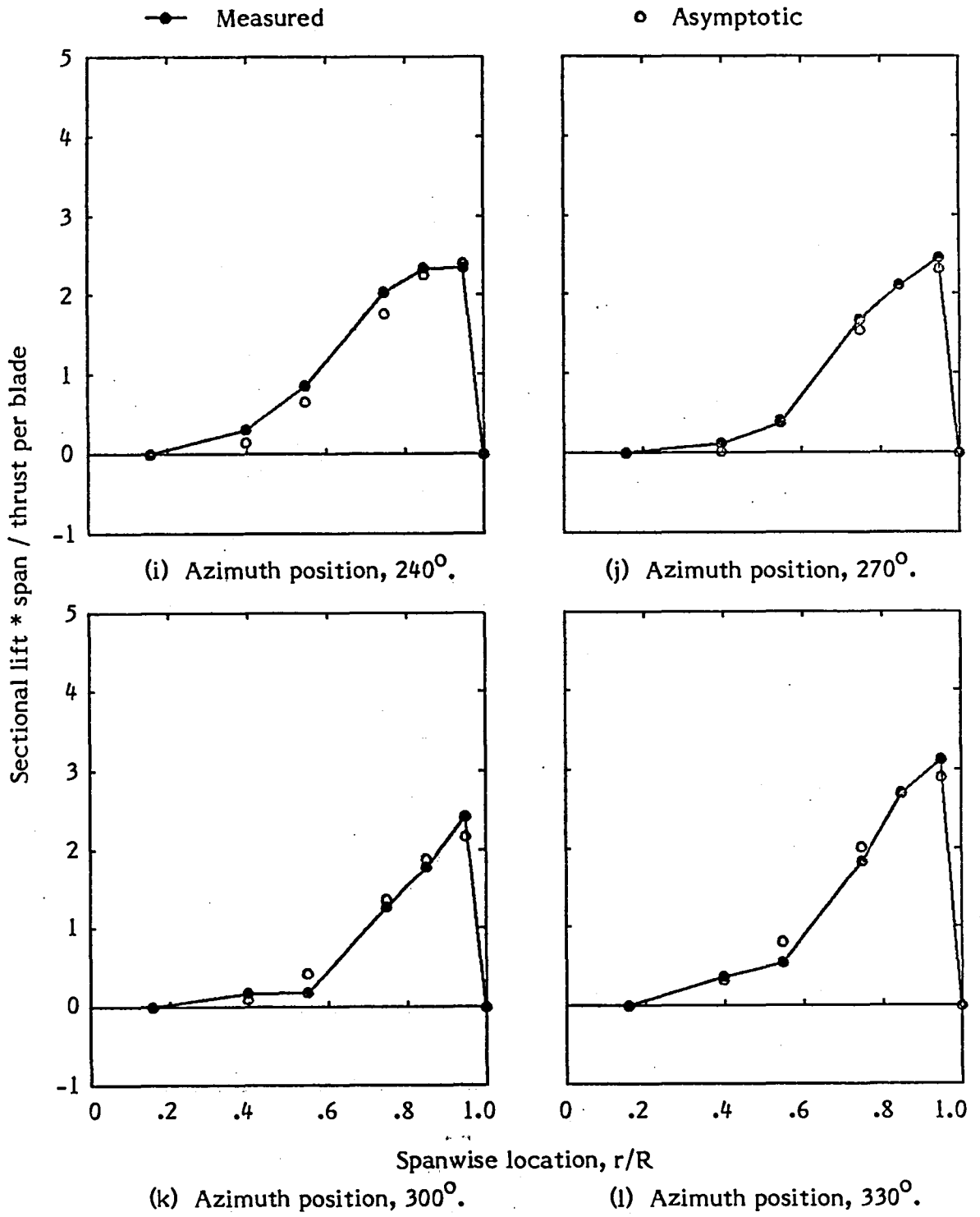
(g) Azimuth position, 270°.

(h) Azimuth position, 315°.
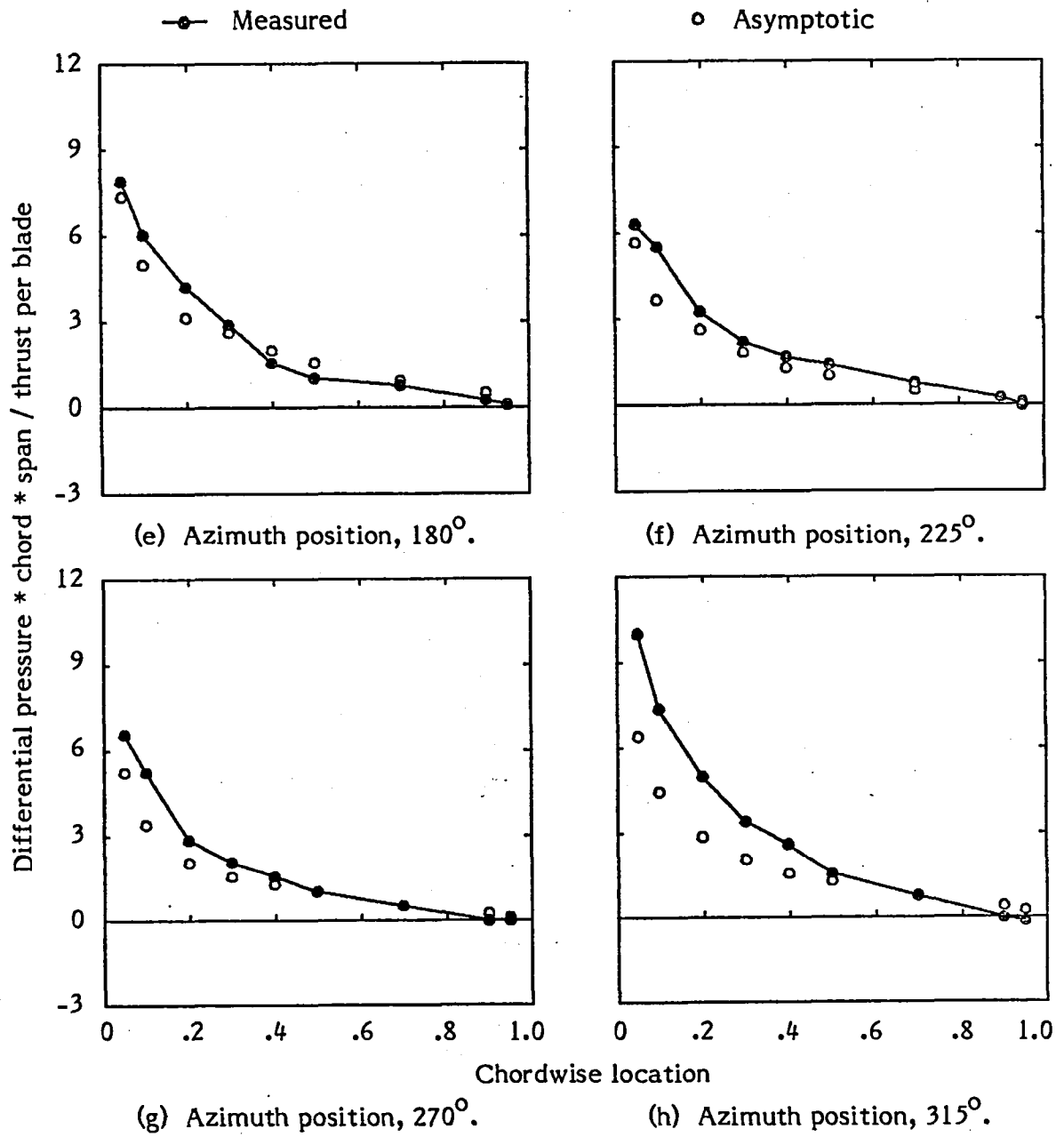
Figure 10. – Concluded.
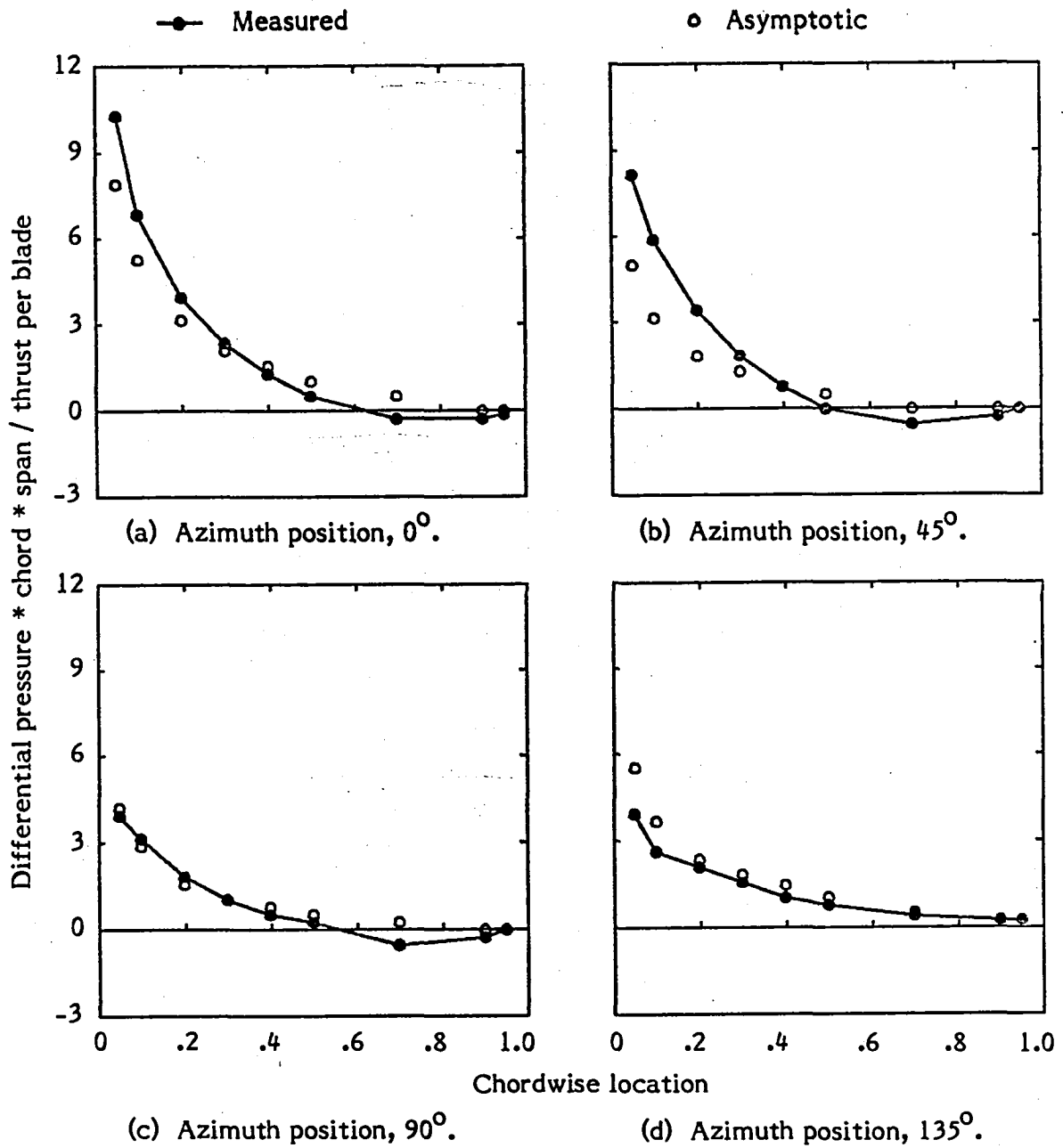
Figure 11. – Differential pressure versus chordwise location for Case 1 with advance ratio of 0.29 at 95 percent span.

(e) Azimuth position, 180°.

(f) Azimuth position, 225°.

(g) Azimuth position, 270°.

(h) Azimuth position, 315°.
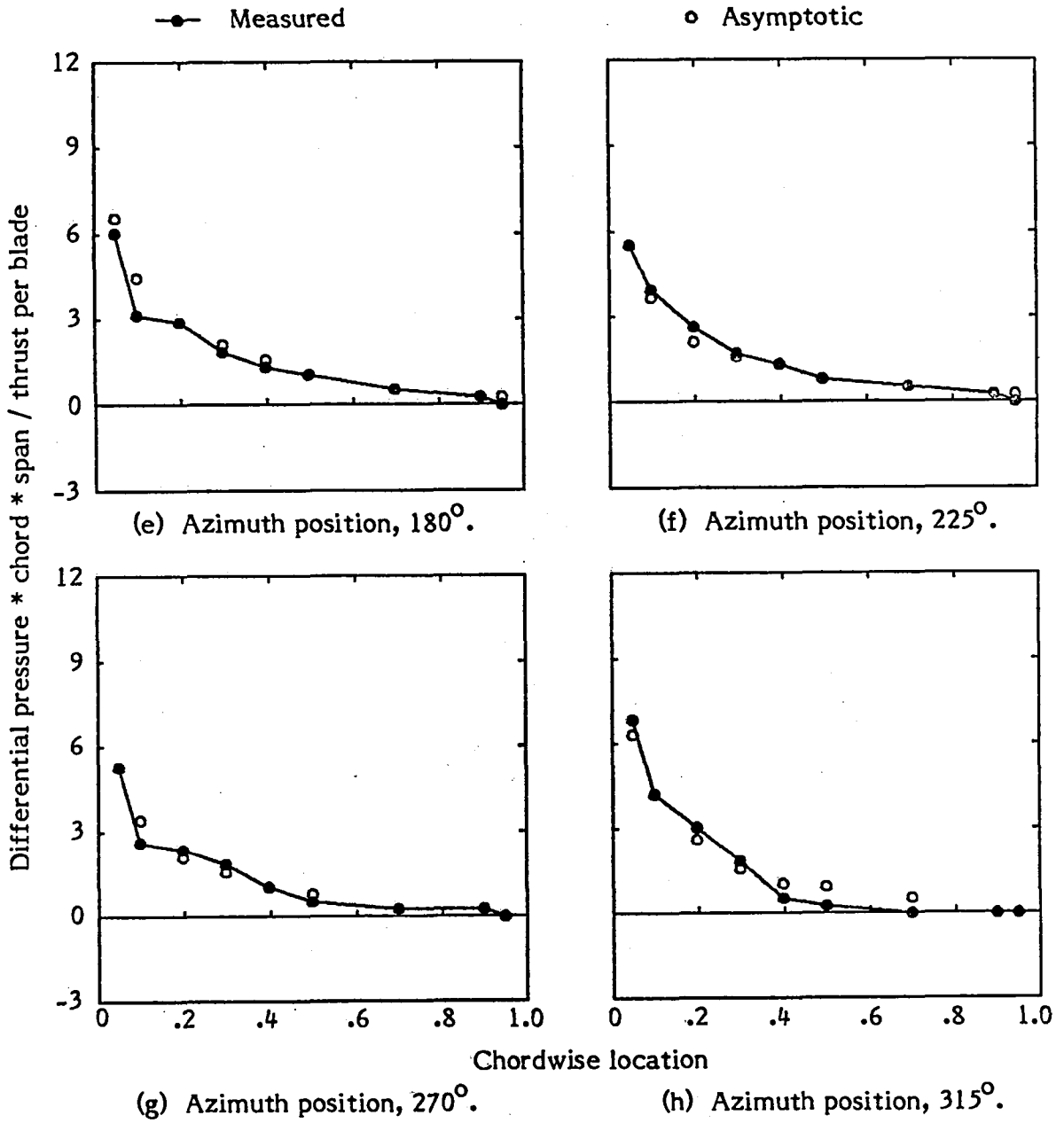
Figure 11. – Concluded.

Figure 12. – Normalized total blade lift versus azimuth position for Case 2.
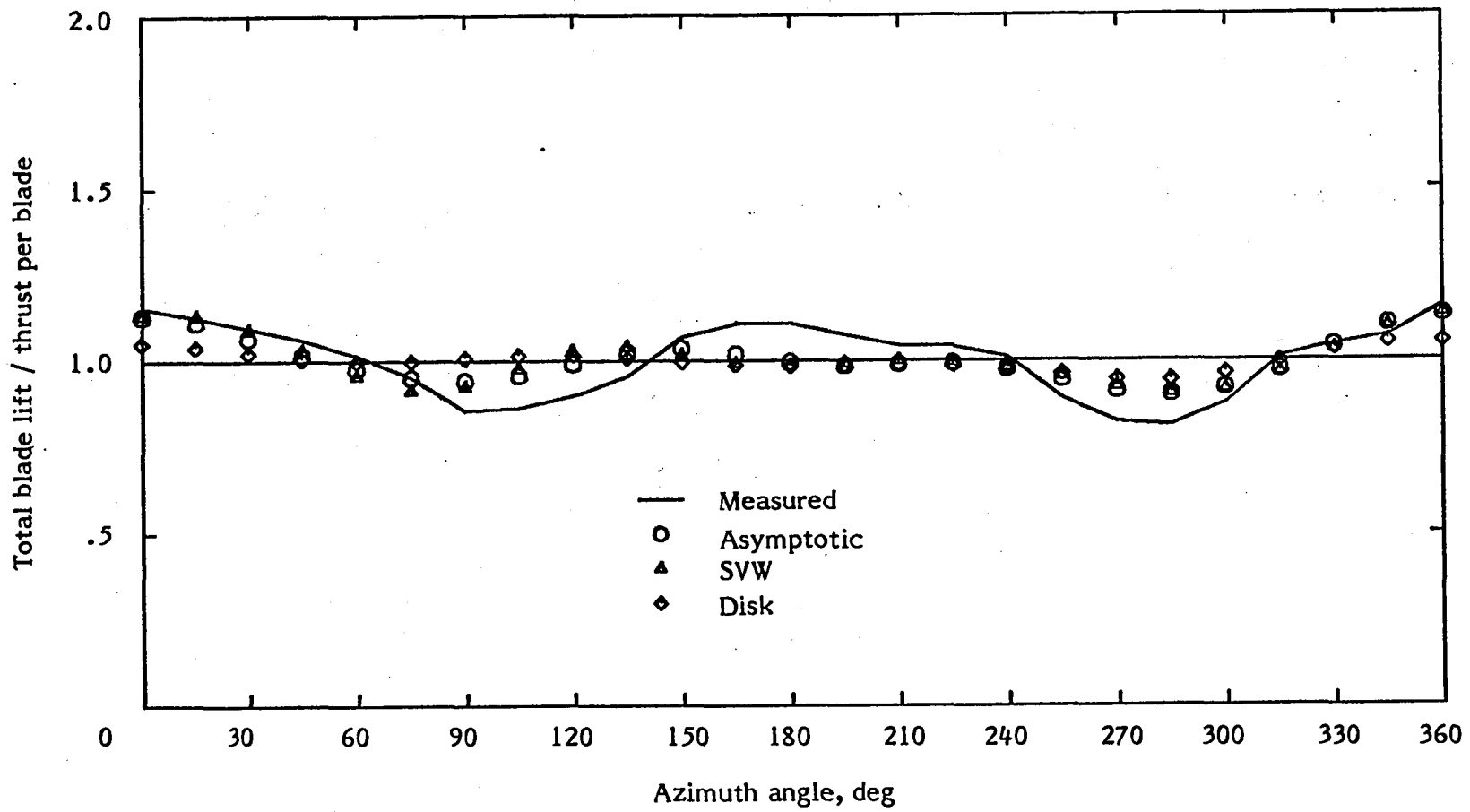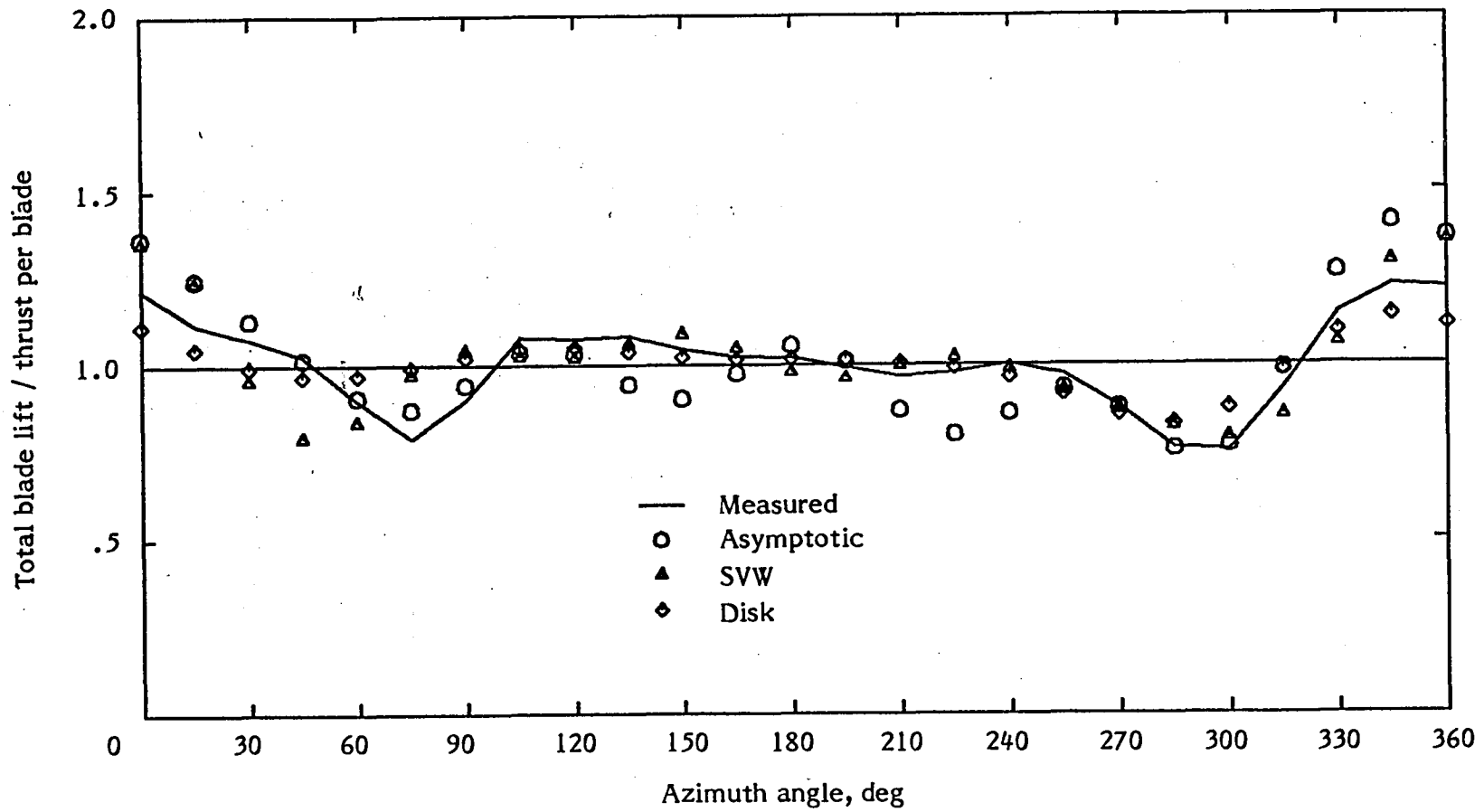
(a) Advance ratio, 0.06.

(b) Advance ratio, 0.13.

Figure 12. - Continued.

(c) Advance ratio, 0.29.

Figure 12. – Concluded.

(a) Azimuth position, 0°.

(b) Azimuth position, 30°.

(c) Azimuth position, 60°.

(d) Azimuth position, 90°.

Figure 13. – Normalized sectional lift versus spanwise location for Case 2 with advance ratio of 0.06.

(e) Azimuth position, 120°.

(f) Azimuth position, 150°.

(g) Azimuth position, 180°.

(h) Azimuth position, 210°.

Figure 13. - Continued.

101

(i) Azimuth position, 240°.

(j) Azimuth position, 270°.

(k) Azimuth position, 300°.

(l) Azimuth position, 330°.

Figure 13. – Concluded.
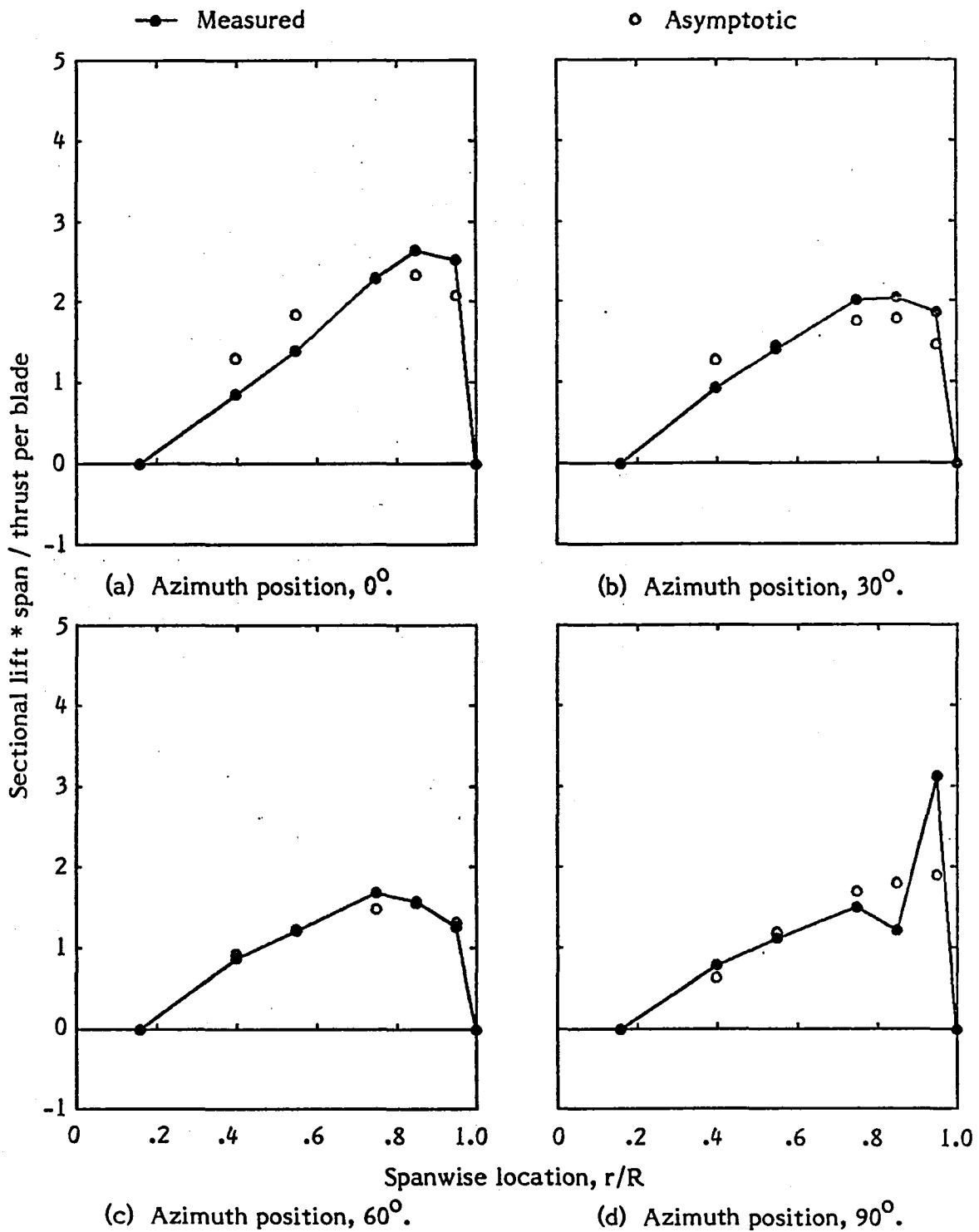
Figure 14. - Normalized sectional lift versus spanwise location for Case 2 with advance ratio of 0.13.

(e) Azimuth position, 120°.

(f) Azimuth position, 150°.

(g) Azimuth position, 180°.

(h) Azimuth position, 210°.

Figure 14. – Continued.

104

(i) Azimuth position, 240°.

(j) Azimuth position, 270°.

(k) Azimuth position, 300°.

(l) Azimuth position, 330°.

Figure 14. - Concluded.
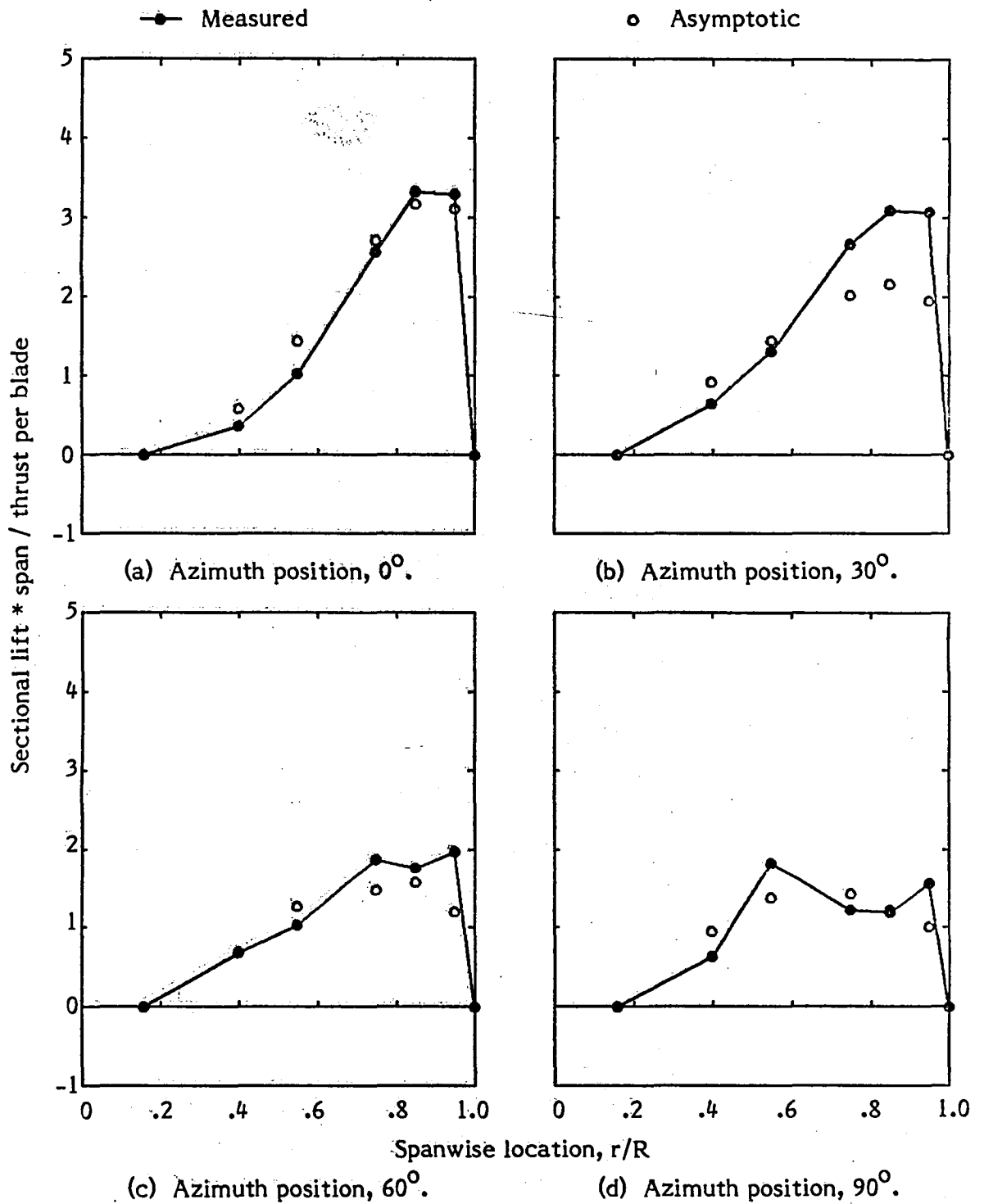
Figure 15. - Normalized sectional lift versus spanwise location for Case 2 with advance ratio of 0.29.

(e) Azimuth position, 120°.

(f) Azimuth position, 150°.

(g) Azimuth position, 180°.

(h) Azimuth position, 210°.

Figure 15. - Continued.

(i) Azimuth position, 240°.

(j) Azimuth position, 270°.

(k) Azimuth position, 300°.

(l) Azimuth position, 330°.

Figure 15. – Concluded.
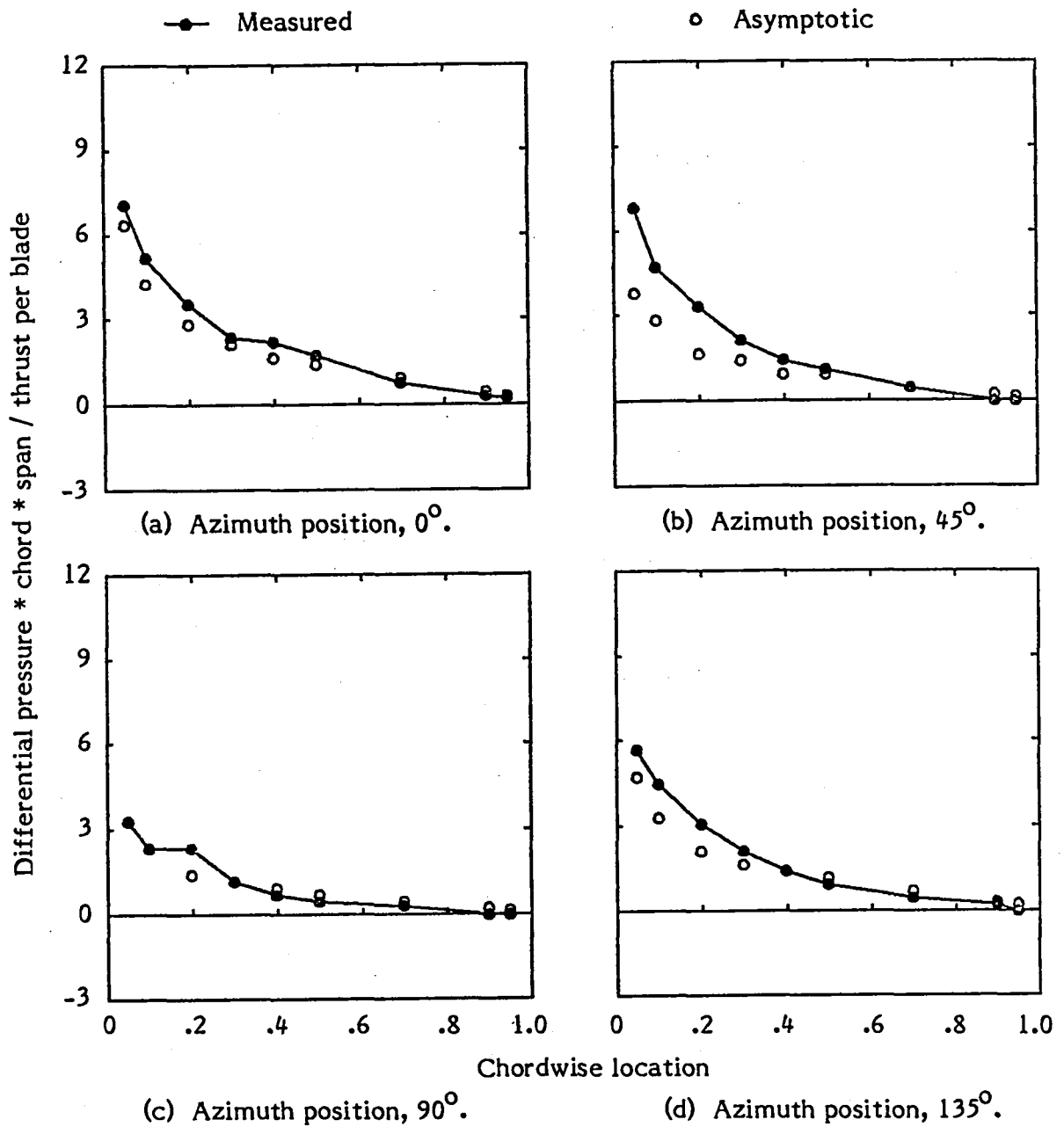
Figure 16. -Differential pressure versus chordwise location for Case 2
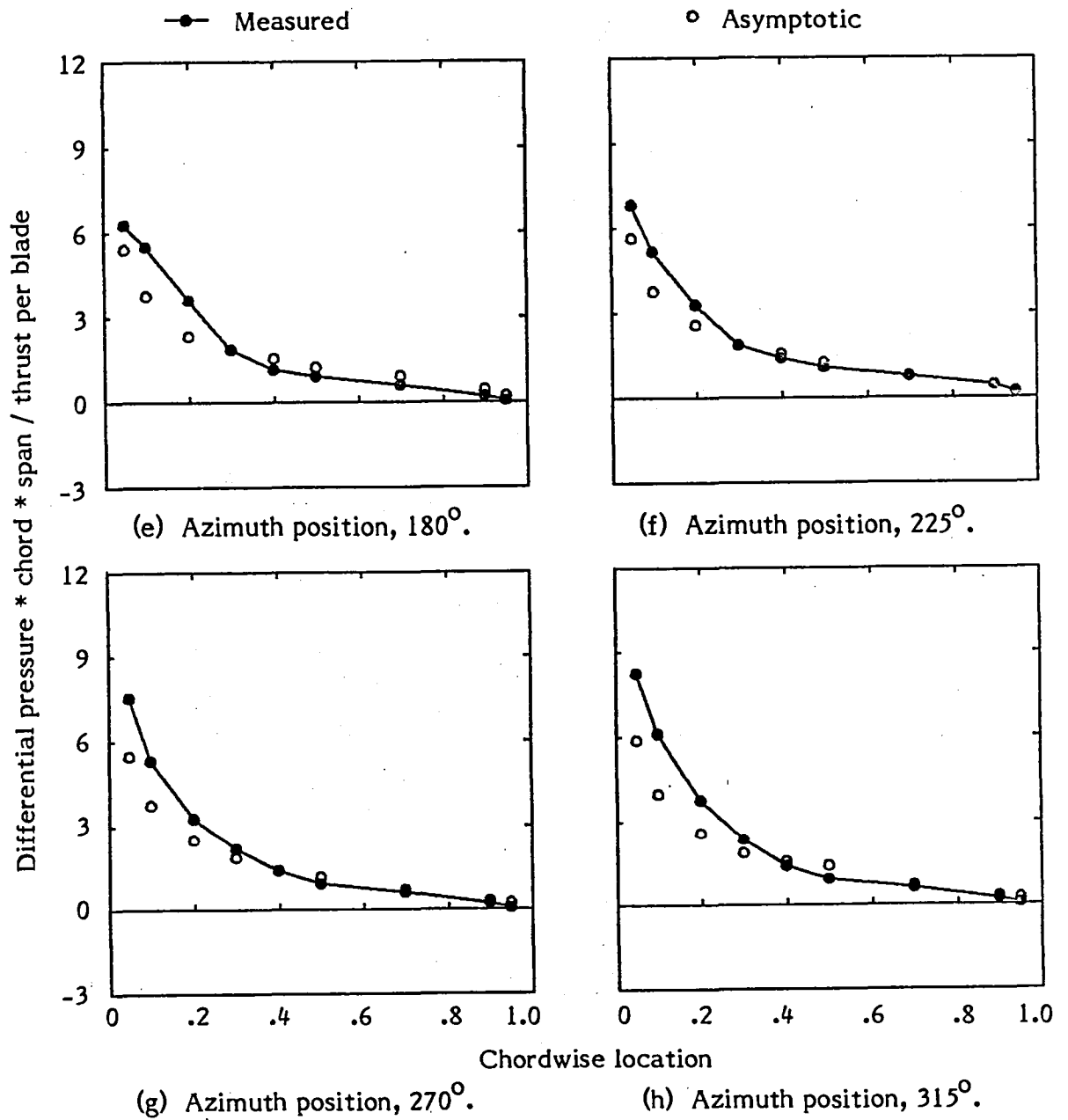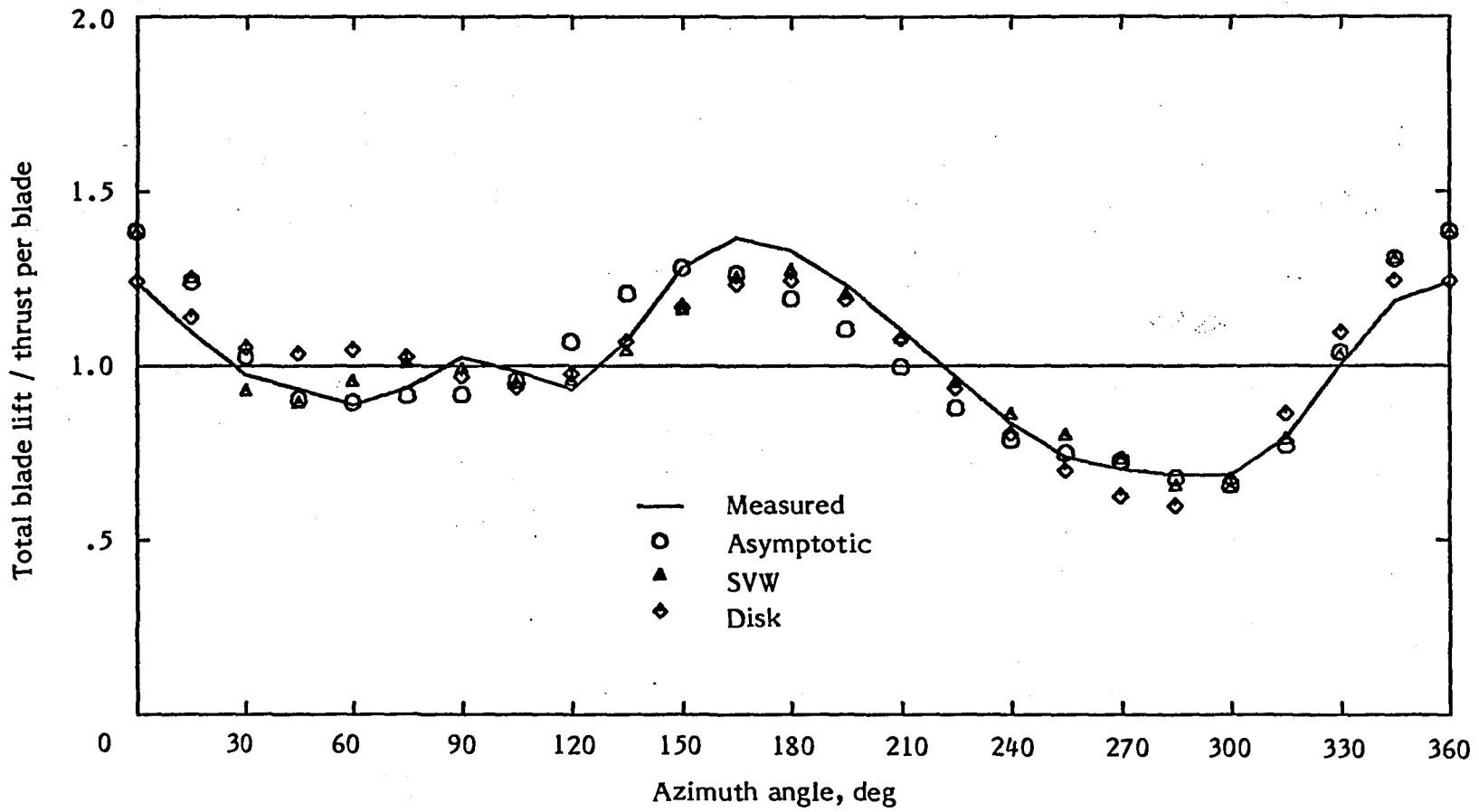with advance ratio of 0.29 at 75 percent span.

(e) Azimuth position, 180°.

(f) Azimuth position, 225°.

(g) Azimuth position, 270°.

(h) Azimuth position, 315°.
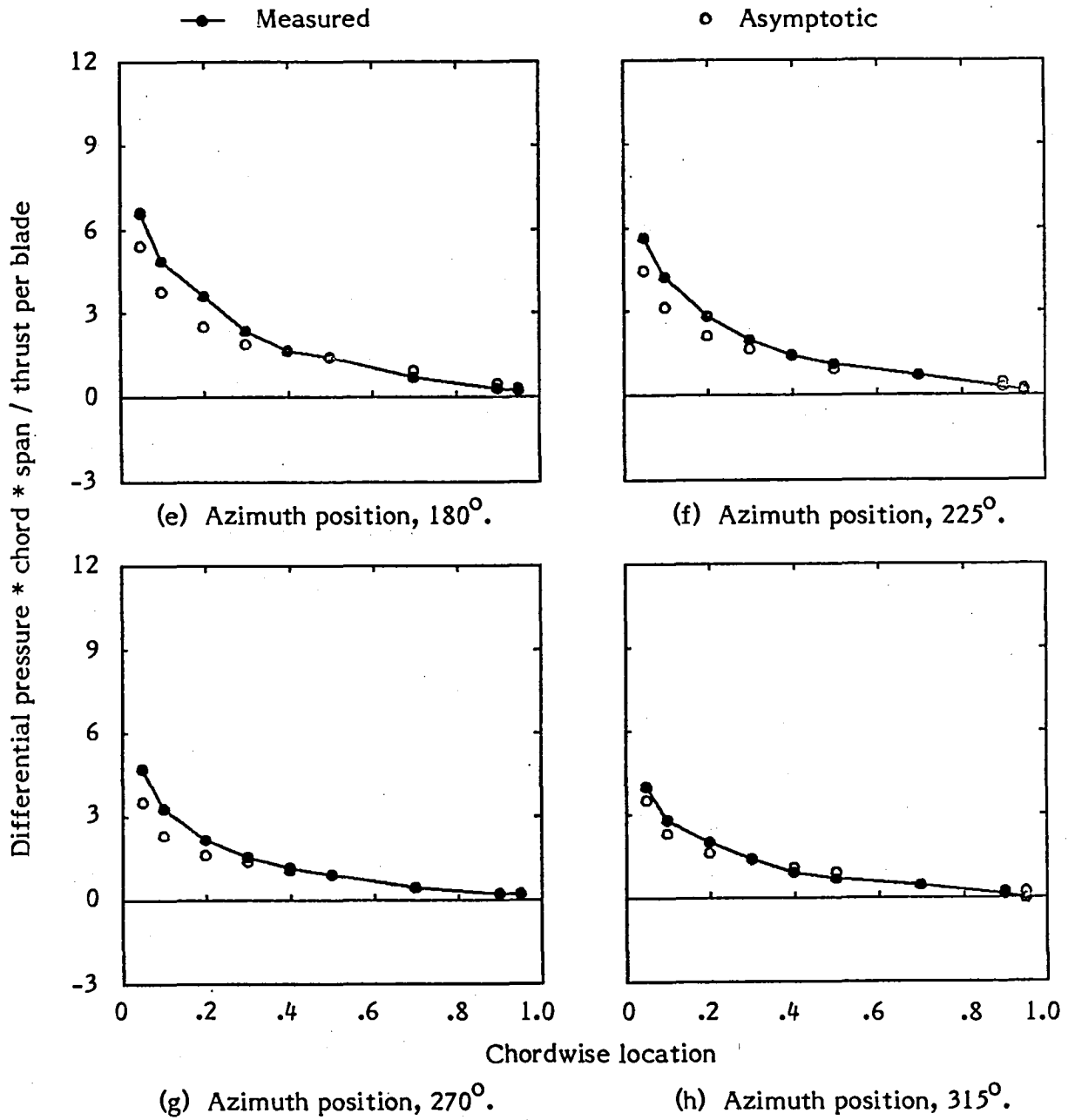
Figure 16. – Concluded.
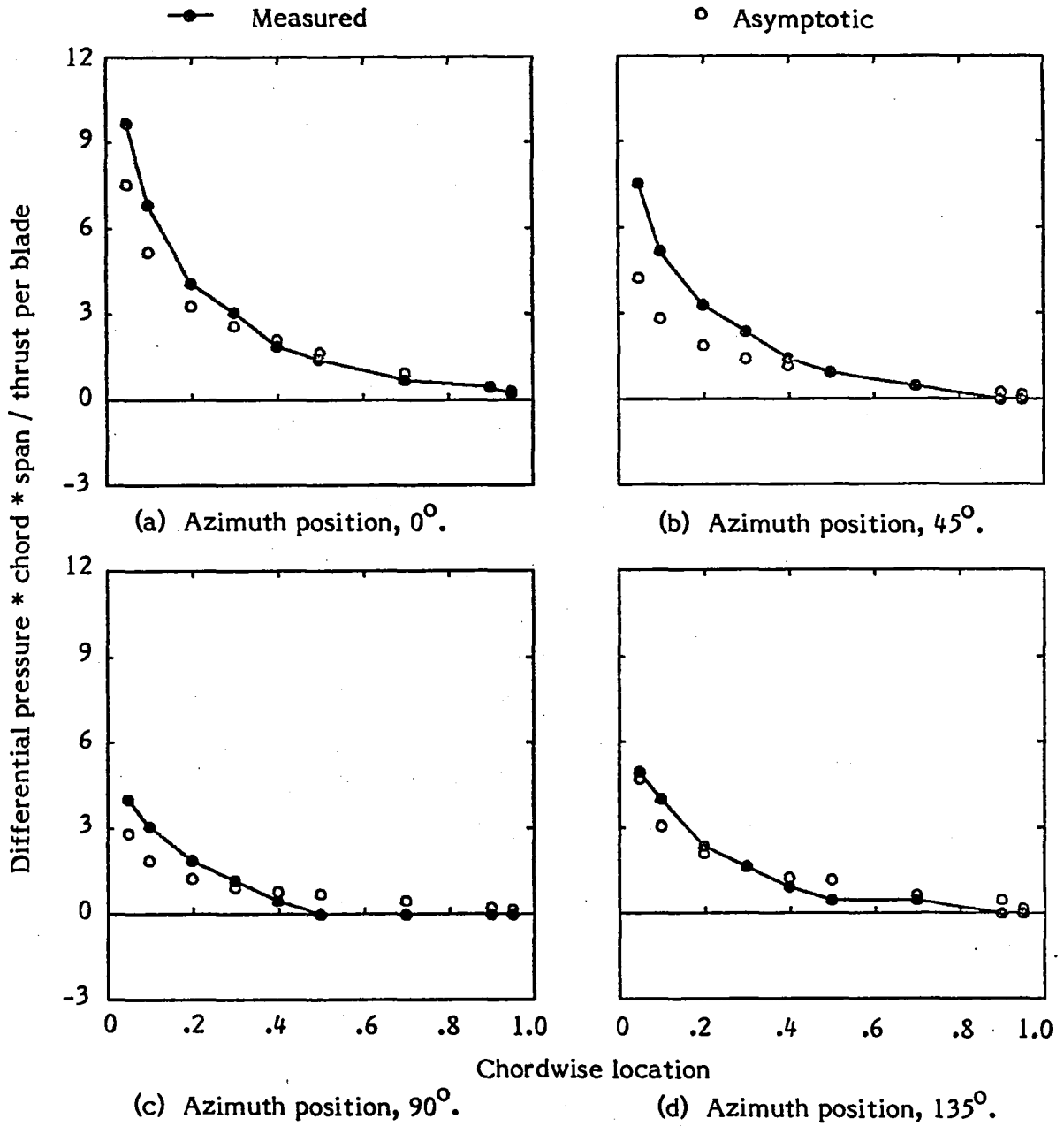
Figure 17. – Differential pressure versus chordwise location for Case 2 with advance ratio of 0.29 at 85 percent span.

(e) Azimuth position, 180°.

(f) Azimuth position, 225°.

(g) Azimuth position, 270°.

(h) Azimuth position, 315°.
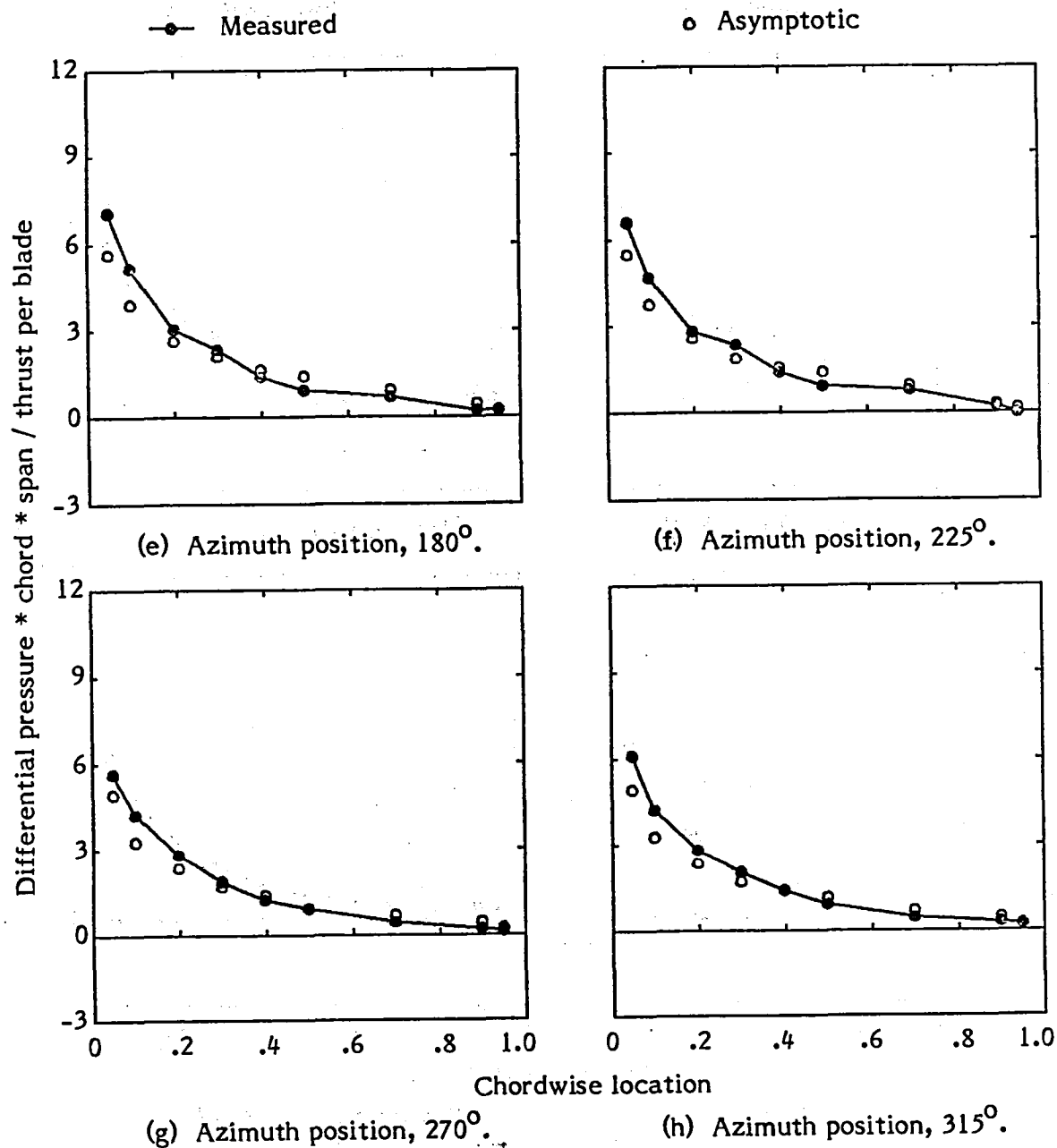
Figure 17. – Concluded.

112
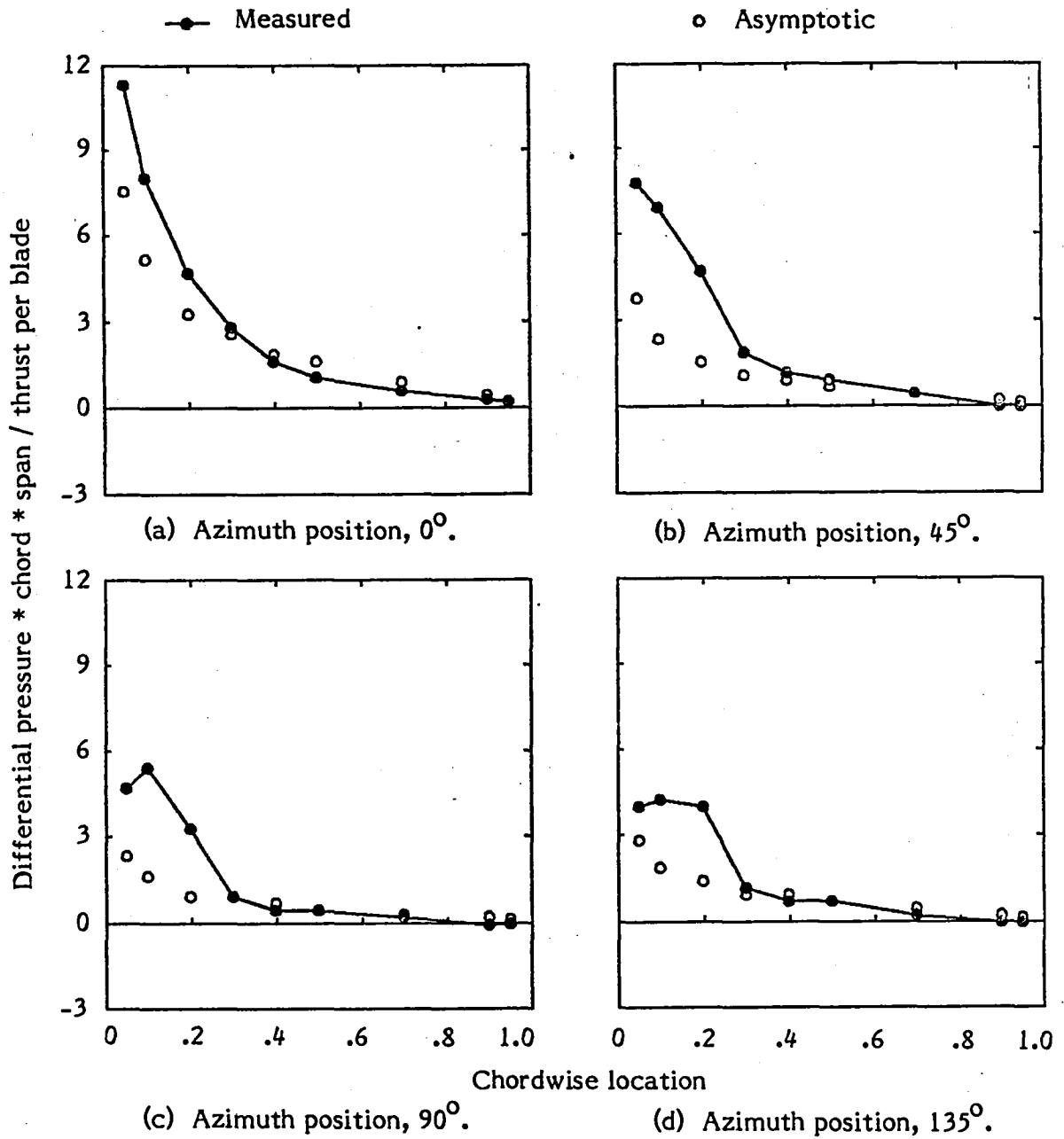
Figure 18. – Differential pressure versus chordwise location for Case 2 with advance ratio of 0.29 at 95 percent span.

(e) Azimuth position, 180°.

(f) Azimuth position, 225°.

(g) Azimuth position, 270°.

(h) Azimuth position, 315°.

Figure 18. – Concluded.

114

(a) Advance ratio, 0.29.

Figure 19. – Normalized total blade lift versus azimuth position for Case 3.
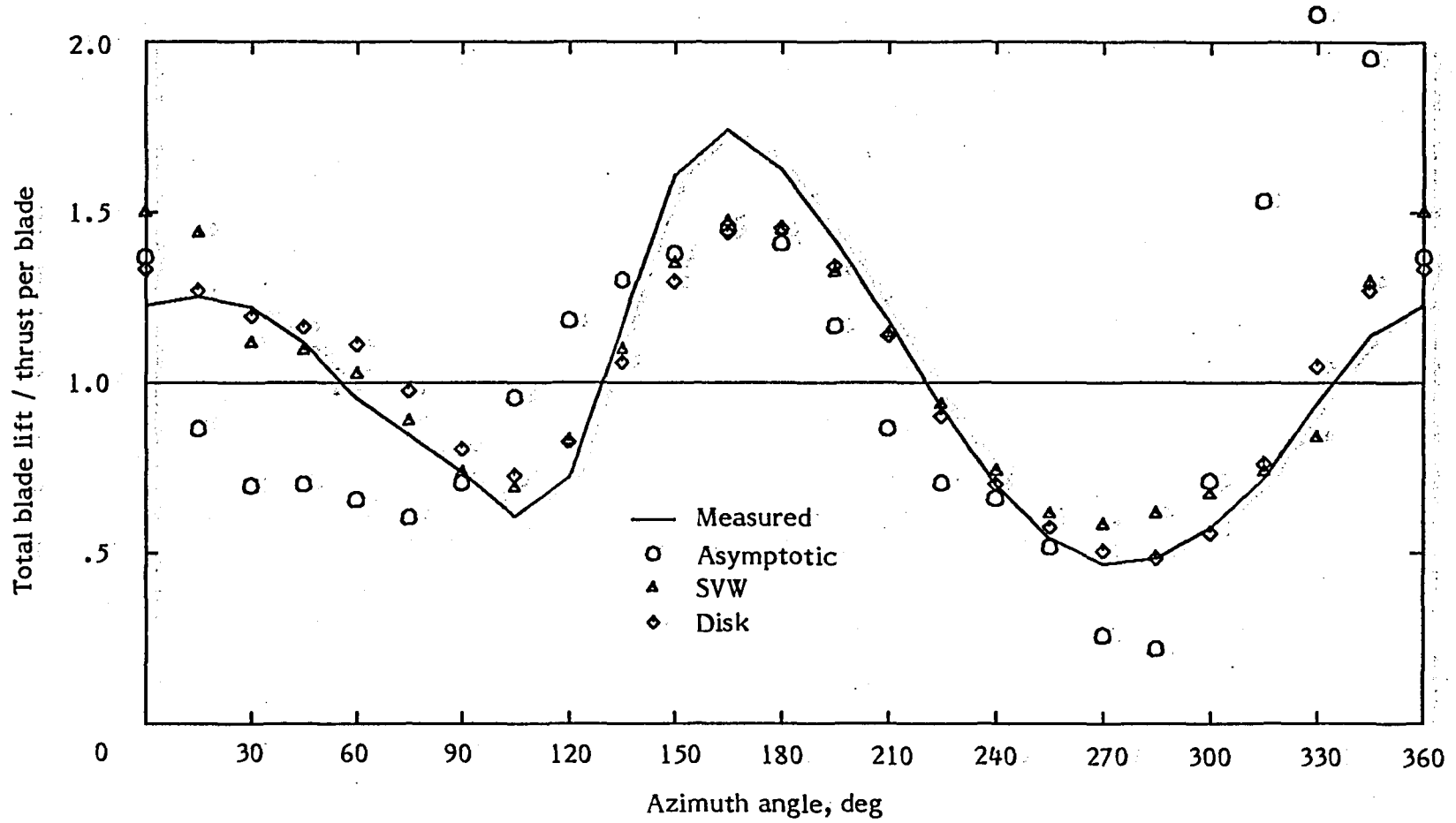
(b) Advance ratio, 0.39.

Figure 19. – Continued.
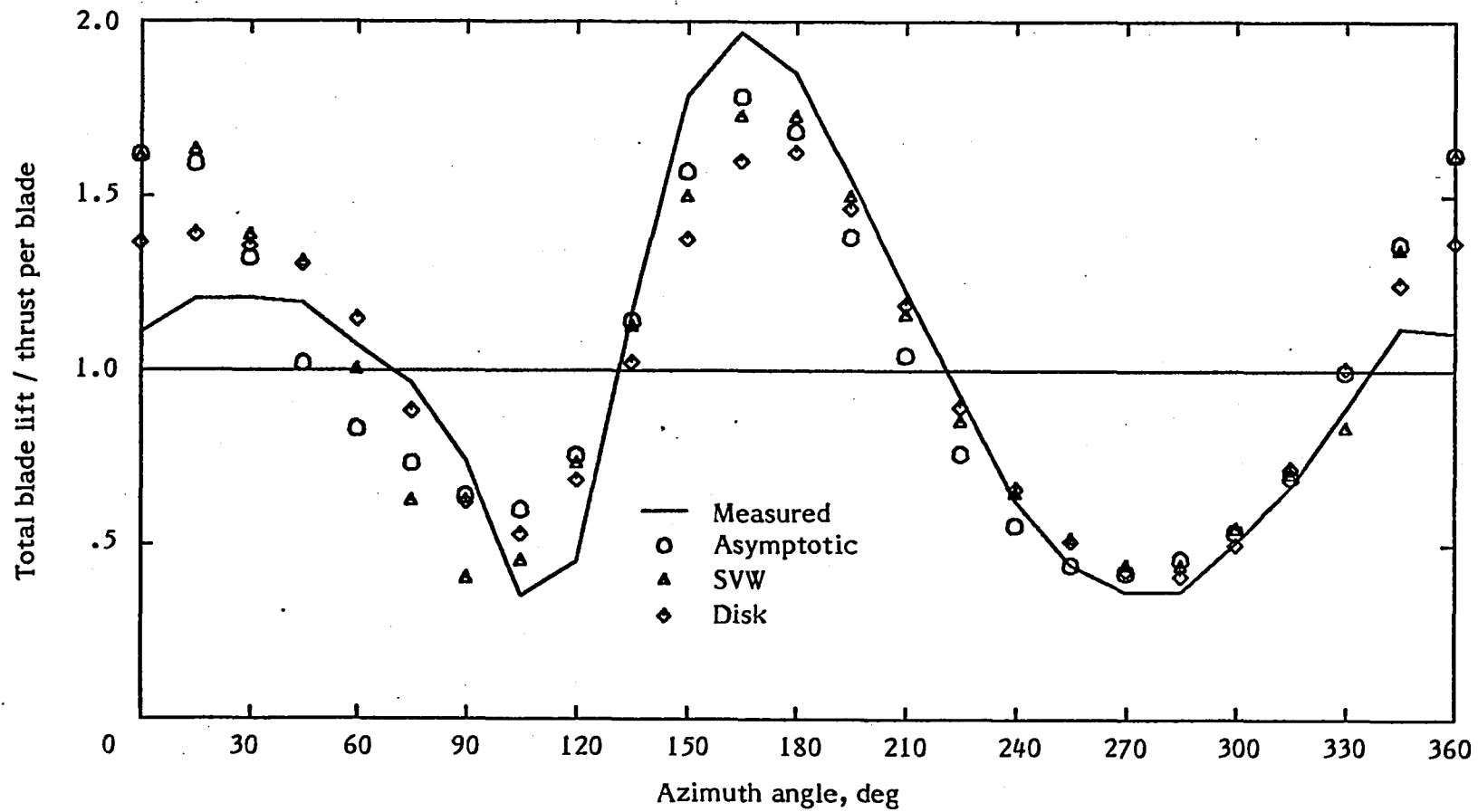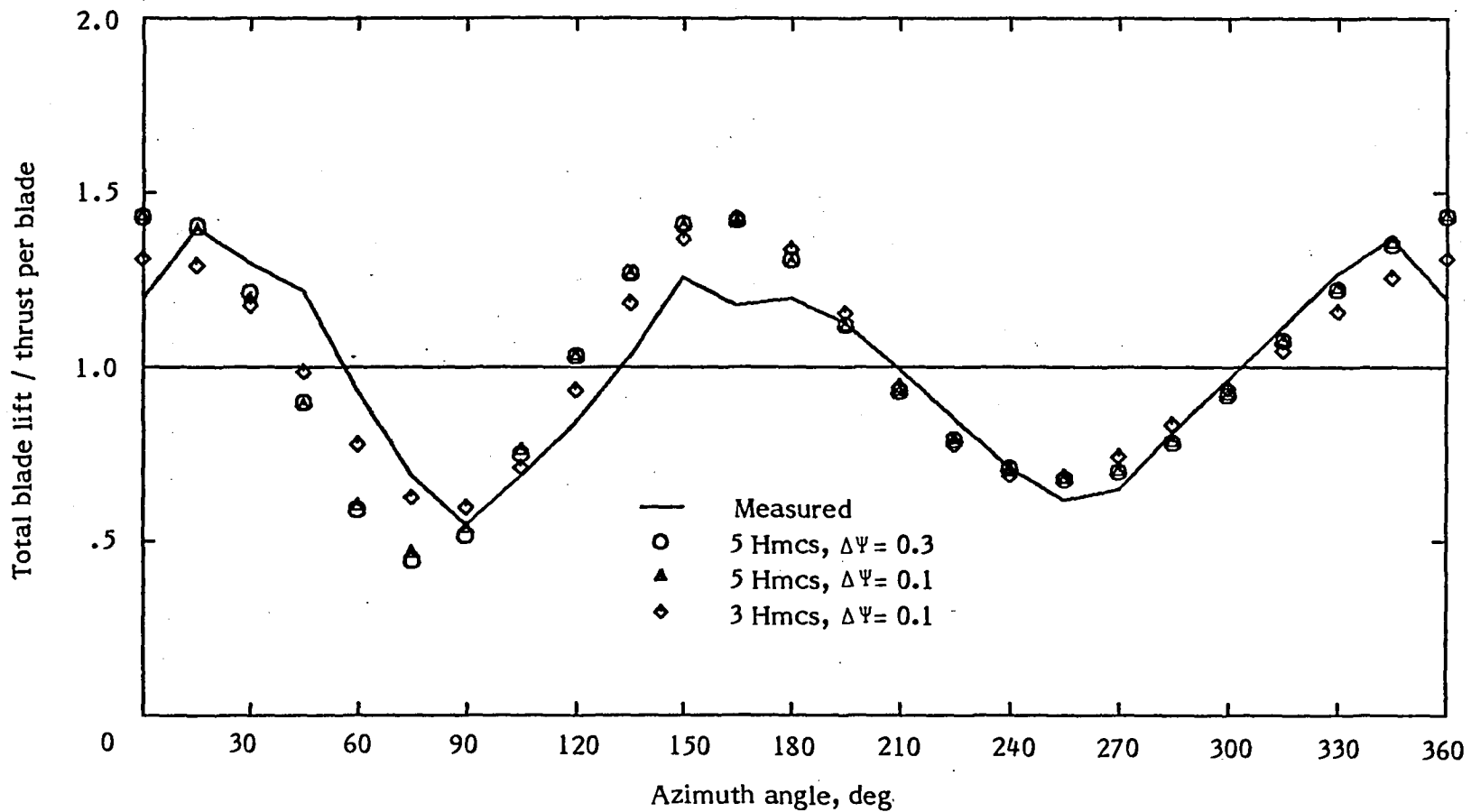
(c) Advance ratio, 0.45.

Figure 19. – Concluded.

Figure 20. - Computational effect on asymptotic total lift for Case 1 with advance ratio of 0.29.
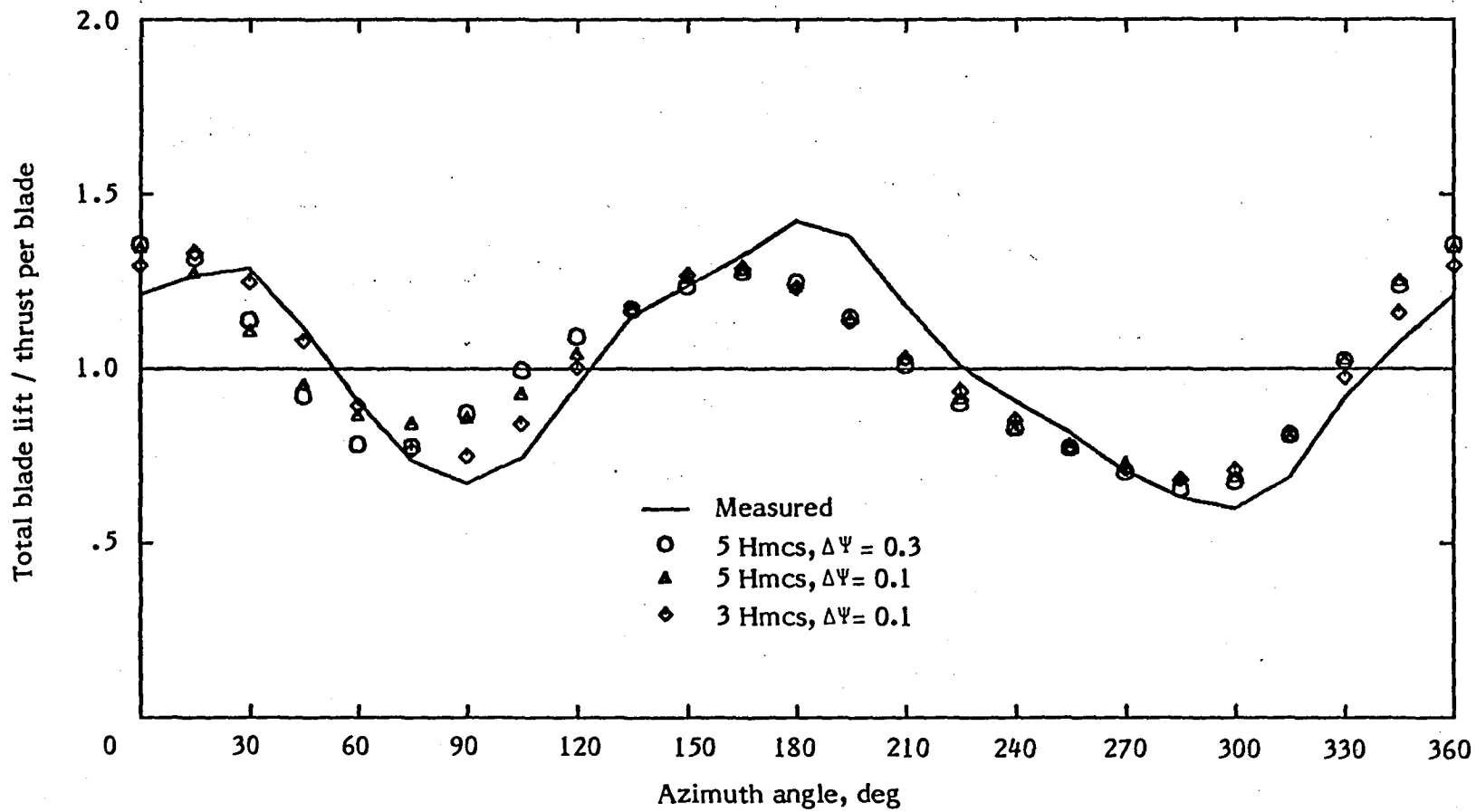
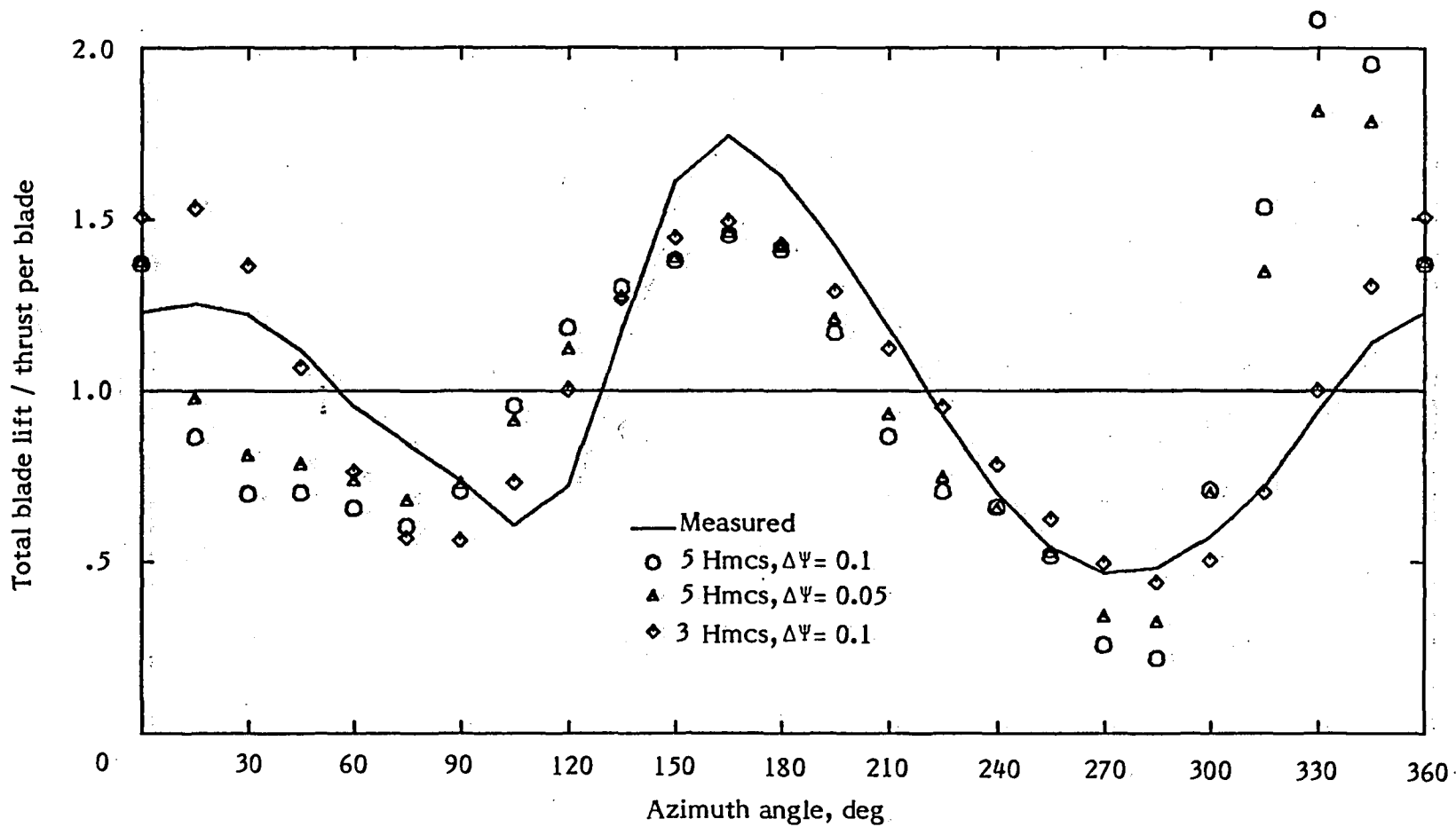Figure 21. – Computational effect on asymptotic total lift for Case 2 with advance ratio of 0.29.

Figure 22. – Computational effect on asymptotic total lift for Case 3 with advance ratio of 0.39.

1. Report No. NASA CR - 165742	2. Government Accession No.	3. Recipient's Catalog No.
4. Title and Subtitle HELICOPTER ROTOR LOADS USING A MATCHED ASYMPTOTIC EXPANSION TECHNIQUE		5. Report Date May 1981
		6. Performing Organization Code
7. Author(s) G. Alvin Pierce and Anand R. Vaidyanathan		8. Performing Organization Report No.
9. Performing Organization Name and Address Georgia Institute of Technology School of Aerospace Engineering Atlanta, Georgia 30332		10. Work Unit No.
		11. Contract or Grant No. NAS 1 - 16222
12. Sponsoring Agency Name and Address National Aeronautics and Space Administration Washington, DC 20546		13. Type of Report and Period Covered Contractor report
		14. Sponsoring Agency Code

16. Abstract

A variety of approximate methods are available for the estimation of airloads on helicopter rotor blades. These methods vary widely in their degree of approximation, accuracy and detail of prediction. One such method has been suggested by Van Holten which uses an acceleration potential description of the flow field and a matched asymptotic expansion technique to calculate unsteady, three-dimensional airloads on a rotor blade in forward flight.

The study presented here was undertaken to examine the theoretical basis and computational feasibility of the Van Holten method, and to evaluate its performance and range of validity by comparison with experiment and other approximate methods. It is found that, within the restrictions of incompressible, potential flow and the assumption of small disturbances, the method does lead to a valid description of the flow. However, due to the nature of the basic assumptions, the method begins to break down under conditions favoring non-linear effects such as wake distortion and blade/rotor interaction.

17. Key Words (Suggested by Author(s)) Unsteady airloads, Helicopter rotor, Potential flow, Asymptotic expansion		18. Distribution Statement Unclassified - Unlimited	
19. Security Classif. (of this report) Unclassified	20. Security Classif. (of this page) Unclassified	21. No. of Pages 123	22. Price